Vrije Universiteit Brussel

FACULTY OF ENGINEERING

Analysis of the energy storage systems in series plug-in hybrid electric vehicles

Karel Fleurbaey

Promoter: Prof. Dr. Ir. Joeri Van Mierlo
Supervisor: Dr. Eng. Noshin Omar
Ir. Mohamed El Baghdadi

Thesis submitted in partial fulfilment of the requirements for the:
Master of Science in Applied Sciences and Engineering:
Electro-Mechanical Engineering

Academic year 2012-2013

Bruface
Brussels
Faculty of
Engineering

VRIJE UNIVERSITEIT BRUSSEL
SCIENTIA VINCERE TENEBRAS

Preface

From an economical, environmental and social point of view, the current energy supply and use is not sustainable. The intensive use of fossil fuels in the energy generation process leads to an increased concentration of greenhouse gasses in the atmosphere. Its effect in terms of global warming is today already described by the International Panel on Climate Change and a global temperature rise of 2°C compared to pre-industrial level can only be stopped if decisive actions are taken quickly. I chose to study engineering because I want to be part of this change towards a more sustainable society. The trend towards renewable electricity generation and more efficient electricity use has been highlighted continuously during our education as energy engineers. However, the technological evolutions in the transport sector, which accounts for 25% of the worldwide CO_2 emissions, were not treated in detail. This master thesis gave me the chance to also get in contact with the research on hybrid drivetrains and energy storage systems of electrified vehicles.

I want to thank everyone who helped me finishing this master thesis.
First and foremost, I want to thank Prof. Dr. Ir. Joeri Van Mierlo for giving me the opportunity to perform research on the rechargeable energy storage systems of plug-in hybrid electric vehicles. I also want to express my gratitude to my supervisors Dr. Eng. Noshin Omar and Ir. Mohamed El Baghdadi for their continuous assistance and support. Their expertise and warm guidance were of great help during this master thesis. I also sincerely thank Dr. Ir. Ricardo Barrero for his help during the design phase of the proposed model.
I want to address special thanks to my girlfriend, my family and friends for their love, support and encouragements during this master thesis.

Abstract

Author: Karel Fleurbaey
Degree: Master of Science in electromechanical engineering – Profile Energy
Academic year: 2012 – 2013
Title: Analysis of the energy storage systems in series plug-in hybrid electric vehicles
Keywords: Matlab, Simulink, Plug-in Hybrid Electric Vehicle, Lithium ion battery, Electrical Double Layer Capacitor

Summary

A model of a series plug-in hybrid electric vehicle in the Matlab/Simulink environment is proposed. This model is used to examine the rechargeable energy storage system (RESS) of the plug-in hybrid electric vehicle. None of the currently existing lithium ion battery technologies are able to meet the industrial demands in terms of energy content, power capability, cycle life, efficiency and cost. To overcome this inconvenience, the combination of an Electrical Double Layer Capacitor (EDLC) system with an energy-optimized battery is analysed. A comparative study between the battery stand-alone system and the hybrid RESS shows the beneficial influence of the EDLC system on the power performance, cycle life, energy efficiency and all electric driving range. The EDLC system however also significantly increases the cost, weight and volume of the RESS, blocking its introduction in modern passenger vehicles.

Abstract

Auteur: Karel Fleurbaey
Graad: Master of Science in de ingenieurswetenschappen: Werktuigkunde – Optie Energie
Academiejaar: 2012 – 2013
Titel: Analyse van energieopslag systemen in serie plug-in hybride elektrische voertuigen.
Trefwoorden: Matlab, Simulink, Plug-in Hybride Elektrische voertuigen, Lithium ion batterij, Elektrische dubbellaag condensator

Samenvatting

In deze master thesis wordt een simulatiemodel voor een serie plug-in hybride elektrische wagen voorgesteld. Dit model wordt gebruikt om het energieopslag systeem van de plug-in hybride wagen te analyseren. Het energieopslag systeem bestaat in de moderne toepassingen uit een lithium-ion batterij, hoewel ook deze technologie (nog) niet aan de industriële eisen kan voldoen wat betreft energie-inhoud, vermogensprestaties, levensduur, efficiëntie en kost. In deze thesis wordt de prestatie van een hybride energieopslag systeem, bestaande uit een energie-geoptimaliseerde lithium ion batterij en een elektrisch dubbellaag condensator (EDLC) systeem vergeleken met deze van een alleenstaand batterijsysteem. De resultaten van de simulatie tonen het positieve effect van het hybride energieopslag systeem op de vermogenprestaties, levensduur van de batterij en efficiëntie van het opslagsysteem aan. Het toevoegen van deze extra component zorgt echter ook voor een aanzienlijke verhoging van de kostprijs, gewicht en volume van het energieopslag systeem, wat de invoering van EDLC systemen in moderne personenwagens tegenhoudt.

Abstrait

Auteur: Karel Fleurbaey
Degré: Master en ingénieur civil électromécanicien – Option Energie
Année académique: 2012 – 2013
Titre: Analyse du système de stockage d'énergie des véhicules hybrides séries rechargeables.
Mots-clés: Matlab, Simulink, Véhicule Hybride rechargeable, Batterie Lithium ion, Condensateur électrique à double couche

Sommaire

Un modèle d'un véhicule hybride rechargeable avec une topologie sérielle est proposé dans cette mémoire. Ce modèle est utilisé pour examiner le système de stockage d'énergie des véhicules hybrides rechargeables, qui consiste typiquement d'une batterie lithium-ion. Pourtant, aucun des batteries lithium-ion ne peuvent répondre aux exigences posées par l'industrie en termes de contenu énergétique, de la capacité de puissance, de la durée de vie, de l'efficacité et du coût. Afin d'améliorer les performances du système de stockage d'énergie, un système de condensateur électrique à double couche (EDLC) est introduit comme système de puissance de crête. Il est démontré que le système de stockage d'énergie hybride améliore la performance de puissance, la durée de vie de la batterie et l'efficacité énergétique du système de stockage vis-à-vis une batterie autonome. Cependant, l'ajout du système EDLC augmente considérablement le coût, le poids et le volume du système de stockage d'énergie, bloquant son introduction dans les voitures modernes.

Table of contents

List of figures

List of tables

List of Acronyms

AC	Alternating Current
ADVISOR	Advanced Vehicle Simulator
AER	All Electric Range
ANL	Argonne National Laboratory
BEV	Battery Electric Vehicle
CD	Charge Depleting
CS	Charge Sustaining
DC	Direct Current
DOE	Department of Energy
DoD	Depth of Discharge
EDLC	Electrical Double Layer Capacitor
EM	Electric Motor
EPA	Environmental Protection Agency
EPR	Equivalent Parallel Resistance
EPRI	Electric Power Research Institute
ESR	Equivalent Series Resistance
FTP-75	Federal Test Procedure driving cycle
HEV	Hybrid Electric Vehicle
HVAC	Heating, Ventilation and Air Conditioning
HWFET	Highway Fuel Economy Driving Schedule
GM	General Motors
ICE	Internal Combustion Engine
IEEE	Institute of Electrical and Electronics Engineers
IEA	International Energy Agency
LFP	Lithium iron phosphate
LMO	Lithium Manganese spinel oxide battery
LTO	Lithium Titanate oxide battery
MIT	Massachusetts Institute of Technology
NA	Not available
NCA	Lithium Nickel Cobalt Aluminium oxide battery
NEDC	New European Driving Cycle
NMC	Lithium Nickel Manganese Cobalt oxide battery
PHEV	Plug-in Hybrid Electric Vehicle
PMSM	Permanent Magnet Synchronous Motor
PPS	Peak Power Storage
PSAT	Powertrain System Analysis Toolkit
RESS	Rechargeable Energy Storage System
RMS	Root Mean Square
SEI	Solid Electrolyte Interface
SLI	Starter, Lightning and Ignition
SoC	State of Charge
SoH	State of Health
USABC	United States Advanced Battery Consortium
VSP	Vehicle Simulation Program

List of Symbols

A	EDLC cell surface	m^2
Acc	Distribution of the acceleration time of a drive cycle	-
AER	All Electric Range	km
A_f	Frontal area of the vehicle	m^2
BF	Brake factor	-
$C_{batt,ref}$	Reference capacity of the battery cell	Ah
C_{el}	Capacitance of an EDLC electrode	F
C_{EDLC}	Capacitance of an EDLC cell	F
$C_{EDLC,mod}$	Capacitance of the EDLC module	F
C_d	Drag coefficient of the vehicle	-
C_r	Rolling resistance coefficient	-
d	Helmoltz distance	m
E^0	Standard reduction potential	V
EPR	Equivalent Parallel Resistance	Ω
ESR	Equivalent Series Resistance	Ω
FE_{final}	Final fuel economy of the vehicle	l/100km
FE_{city}	Fuel economy of the vehicle during city driving	l/100km
FE_{hw}	Fuel economy of the vehicle during highway driving	l/100km
F_t	Tractive effort	N
F_g	Gradient resistance	N
F_r	Rolling resistance	N
F_w	Aerodynamic resistance	N
g	Gravitational constant	N/kg
I_{EDLC}	current through the EDLC system	A
I_{batt}	Battery current	A
$I_{batt,max}$	Maximum current through the battery system	A
$I_{batt,min}$	Minimum current through the battery system	A
$I_{batt,RMS}$	RMS current of the battery system	A
I_c	Battery current during charging	A
I_d	Battery current during discharging	A
i_g	Transmission ratio	-
Impr	Improvement factor	%
I_{ref}	Reference battery current	A
$I_{RMS,impr}$	Improvement factor of the battery RMS current	%
$I_{RMS,batt,s-a}$	RMS current of the stand alone battery system	A
$I_{RMS,batt,hybrid}$	RMS current of the battery in the hybrid RESS	A
M	Limitation factor for the EDLC power	-
m	Mass of the vehicle	kg
m_{batt}	Mass of one battery cell	kg
$m_{batt,module}$	Mass of the battery module	kg
m_{curb}	Curb weight of the vehicle	kg
$m_{EDLC,cell}$	Mass of one EDLC cell	kg
n	Peukert constant	-

$n_{EM,max}$	Maxiumum angular velocity of the electric motor	rpm
N_p	Number of EDLC cells connected in parallel	#
N_s	number of EDLC cells connected in series	#
P_{aux}	Auxiliary power demand	kW
P_{avg}	Average power demand of the vehicle	kW
P_{batt}	Power demand of the battery system	kW
P_{diss}	Dissipated power	kW
P_{EDLC}	Power demand of the EDLC system	kW
$P_{EDLC,lim}$	Limited power of the EDLC system	kW
PF	Penalty factor	-
P_{HVAC}	HVAC power demand	kW
$P_{max,batt}$	Maximum power of the battery	kW
$P_{n,EM}$	Estimated nominal power of the electric motor	kW
P_{ress}	Power demand of the RESS	kW
Q_c	Charge during charging of the battery system	C
Q_d	Charge during discharging of the battery system	C
R_{int}	Internal resistance of the battery	mΩ
r_w	Radius of the wheel	m
SoC_{batt}	State of Chargge of the battery system	%
SoC_{EDLC}	State of Charge of the EDLC system	%
SRF	System Regeneration Factor	%
t	Time	s
t_a	Acceleration time	s
t_c	Charging time	s
t_d	Discharging time	s
Te	Torque	N.m
$U_{batt,max}$	Maximum battery voltage	V
$U_{batt,min}$	Minimum battery voltage	V
U_{EDLC}	Voltage of the EDLC cell	V
$U_{EDLC,max}$	Maximum voltage of one EDLC cell	V
$U_{EDLC,mod}$	Voltage of the EDLC module	V
$U_{n,batt}$	Nominal voltage of the battery cell	V
$U_{n,EDLC,mod}$	Nominal voltage of the EDLC module	V
U_{oc}	Open circuit voltage of the battery system	V
U_c	Voltage during charging of the battery system	V
U_d	Voltage during discharging of the battery system	V
v	Velocity of the drive cycle	m/s
V_{batt}	Volume battery cell	cm^3
V_b	Base velocity of the electric motor	m/s
V_f	Final velocity of the vehicle	m/s
V_{max}	Maximum velocity of the drive cycle	m/s
VPE	Vehicle Propulsion Efficiency	%
VRE	Vehicle Regeneration Efficiency	%
W_{batt}	Energy content of one battery cell	Wh
$W_{batt,mod}$	Energy content of the battery module	kWh

W_{brake}	Braking energy	kWh
$W_{brake,max}$	Maximum braking energy	kWh
W_c	Energy demand during charging of the battery	kWh
W_d	Energy demand during discharging of the battery	kWh
$W_{DC\text{-}bus}$	Consumed energy at the DC-bus	kWh
W_{tot}	Energy consumption during the drive cycle	l
W_{EDLC}	Energy content of an EDLC cell	Wh
$W_{EDLC,max}$	Maximum energy content of the EDLC cell	Wh
$W_{EDLC,us}$	Usable energy content of one EDLC cell	Wh
w_i	Weighting factors for i=1,…,4	-
W_n	Normalised energy consumption	l/100 km
W_{diss}	Dissipated energy	Wh
W_{propel}	Energy required to propel the vehicle, measured at the wheels	kWh
$W_{source,propel}$	Energy required to propel the vehicle, measured at the energy sources	kWh
W_{reg}	Brake energy, measured at the wheels	kWh
$W_{source,reg}$	Brake energy stored in the energy sources	kWh
$W_{aux,reg}$	Brake energy used to power the auxiliary systems	kWh
α	Slope	°
δ_J	Rotational inertia coefficient	-
ΔSoC_{batt}	Operating window of the battery state of charge	%
$\Delta V_{DC\text{-}bus}$	Difference maximum and minimum DC-bus voltage	V
ε_0	Permittivity constant of vacuum	F/m
ε_r	Relative dielectric constant of insulating material	-
η_c	Coulomb efficiency	%
η_w	Energy efficiency	%
η_{impr}	Efficiency improvement factor	%
η_{hybrid}	Efficiency of the hybrid RESS	%
$\eta_{s\text{-}a}$	Efficiency of the battery stand-alone system	%
η_{trans}	Efficiency of the transmission	%
η_{RESS}	Efficiency of the RESS	%
ρ_{air}	Density of air	kg/m^3
τ	Time constant of the low pass filter	s
ω	1ngular velocity	rad/s

1 Introduction

1.1 Background

The automobile sector today faces big challenges. Increasing environmental concerns combined with the decreasing fossil fuel reserves and their increasing price cause interest in efficient and clean technologies in the transport sector. Currently, the transport sector is responsible for 31 % of all the energy consumption in the European Union [1]. The International Energy Agency (IEA) expects a worldwide increase in energy use and $C0_2$ emissions of the transport sector by 50% against 2030 and by 80% against 2050 [2].

In order to deal with these challenges, a lot of research is put in energy efficient systems and powertrains. Electrically propelled vehicles or hybrid electric vehicles are possible solutions with their advantages of a high efficiency electric motor, regenerative braking possibility and reduced dependence on finite oil resources. However, the limited range of Battery Electric Vehicles (BEV) still presents an important drawback. Transitional technologies like Hybrid Electric Vehicles (HEV) and Plug-in Hybrid Electric Vehicles (PHEV) are combining the conventional internal combustion engine (ICE) driven on fossil fuels with an electric motor (EM) fed by a battery system in order to obtain an efficient vehicle with an acceptable driving range. These technologies will play an important role in reducing the oil dependence and greenhouse gas emissions of the transport sector. To achieve the target of 50% less CO_2 emissions by 2050, the Blue Map Scenario presented by the IEA envisages an annual sale of about 50 million BEVs and 50 million PHEVs (see Figure 1) [3].

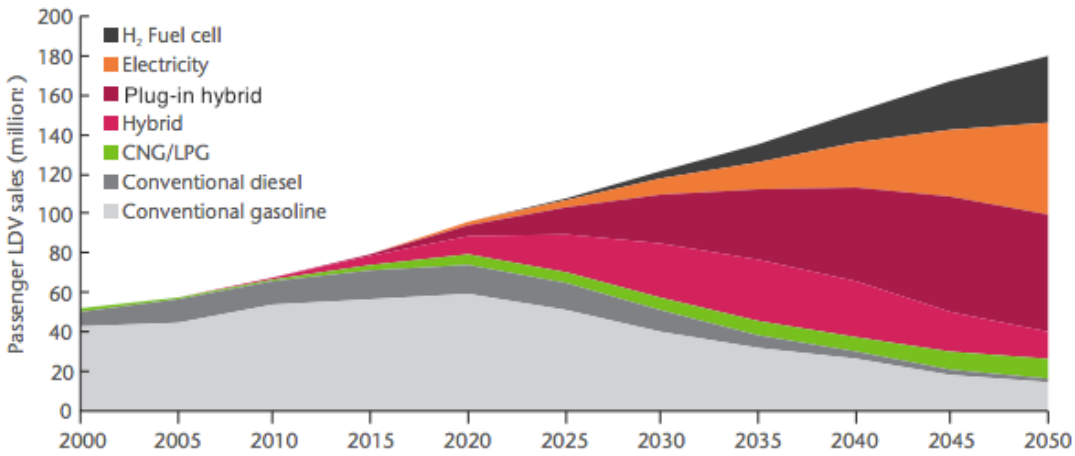

Figure 1: Evolution of vehicle propulsion technologies according to the Blue Map Scenario [3]

Battery Electric Vehicles such as the Nissan Leaf and Tesla Roadster are only powered by their battery system. To reach an acceptable driving range, the battery system must be optimized to store a high energy content.

Hybrid Electric Vehicles (Toyota Prius, Honda Insight, …) use a hybrid energy storage system containing two or more energy sources, for example an ICE fed by gasoline and an EM powered by a battery system. These energy sources are simultaneously working together to power the vehicle. While the ICE delivers the mean power, the rechargeable energy storage system (RESS) deals with the power peaks and is optimized for high power capacity.

Plug-in Hybrid Electric vehicles are something in between BEVs and HEVs. During their All Electric Range (AER), the vehicle is driven only with power coming from the RESS, just like a BEV. When the stored energy in the RESS becomes too low, the ICE will contribute together with the battery to power the vehicle, just like in an HEV. A PHEV combines the advantage of driving a certain distance purely electric – today typically 20 to 80 km –without the drawback of the limited range. PHEVs can also be charged from the grid like BEVs. The main challenges today for the PHEVs are the increased cost due to the extra components and the performances of the battery system. The Chevrolet Volt, with its European variant Opel Ampera, and the Plug-in version of the Toyota Prius are the most known PHEVs [4-6].

1.2 Thesis objectives

In this master thesis, the RESS of a PHEV is investigated more in detail. The major challenge of PHEVs is the performance and cost of the RESS. As explained in [7] and [8], different research organisations such as the United States Advanced Battery Consortium (USABC) and Electric Power Research Institute (EPRI) have proposed battery goals in terms of energy content, power capacity, cycle life, safety and cost. However, none of the currently existing battery technologies is able to meet these objectives.

The performance of the RESS can be improved by combining an energy-optimized lithium-ion battery with an Electrical Double Layer Capacitor (EDLC) system. In [9] and [10], EDLCs are presented as a promising technology to contribute during peak power demand and have a beneficial effect on the cycle life of the battery, energy efficiency of the drivetrain and driving range of the vehicle. Although the cost of an EDLC cell has decreased with 90% [9] during the last 10 years, the addition of a peak power unit introduces important extra challenges towards the cost, weight and volume of the RESS. Due to these reasons, the EDLC technology is preferably used in heavy transport applications such as buses [11], trams and metros [12] and not yet in passenger vehicles. However, different analyses of the performance of the hybrid battery-EDLC system are presented in literature for HEV [13-14] and BEV [9] applications. PHEVs however demand an RESS with both a high energy content and high power capability [15], leading to the research of the performance of the hybrid RESS in a Series PHEV in this master thesis.

In this master thesis, a model of a Series Plug-in Hybrid Electric Vehicle is made in MatLab/Simulink. The model is used to analyse the characteristics of the hybrid RESS and present a comparative study of the battery stand-alone system and hybrid RESS. The effect on the fuel consumption and driving range, power capability, energy and regenerative braking efficiency, cycle life and cost is examined.

1.3 Master thesis outline

This master thesis is divided into six chapters. In the *first chapter*, the context of this master thesis is drawn and the problem statement and objectives of the master thesis are highlighted.

In the *second chapter*, a literature review about PHEVs and the current RESS technologies is presented. The investigation of the RESS is concentrated on the energy sources of interest for this master thesis: a battery systems, EDLC system and the possibilities to connect both types. The review is completed with a summary of the most important RESS technological objectives. In order to compare these goals with the current status of the RESS of PHEVs, a non-exhaustive list of different commercial and prototype BEVs and PHEVs and their main specifications is presented.

In order to investigate the RESS, a simulation model is proposed in the *third chapter*. First, a summary of the existing modelling techniques and most important modelling programmes for vehicular applications is presented. Then, the exact modelling technique of each component and the control strategy used in the proposed simulation are explained.

Chapter four handles the dimensioning of the components. The model is based on the Chevrolet Volt, as it is currently the most popular PHEV. This means that the design parameters (curb weight, drag coefficient, rolling resistance coefficient…) of the Chevrolet Volt are used in this simulation in order to simulate the behaviour of the car. Starting from this basic case, the different components are all independently modelled and dimensioned. The sizing methodology is highlighted for the different RESS parts.

The results of the proposed model are shown in *chapter five*. The model is first validated by comparing its fuel consumption with the official fuel economy ratings of the Chevrolet Volt 2011. The behaviour of the hybrid RESS is optimized by defining the best time constant of the filter used to control the power flows. A comparison is made between the battery stand-alone system and hybrid RESS, with emphasizing the five most important RESS parameters: energy content, power capability, lifetime, efficiency and cost.

The conclusions and future work of this master thesis are presented in *chapter six*.

2 State-of-the-Art

2.1 Hybrid Topologies

In order to overcome the problem of range for Battery Electric Vehicles (BEVs), Hybrid Electric Vehicles (HEVs) combine two or more energy sources to power the vehicle simultaneously. In most cases, an internal combustion engine (ICE) fed by fossil fuels and an electric motor (EM) powered by a battery are used. There exist different topologies to combine the used components. Three main extinctions can be made: series HEV parallel HEV and combined series-parallel HEV.

2.1.1 Series HEV

The Series HEV is characterised by a series coupling of the energy sources. The ICE is connected to a generator that transforms the mechanical energy into electrical energy. The electric energy arrives at the DC bus, where it can be used to power to the electric motor or the battery. In the series PHEV, all the traction power is delivered by the electric motor and there is no mechanical contact between the ICE and the wheels. This allows decoupling ICE of the wheels and running it constantly in its most efficient region. However, the total efficiency of the driveline suffers by the extra energy conversion. Series HEVs are mostly used for heavy applications like buses or in urban vehicles that have to start and stop often.

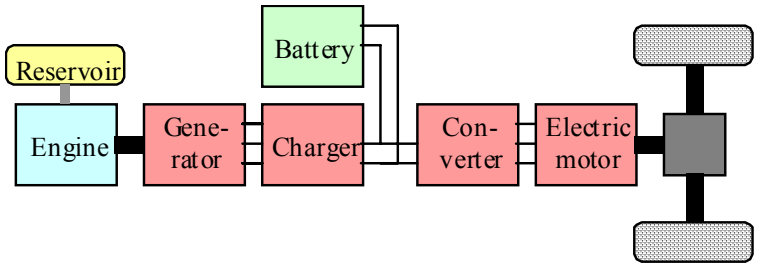

Figure 2: Series HEV Topology [16]

2.1.2 Parallel HEV

In a Parallel HEV, the power flow to the wheels happens in parallel, meaning that both the ICE and the EM can perform traction. They are coupled through a gearbox to one shaft that drives the wheels and clutches can be used to disconnect each motor. The parallel HEV topology has the advantage that the operating engine can be chosen in function of the driving behaviour. The EM will drive the vehicle during situations where the ICE is least efficient, thus at low loads and during starting while the ICE will deliver power at high speeds. The Honda Insight is an example of a commercial hybrid car with the parallel topology.

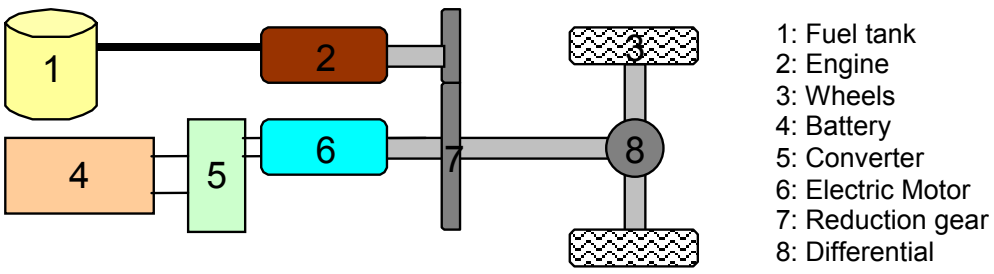

Figure 3: Parallel HEV Topology [16]

2.1.3 Combined HEV

Combined HEVs use the advantages of both the series and the parallel hybrid topologies:

- It is possible to generate electricity with the ICE at maximum efficiency (series);
- It is possible to only drive purely electric/ only with the ICE/ using both (parallel).

As Figure 4 shows, the configuration now becomes more complex and one has to make use of a power split device. This practically means a planetary gear, where the sun represents the generator, the planets the ICE and the ring the EM during driving and the wheels during deceleration. The Toyota Prius is the most known example of a HEV with combined series-parallel drivetrain [5,6,16-18].

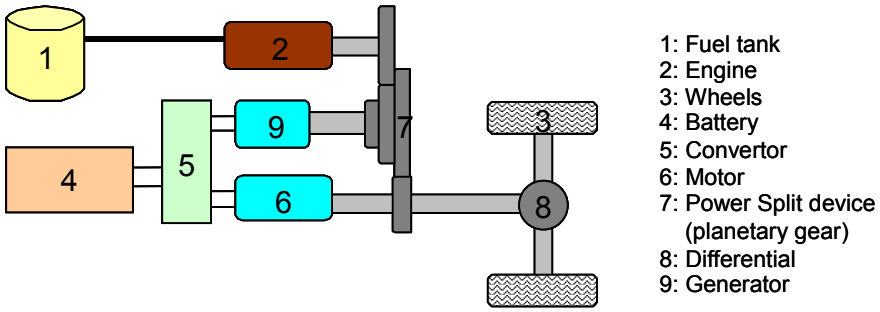

Figure 4: Combined HEV Topology [16]

As explained above, each topology has its own advantages and drawbacks. However, aside from the architecture of the drivetrain, the power management strategy also has a huge impact on the driving comfort and system efficiency. The power management strategy brings the components together by deciding which power source operates under which conditions [6,16].

2.2 Plug-in Hybrid Electric Vehicles

As explained above, Plug-in Hybrid Electric Vehicles combine the main benefit of BEVs (driving purely electric) with that of HEVs (no range limitation).

PHEVs can be driven in two different modes depending on the State of Charge (SoC) of the battery system: Charge Depleting (CD) and Charge Sustaining (CS). During CD, the battery is delivering the main power to move the vehicle, causing a decrease in SoC of the battery system. A further distinction can be made between *all electric* and *blended* mode. In the first mode, the ICE will not deliver any contribution to power the vehicle, exactly like with BEVs, while the ICE does contribute in the blended mode. During CS, the average SoC will be constant and the battery handles the power peaks while the ICE delivers the mean power. The main advantage of a PHEV is that they are able to run in both CD and CS, while a BEV and HEV respectively only support CD and CS (see Figure 5) [7,19].

PHEVs are usually described according to their CD range: PHEV – x, where x denotes the distance that can be driven in CD mode (in km or in miles). This description however does not make any distinction between AER or blended, nor does it specify the driving conditions under which the proposed distance can be attained.

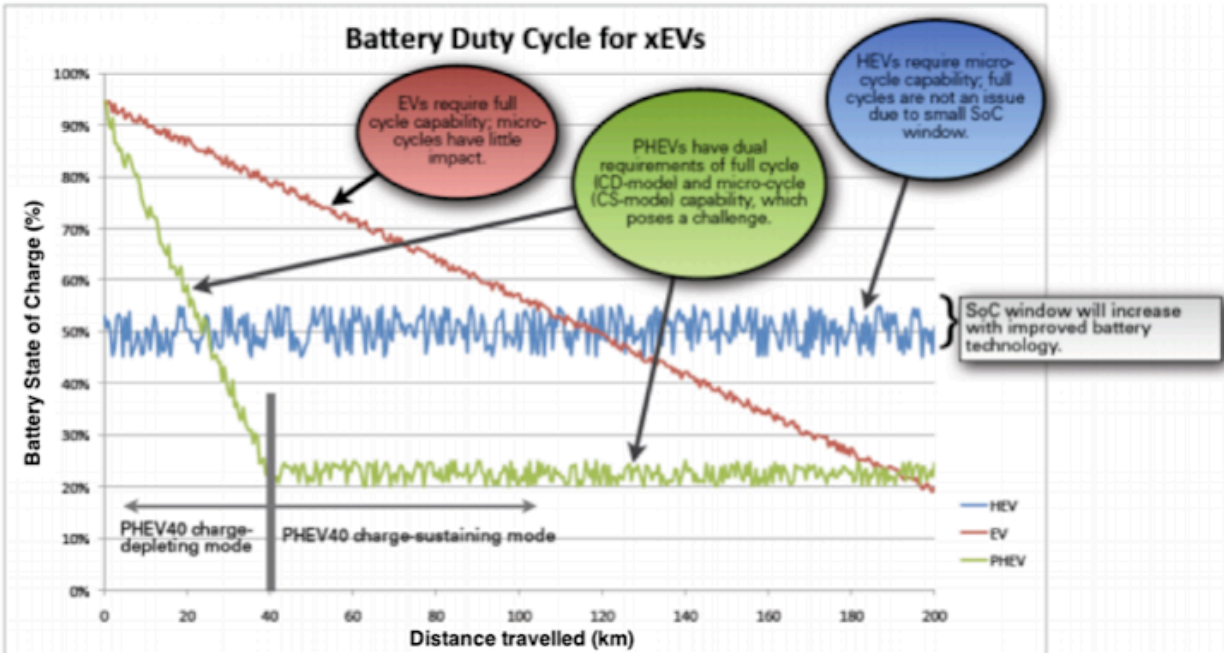

Figure 5: Charge Depleting and Charge Sustaining driving mode [19]

2.2.1 Advantages:

- *Runs in CD and CS:* the main advantage of the PHEV is its ability to drive in both CD and CS mode. Thanks to this feature, a PHEV is able to drive with the benefits of a BEV (high efficiency, no pollution, charging at home) without its range limitations. A typical BEV is able to drive 150 km, while this range can be extended to more than 500 km for PHEVs [5].
- *Environmental benefits:* with their typical AER between 20 and 80 km, PHEVs have the possibility to satisfy a significant share of the daily drives in all electric mode. The IEA reports that 50% of the trips in Europe are less than 10 km and 80% are less than 25 km [3]. During driving in all electric mode, no pollution is emitted during driving, benefitting the local air quality (no particle matter, carbon monoxide or volatile organic compounds) and a reduction of noise [6].
- *Operating cost*: fuel cost can be reduced because of the low price of electricity compared with oil. Based on data of the US Department of Energy, running a conventional car for 100 miles costs $13.3 while the same distance costs $7.10 for its PHEV equivalent [20].
- *Vehicle to grid:* the electrification of the transport sector opens the possibility to couple an electric vehicle to the grid. By integrating vehicles with the electricity grid, the energy stored in the vehicle can play a role in the balancing of the power system [21].

2.2.2 Disadvantages:

- *Performance RESS:* The main challenge for PHEV is to develop a RESS that is able to satisfy the costumer's requirements. Although different battery technologies already exist today, none of them is already able to meet the industrial requirements set by the US Advanced Battery Consortium in terms of power and energy density, calendar life, safety and cost.
- *Higher initial cost:* The initial cost of a PHEV is higher than for a conventional car because of the extra components of the hybrid drivetrain. According to reference [2], the cost for the manufacturer of a PHEV-40 is expected to be about $14000 to $18000 more, where the largest share is the battery pack with $10000 to $14000.

2.3 Rechargeable Energy storage systems

The Rechargeable Energy Storage system (RESS) is one of the most important components of PHEV. The energy system must combine the energy and power requirements of the vehicle together with a large lifetime, safety requirements and a low cost. The RESS in currently existing electrically propelled vehicles exists out of a battery system.

2.3.1 Batteries

For vehicular applications, secondary or rechargeable batteries are used. During discharging of the battery, an electric circuit arises by connecting the electrochemical cell with a load: electrons are flowing from the anode (which is oxidized) through the load to the cathode, where they are accepted and the cathode material is reduced. The electric circuit closes by the movement of anions and cations through the electrolyte. During charging, the current flows in the opposite direction by implementing a voltage difference over the electrochemical cell [22,23].

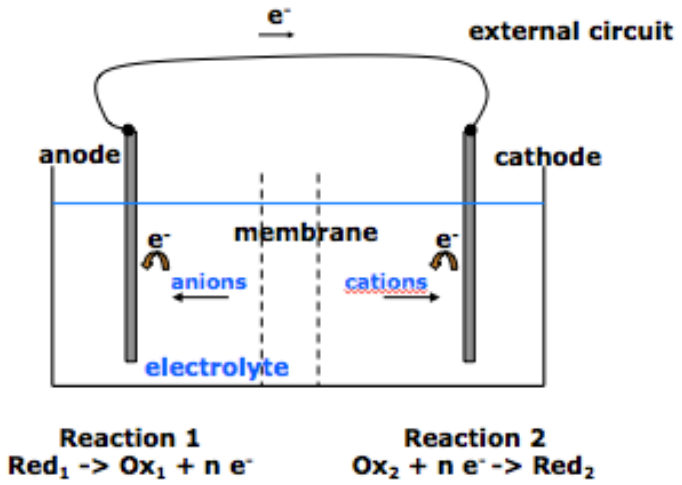

Figure 6: Discharging mechanism of an electrochemical cell [22]

The parameters that are important for battery performances in PHEV are lifetime, power capacity, energy content, battery efficiency and cost. The *lifetime* reports the ageing of the battery due to side reactions. It can be defined as the calendar life and cycle life, respectively representing the amount of years and the amount of charging and discharging cycles possible before the battery loses its ability to hold a certain charge level, typically 80% of its initial charge [24]. Important for the cycle life is the depth of discharge (DoD)[1]. *Battery efficiency* represents the battery losses during charging and discharging. *Specific energy* denotes the energy content of the battery, expressed in Wh/kg. The energy content determines the range of the PHEV in all electric mode. *Specific power* (W/kg) describes the maximum power that can be drawn from the battery and determines the acceleration performance of the vehicle. Other important characteristics for PHEVs are the operating temperature, the charging rate, the volume and weight. Battery design inherently incorporates trade offs between these characteristics: optimizing one characteristic always has a negative impact on another one. For example, a battery can be designed for optimal energy density or for high power density by changing the shape of the electrodes: high power electrodes are very thin in order to make fast intercalation possible, while high energy electrodes need to be thick to store a lot of ions [7,23,25].

[1] The difference between the maximum and minimum SoC of a battery during operation

During history, different battery technologies have been designed and used for vehicular applications. The Ragone chart (Figure 7) shows these technologies, emphasizing their energy and power capabilities. It clearly shows that Lithium ion batteries is the most performant technology due to their high energy content and power capabilities. An overview of the most important battery technologies is presented below.

2.3.1.1 Lead acid batteries

The lead battery is the oldest and best-known type of battery. It has been used traditionally as SLI battery (starter, lightning, ignition) in conventional cars with the main advantage of being a cheap and mature technology. It however faces important limitations for electrical vehicles: low energy density (30 Wh/kg), power density (70-200 W/kg) and restricted lifetime [6,7,25].

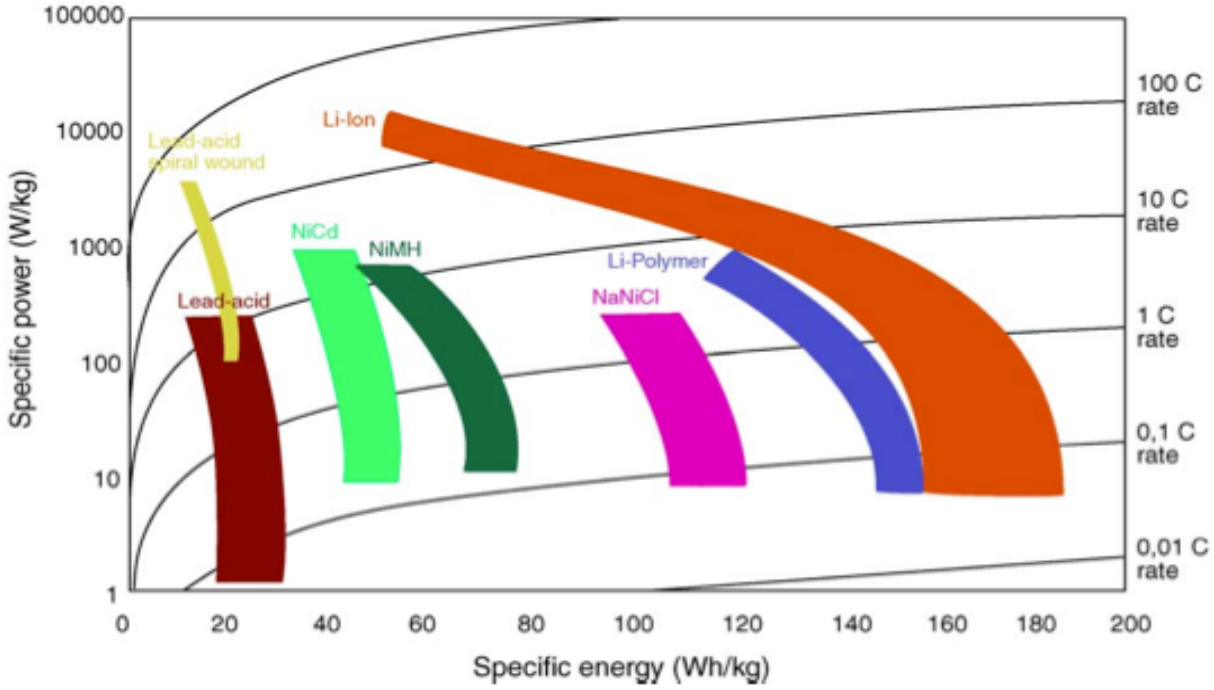

Figure 7: Ragone chart [25]

2.3.1.2 Nickel metal hydride batteries

Nickel Cadmium batteries (NiCd) have a much higher specific energy content (50 Wh/kg) than the lead acid batteries. Its favourable power performances and cycle life allowed its introduction in some BEVs (eg. Renault Clio RT, Peugeot 106 Electric), but the European Commission banned NiCd batteries from vehicular and consumer applications in 2006 due to the toxic nature of Cadmium. They also suffer from the memory effect[2] [6,7,25].

The improved version of the NiCd battery is the Nickel metal hydride battery (NiMH). It has comparable performances but uses a special alloy instead of the toxic Cadmium. The NiMH battery has found its application in early BEVs (e.g. GM EV1) and in most HEVs (Toyota Prius, Honda Civic). Their low nominal voltage (1,2V) and low energy efficiency (60-80%) are the main drawbacks of NiMH batteries. No significant new technological improvements or cost reductions are expected in the future [7,15,19,25].

[2] The battery looses its maximum energy capacity if it is recharged after being only partially discharged.

2.3.1.3 High temperature batteries

High temperature batteries as the sodium-nickel-chloride battery (Zebra battery) use molten electrodes and operate at high temperatures (around 300°C). They have a very high specific energy up to 100 Wh/kg. The battery however has to be heated during periods that it is not used, making this type of batteries more suitable for intensively used fleet vehicles [6,7,25].

Table 1: Characteristics of different energy storage types [25]

	Lead acid	NiMH	Zebra	Li-ion	EDLC
Cell voltage (V)	2	1,2	2 – 2,5	3,3 – 3,7	2,7
Energy density (Wh/kg)	30-35	50-80	90-130	80-170	5
Power density (W/kg)	70-200	175-700	100-160	400-2500	6000
Energy efficiency (%)	80-85	60-80	80-90	85-95	92
Cycle life (cycles)	300-1000	1500-2000	600-1000	>1000	1.000.000
Cost (€/kWh)	100-200	400-500	150-400	300-800	6000-12000

2.3.1.4 Lithium ion batteries

Lithium ion batteries are the most promising battery technology. As can be seen on Figure 7, their high energy and power density in comparison with the other battery types makes the lithium ion battery the most appropriate technology. Their low standard reduction potential (E^0 = -3,04V) makes lithium an attractive negative electrode to get a high cell voltage. This potential combined with their low equivalent weigh (M = 6,94 g/mol) results in a very high specific energy cell. However, the high reactivity of lithium also has drawbacks in terms of safety and the cost is currently high in comparison with the other RESS technologies [15,23].

Rechargeable lithium ion batteries do not have the same mechanism as the traditional redox reaction batteries. The lithium ions transport their charge according to the intercalation process. The intercalation process is characterised by an insertion of an atom or molecule into a host structure without changing its structure. During discharge, the lithium ions are extracted out of the anode material (see Figure 8). They migrate through the electrolyte into the crystal lattice of the cathode, without changing its structure. During charging, the same reaction occurs in the opposite direction [7,19,22,25-27].

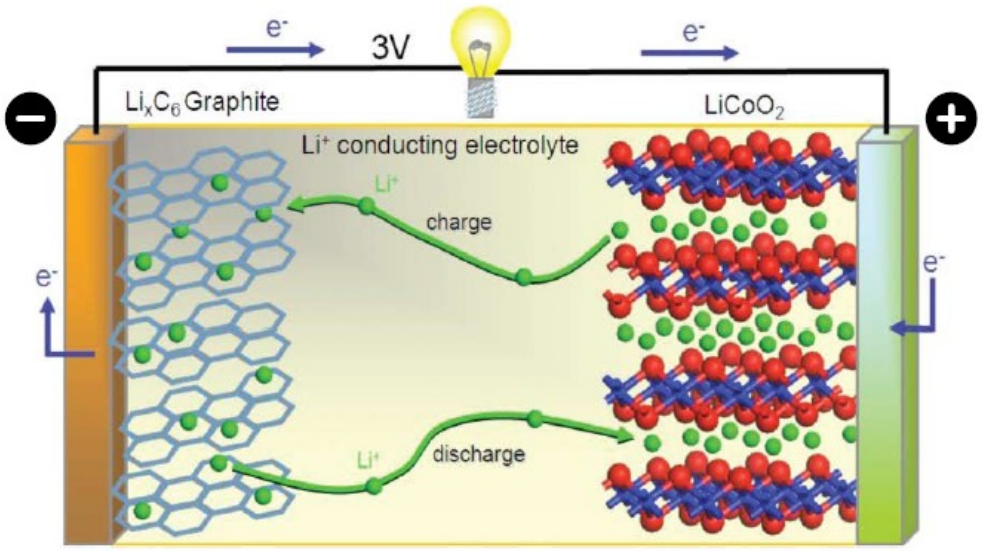

Figure 8: Charging and discharging mechanism of lithium ion batteries [27]

Rechargeable lithium-ion batteries encompass a variety of technologies based on the materials that are used as anode, cathode and electrolyte. The electrolyte is a liquid (or polymer/liquid), mostly a lithium salt dissolved in organic solvents that conduct ions (for example Lithium hexafluorophosphate ($LiPF_6$) or Lithium tetrafluoroborate ($LiBF_4$)) [23,28]. Most of the chemistries use graphite anodes, making it possible to name the battery type to the chosen cathode material. According to a report of the Boston Consulting Group, the lithium ion battery technologies that can play an important role in PHEV applications are [29]:

- Lithium nickel cobalt aluminium oxide (NCA);
- Lithium iron phosphate (LFP);
- Lithium nickel manganese cobalt oxide (NCM);
- Lithium manganese spinel oxide (LMO);
- Lithium titanate oxide (LTO).

Historically, the lithium cobalt oxide or LCO ($LiCoO_2$) battery has gained a superior position in portable applications such as laptops and cell phones. Although also the Tesla Roadster uses a LC0 battery system, their lifetime, cost and thermal stability make them not appropriate for the automobile industry. The *lithium nickel cobalt aluminium oxide* or *NCA* ($LiNi_{0,85}Co_{0,15}Al_{0,05}O_2$) electrode is less sensitive to the dissolution of Cobalt, which reduces electrode capacity, and the formation of the CoO_2 layer that reduces the cathode surface. NCA has a very high energy and power density but still faces limitations in terms of thermal stability: at higher temperatures, oxygen can be released which can react with the electrolyte and result in a thermal runaway[3].

Using *lithium iron phosphate* ($LiFePO_4$) cathodes inherently results in a higher thermal stability. It has a lower cell potential than the NCA battery, what reduces the oxidation of the electrolyte and causes more stability. This lower cell voltage however also has a downside in the form of a lower energy content. LFP does not use any toxic cobalt oxide and is cheaper due to the larger availability of the raw materials. The BYD F3DM and Fisker Karma use an LFP battery.

Lithium manganese spinel oxide (LMO) ($LiMnO_4$) can also be used as a cathode material. Thanks to its spinel crystal structure, the ion flow on the electrode is improved what results in a lower internal resistance and fast charging and discharging. When fully charged, it has only little excess of lithium ions providing only very little undesirable lithium metal deposition on the negative electrode in overcharge. But the dissolution of manganese in the electrode can poison the graphite electrode and reduce the lifetime of the battery.

A *lithium nickel manganese cobalt oxide* or *NCM* ($LiNi_{0,33}Co_{0,33}Mn_{0,33}O_2$) battery has good storage capacity at higher voltages, but has drawbacks in terms of lifetime and safety because the NCM electrode doesn't form a stable couple with the graphite electrode. Graphite based anodes are sensitive to the formation of the solid-electrolyte interface (SEI) layer. This is a protective layer formed at the interface of the electrode with the electrolyte during the first time that the battery is charged. The SEI layer prevents continued, uncontrolled reaction of lithium with the electrolyte and acts as a protective layer, but goes hand in hand with a smaller electrode capacity. Like with the LMO battery, the dissolution of manganese reduces the lifetime.

[3] Positive loop where an increase in temperature results in a higher reaction rate and more heat release.

To avoid this, titanium oxide can be chosen as negative electrode. *Lithium titanate (LTO)* batteries make use of an anode based on nano particles of $Li_4Ti_5O_{12}$. The LTO cathode has a lower capacity (180 mAh/g) than the graphite one (360 mAh/g) and the cell voltage decreases (2,4V versus 3,6V for NCA) causing a lower specific energy. However, the high safety and cycle life are advantages that can make up for the lower energy density [15,23,28-36].

The research and development for new chemistries in lithium ion batteries is a continuously evolving process. However, new chemistries need time to reach the market and first reach the electronics market due to the smaller battery sizes. As no new chemistries are yet available in consumer applications today and no new breakthroughs are reported in literature, it is reasonable to assume that only a gradual improvement in performance of the existing lithium-ion technologies can be expected up to 2020. Lithium sulphur and lithium air batteries show great potential to deliver much higher specific energy, but still face big challenges [23,29,31].

Table 2: Comparison of different Lithium ion technologies [30]

	Chemistry: Neg/pos electrode	Cell voltage (max/nom)	Capacity (mAh/g) Anode/cathode	Energy density Wh/kg	Cycle life (deep)	Thermal stability
NCM	Graphite / $NiCoMnO_2$	4,2 / 3,6	360 / 180	100 - 170	2000-3000	Fairly stable
LMO	Graphite / Mn spinel	4,0 / 3,6	360 / 110	100 - 120	1000	Fairly stable
NCA	Graphite / $NiCoAl0_2$	4,2 / 3,6	360 / 180	100 - 150	2000-3000	Least stable
LFP	Graphite / Iron phospate	3,65 / 3,25	360 / 160	90 - 115	> 3000	Stable
LTO	Lithium titanate/ Mn spinel	2,8 / 2,4	180 / 110	60 - 75	> 5000	Most stable

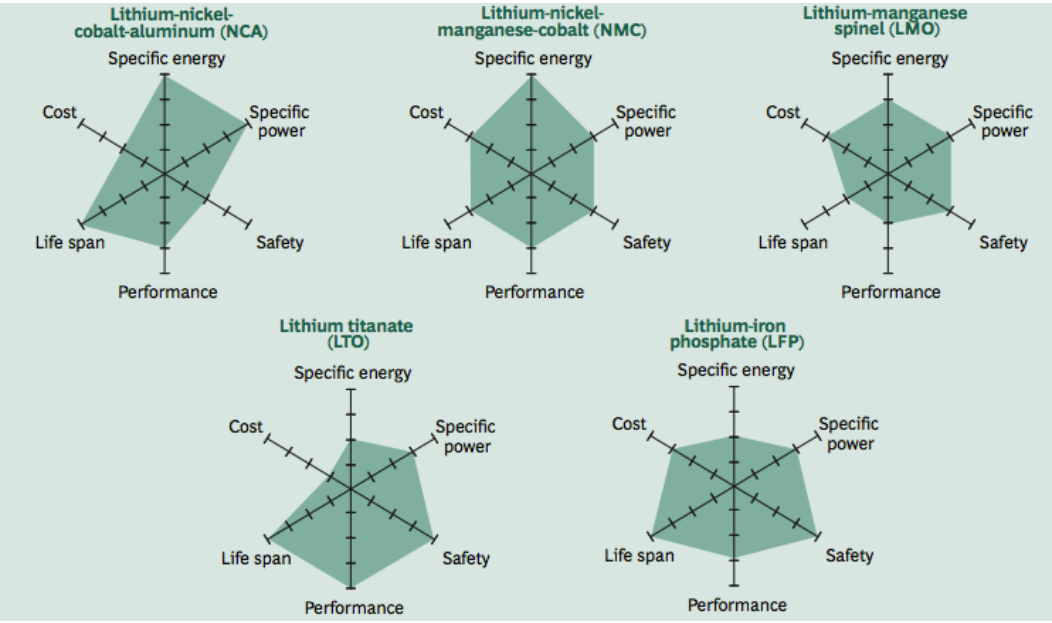

Figure 9: Comparison lithium ion technologies [29]

2.3.2 Electric double-layer capacitors

Since the beginning of the 1990, the Electrical Double Layer Capacitor (EDLC) – also known as supercapacitor or ultracapacitor - has been introduced as a RESS technology for high power applications. EDLCs are characterised by a low energy density and high power capacity and can play an important role in vehicular applications to overcome the limited power performance of energy-optimized batteries. Especially PHEVs need both a high energy density and high power capability to respectively allow an adequate driving range and acceleration performance.

The outlook of an EDLC cell is shown in Figure 10. By applying a voltage over the electrodes, each electrode will attract ions with the opposite charge to satisfy the principle of electro-neutrality. The accumulation of ions around the electrode generates a double layer that stores their charge electrostatically like a conventional capacitor. Important to notice is that there is no charge transfer taking place at the electrode - electrolyte interface, as in the case of redox batteries or lithium-ion batteries (intercalation). The process taking place in the EDLC is non-faradaic and the appearing current is a displacement current needed to rearrange the charges around the electrodes. The non-faradaic mechanism allows EDLC cells to reach a lifetime of 15 years (1 million cycles) and to have a very low internal resistance and high efficiency (95-98%). Their main drawbacks are their limited energy content and high cost [9,10,22,28,37].

The typical capacitance of one electrode is

$$C_{el} = \varepsilon_0 . \varepsilon_r . \frac{A}{d} \tag{2.1}$$

where

C_{el} = capacitance of the electrode (F);
ε_0 = permittivity constant of vacuum (F/m);
ε_r = relative dielectric constant of the insulating material between the plates (-);
A = EDLC cell surface area (m^2) ;
d = Helmholtz distance (m).

By using carbon electrodes, one can obtain a very large surface area A ($1000 m^2/g$). Combined with a small distance d (practically 5-10Å), the final capacitance of an EDLC is much higher than for conventional capacitors. A typical capacitance of a carbon-based electrode is about 100F/g [7]. One should remark that the double layer appears at both the electrodes, creating a cell that corresponds to two capacitors in series. The total capacitance becomes:

$$C_{EDLC} = \left(\frac{1}{C_{el1}} + \frac{1}{C_{el2}} \right)^{-1} \tag{2.2}$$

The energy that can be stored in an EDLC cell is

$$W_{EDLC} = \frac{C_{EDLC} * {U_{EDLC}}^2}{2} \tag{2.3}$$

where

W_{EDLC} = stored energy (J);
C_{EDLC} = capacitance of the EDLC cell (F);
U_{EDLC} = voltage difference over the EDLC cell (V).

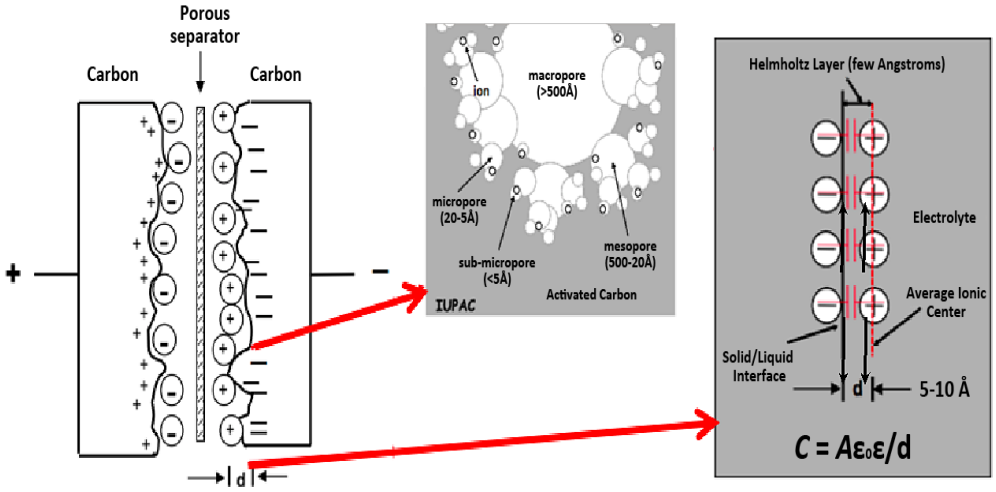

Figure 10: Mechanism of EDLC [23]

Typically, an EDLC cell is able to store 5 Wh/kg. Relation 2.3 shows the link between voltage difference and stored energy in the EDLC cell. In order to stay in a safe operating region and have an efficient energy transfer, the voltage of an EDLC system is only allowed to vary between 50% and 100% of its maximum voltage, meaning that only 75% of the energy of an EDLC cell can be used.

The limited energy density of an EDLC cell can be improved by using pseudo-capacitors. A pseudo-capacitor is a device where the ions in the double layer combine with the atoms on the surface of the electrode. They use one carbon based electrode and one battery-like electrode. The Faradaic electrode is chosen out of the family of Lithium-ion chemistries to enlarge the voltage range of the pseudo-capacitor, resulting in an increased energy density. The significantly higher specific energy has a trade off in lower power density and reduced cycle and calendar life [4,7,10,38].

2.3.3 Hybrid RESS

The RESS of a PHEV must have a high energy and high power density in order to meet the costumer's demand in terms of driving range and accelerations. To meet these requirements, EDLCs can be combined with an energy optimized battery system. In this hybrid RESS, the battery system delivers the average power demand while the peak power comes from the EDLC system. Using a hybrid RESS has proven to extend the lifetime of the battery, its efficiency and limits the temperature rising in the battery due to the averaging of the power drawn from the battery system [9,39,40].

In Figure 11, the different hybrid architectures are shown. In *topology A*, both the battery and EDLC system are directly connected to the DC-bus. The direct connection however imposes the EDLC size, since the terminal voltage of both sources cannot be different. Moreover, the current distribution between the EDLC system and battery is completely defined by their internal resistances. This means that the power flows in the RESS cannot be controlled.

The addition of a DC/DC converter in between an energy source and the DC-bus allows regulating the output voltage and current of the energy source, thus allows controlling and optimizing the energy exchange between the sources. In *topology B,* two bidirectional DC/DC converters are used to connect the energy sources with the DC-bus in order to control the DC-

bus voltage in all situations. The improved DC-bus voltage stability however doesn't compensate for the cost and extra losses in the two DC/DC converters. *Topology C* only uses one DC/DC converter, in between the battery system and the DC-bus. It allows controlling the DC bus voltage in function of the EDLC system's voltage, which is subjected to large variations because of the relation between the stored energy in an EDLC and its voltage (equation 2.3).

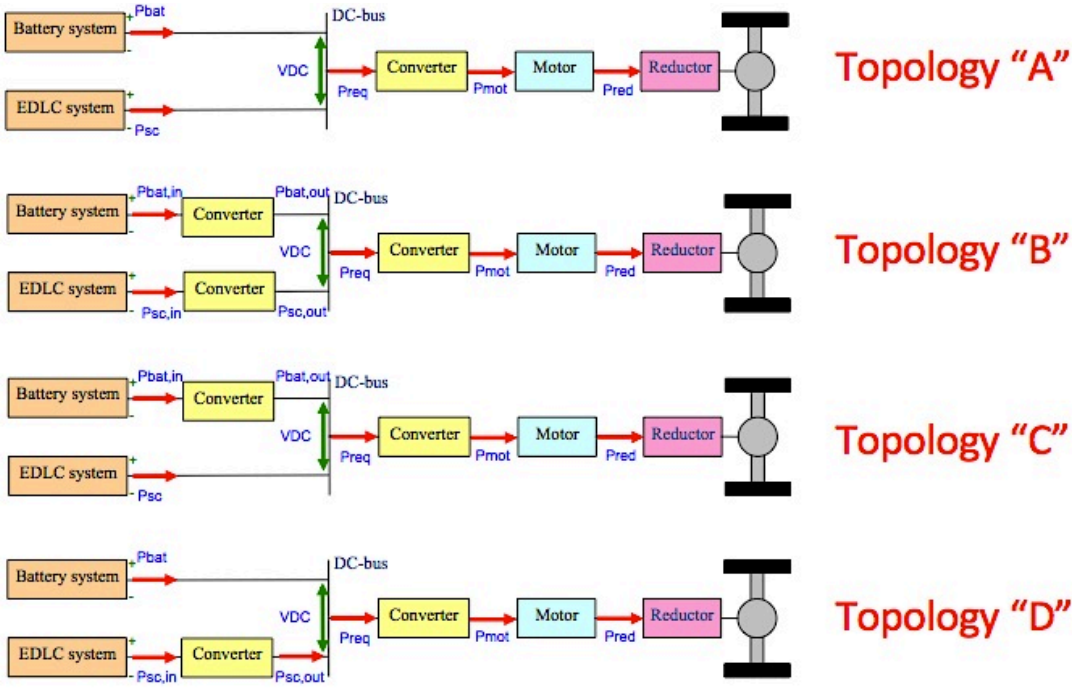

Figure 11: Hybrid RESS topologies [9]

The preferred solution is *topology D*, where the EDLC system is connected to the DC-bus through a bidirectional DC/DC converter. The converter allows controlling the EDLC system's voltage in function of the DC-bus voltage, which is imposed by the battery system and shows much smaller variations. The benefit of controlling the power flows in the RESS at a minimum cost (only using one converter) and with a relatively stable DC-bus voltage justifies the choice to use topology D in this master thesis [9,41].

2.4 Current status of PHEV

For commercial PHEV design, the RESS' requirements are high power and energy content, high energy efficiency, long lifetime, safe operation and cost. These requirements are different for every PHEV, depending on its CD driving mode (all electric or blended), on the assumed drive cycle, vehicle weight etcetera. In literature, different goals and targets are proposed for the battery characteristics. An overview of the most influential goals is presented in Table 3.

The United States Advanced Battery Consortium (USABC) proposes RESS requirements for two PHEVs with a different AER: a power optimized PHEV-10 mile and energy optimized PHEV-40 mile. Both PHEVs are assumed to drive in all electric mode. The PHEV-10 goal focuses more on high power capacity, while the higher energy content has its trade-off in the form of lower power performances in the PHEV-40. USABC uses the Urban Dynamometer Driving Schedule (UDDS), a driving cycle that represents typical city driving behaviour, to define their battery requirements.

The Electric Power Research Institute (EPRI) requirements consider a PHEV-20 and PHEV-60 in all electric driving mode. They are less ambitious in terms of energy and power density due to the higher proposed battery mass. EPRI takes a Depth of Discharge (DoD) of 80% into account, while the other goals are based on 70% DoD. Aside from the UDDS, EPRI also uses the Federal Highway Schedule driving cycle (HWFET) to take highway driving behaviour into account. The Sloan Automotive Laboratory at Massachusetts Institute of Technology (MIT) proposes requirements for the RESS of a PHEV-30 sedan. MIT bases its battery targets on the UDDS, HWFET and US06 driving cycles. The last one is a more aggressive driving cycle with longer accelerations and higher top speed. The CD driving mode is blended, what makes it possible to design the battery for better power performances.

Table 3: RESS industrial requirements and goals [15]

	Units	USABC		MIT	EPRI	
Vehicle Assumptions						
CD Range	miles	10	40	30	20	60
CD Operation	-	AE	AE	blended	AE	AE
Body Type	-	SUV	Mid car	Mid car	Mid car	Mid car
Total Battery Mass	kg	60	120	60	159	302
Total Vehicle Mass	kg	1950	1600	1350	1664	1782
Battery Goals						
Peak Power	kW	50	46	44	54	99
Energy Capacity	kWh	6	17	8	6	18
Calender Life	years	15	15	15	10	10
CD Cycle Life	cycles	5000	5000	2500	2400	1400
CS cycle Life	cycles	300000	300000	175000	<200000	<200000

EPRI and MIT both provide actual requirements for current batteries, while the proposed battery characteristics of USABC are more ambitious and can be seen as goals rather than as requirements. There is no battery able to meet all the specified requirements of USABC yet. However, Axsen et al make in [8] the consideration that these goals are too ambitious, certainly in comparison with the costumer's demands [7,8,15,42].

In Table 4, a non-exhaustive list of PHEVs and some BEVs (Tesla Roadster, Mitsubishi iMiev and Nissan Leaf) is shown together with their main characteristics. The major difference between the BEVs and PHEVs is found in the energy content of the battery. BEVs need a larger energy content in order to obtain a reasonable range, while PHEVs rely on the ICE to extend their range. One can observe that the modern batteries are all of the lithium-ion family. Another remark is that a PHEV is a very young technology, with the first commercial car – the BYD 3FDM - only released in 2008 by the Chinese manufacturer BYD, although the sale of the BYD 3FDM to the general public only began in March 2010 in China and in 2011 in the USA [43]. The Chevrolet Volt (with the Opel Ampera variant in Europe) is currently the most successful PHEV. The wide variation in specific energy of the RESS can partly be explained by the chosen driving mode: the Chevrolet Volt runs in all electric mode during CD, asking more energy than for example the Toyota Prius that runs in blended mode.

Table 4: List of commercial PHEVs [5,44-56]

Car		Price ($)	Release date	Range (km): AER/full	Battery type	Energy content (kWh)	Power (kW)
Cars on the market							
Tesla	Roadster	109 000	Feb-08	394	Li-ion / LCO	56	225
BYD	F3DM	21 900	Dec-08	100 / 483	Li-ion / LFP	16	50
Mitsubishi	iMiev	29 125	Jul-09	100	Li-ion / LMS	16	49
Nissan	Leaf	35 200	Dec-10	118	Li-ion / LMS	24	80
Chevrolet	Volt	39 145	Dec-10	56 / 604	Li-ion / LMS	16	111
Fisker	Karma	102 000	Jul-11	80 / 483	Li-ion / LFP	20,1	240
Toyota	Prius PHEV	32 000	Jan-12	18 / 870	Li-ion / NCA	4,4	60
Ford	C-max Energi	33 745	Oct-12	34 / 885	Li-ion / NA[1]	7,6	68
Cars coming on the market							
Volvo	V60 Plug-In Hybrid	81 000	Nov-12	51 / 901	Li-ion / NA	12	50
Honda	Accord Plug-in Hybrid	39 780	Jan-13	21 / 805	Li-ion / NA	7,6	124
Ford	Fusion Energi	39 495	2013	34 / NA	Li-ion / NA	NA	NA
Suzuki	Swift Plug-in	24 900	2013	30 / NA	Li-ion / NA	2,66	55
Porsche	918 Spyder	845 000	Dec-13	25 / NA	Li-ion / NA	6,8	200
BMW	i8	NA	2013	35 / 700	Li-ion / NA	7,2	96
Audi	A1 e-tron	NA	NA	50 / 249	Li-ion / NA	12	45
Volkswagen	Golf Variant Twin Drive	NA	NA	57 / 900	Li-ion / NA	11,2	85
Mercedes Benz	Blue ZERO E-cell Plus	NA	NA	100 / 600	Li-ion / NA	18	70
Lotus	Evora 414E hybrid	NA	NA	48 / 483	Li-Polymer	17	304

[1]: NA = Not available

3 Modelling

3.1 Introduction

The investigation of hybrid vehicles and their performances is a complex task. To efficiently design, analyse and evaluate a (hybrid) vehicle, modelling and simulation tools are indispensable. Simulations allow gaining a clear view on the performances, efficiency, consumption and etcetera without the expensive and time-consuming process of prototyping. Regarding the modelling of Plug-In Hybrid Electric Vehicles (PHEVs), different approaches can be found in literature. The simulation techniques vary in their degree of detail of the used (sub)model and in the direction of calculation of the power.

Apart from the chosen model, two different modelling techniques do exist depending on the direction of the calculation. The *forward approach* or cause-effect method, computes the power starting from the energy source to the wheels, according to the physical direction of the power flow. The *backward approach* or effect-cause method calculates the power in the reverse direction, opposite to the physical direction of the traction power.

The *backward* simulation technique starts with a driving cycle that defines the velocity profile. The required traction effort at the wheels is obtained by computing the required acceleration force and resistances that the vehicle has to overcome. This traction force is then translated into the torque and speed, which flow upstream through the drivetrain to the energy sources. The powerflow is calculated backwards through each component, taking their efficiency into account. To do this, maps and look-up tables are used to model the components, making it simple and allowing a fast computation of the result. The use of maps however has the disadvantage that the dynamic effects are not taken into account. For real-time simulations, for example to know the exact behaviour of a component, the use of the *forward approach* is preferred. The forward modelling technique uses a controller (cf. driver) that tries to follow a driving cycle. This allows obtaining best effort performances, while the backward model can encounter problems when it is not able to follow the driving cycle. Its main disadvantage is that the increased accuracy is associated with an increased computation time [17,57-61].

3.2 Simulation tools

During the last two decennia, different simulation tools have been developed for the investigation of vehicles. An overview of the most prominent simulation software is presented.

3.2.1 ADVISOR

Advanced VehIcle SimulatOR or ADVISOR was a vehicle simulation programme of the National Renewable Energy Laboratory of the USA. It was developed in 1994 to support the US Department of Energy (DOE) in its research in Hybrid Electric Vehicles (HEVs). It has been widely used, both in industry and research institutes to assess the performance, fuel economy and emissions of both conventional vehicles and HEVs. ADVISOR is a simulation program written in the MatLab/Simulink environment. It uses a combined backward/forward technique, which allows both the benefits of fast computation and best effort calculations. ADVISOR contains a number of predefined data and models for the chosen components. The user can both change these data - by editing the associated MatLab file - and the model itself [9,27,57].

3.2.2 PSAT and Autonomie

The *Powertrain System Analysis Toolkit* or *PSAT* was developed at Argonne National Laboratory (ANL) in 1999. The US DOE sponsored the development of PSAT. Just like ADVISOR, it is written in MatLab/Simulink, but PSAT's calculation method is based on the forward approach. Simulations can be carried out with one of the 200 predefined configurations for conventional vehicles and various hybrid vehicles and topologies. The level of detail varies from the use of look-up tables to the implementation of dynamic models, what makes it possible to obtain more accurate results than with ADVISOR [58].
In 2007, ANL developed in corporation with General Motors a new simulation programme: *Autonomie*. The purpose of the new version is to deal with the increasing complexity and diversity of the powertrain. It contains several new features, among which the possibility to run only one single component (e.g. only the ICE) and the option to customize the powertrain configuration [9,63].

3.2.3 Dymola

Dynamic Modeling Laboratory or Dymola was developed by Dynasim in Lund, Sweden in 2000. It is based on Modelica models, which is a programming language, intended to design physical systems. It suits the modelling of larger and more complex systems, making it possible to analyse the behaviour of your components in detail. To describe these complex systems, Modelica uses differential algebraic and discrete equations [62].

3.2.4 Vehicle Simulation Programme (VSP)

Vehicle Simulation Programme (VSP) was created at the Vrije Universiteit Brussel in 2000. It works in the LabVIEW environment and makes use of the backward simulation approach. It has been used in different research and industrial projects. It is developed in order to study the power flows in different drivetrains and compare them, both on the level of energy consumption and performance. The submodels can also be modified to obtain the desired simulation [24,60].

Aside from the discussed programs, other simulation tools can be found in literature such as SIMPLEV, MapleSim and ELVIS.

3.3 Proposed Model

3.3.1 General overview

To analyse the power flows in the drivetrain of a series PHEV, a dynamic simulation in the Matlab/Simulink environment is build. The objective of the simulation program is to examine power flows in the drivetrain and in the Rechargeable Energy Storage System (RESS) of the vehicle in order to analyse the influence of the Electrical Double Layer Capacitor (EDLC) system.

Figure 12 shows the topology of the drivetrain of a series PHEV. An Internal Combustion Engine (ICE), battery system and/or EDLC system deliver the power to propel the vehicle. These three sources are connected to the DC bus, where a DC/AC converter controls the electric motor (EM) that propels the wheels through a transmission. The introduction of a DC/DC converter in between the EDLC system and the DC-bus allows controlling the power flow from and to the EDLC system (see 2.3.3 Hybrid RESS). The amount of the power coming from each source at a certain time is defined by the control strategy.

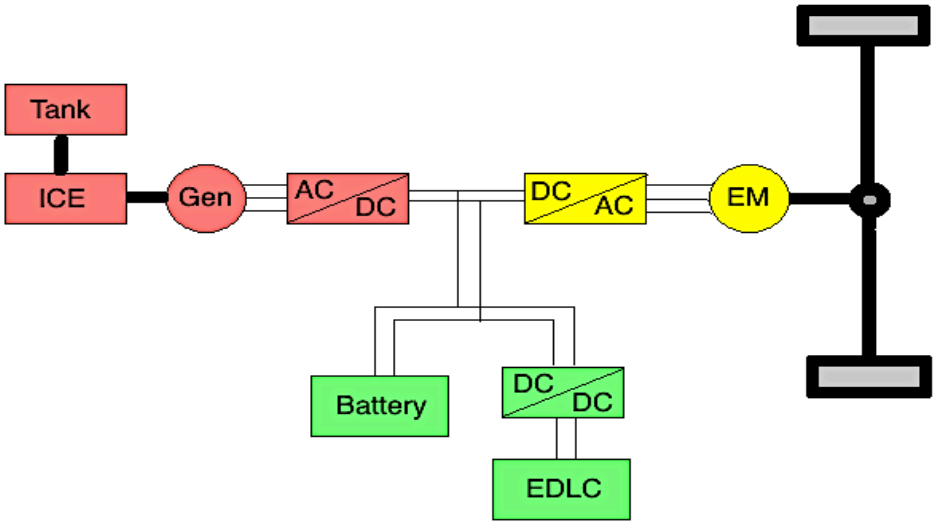

Figure 12: Topology Series PHEV with EDLC

To simulate the Series PHEV, a combined backward and forward model has been built. The 'main' program is written by using the backwards approach for reasons of simplicity and computation time [59]. The driving cycle and efficiency of the different components in the drive cycle define the power that needs to be delivered by the energy sources. The backwards simulation however always assumes that the velocity profile can be followed. In situations where the required power (or other magnitude like torque, speed, current, …) is higher than what can physically be delivered by the vehicle's components, this assumption is not valid anymore. The backwards approach will thus impose a velocity that cannot be reached at the next step of the simulation. In order to take the real performance of the vehicle into account, a forward model is also implemented. In the forward part of the program, the maximum available power coming from the energy sources is used to compute the maximum achievable acceleration and velocity for the next step. At those moments that the required velocity of the drive cycle cannot be followed, the simulation continues with the obtained maximal achievable speed until the drive cycle can again be followed. This moment is defined by also taking the difference in distance due to the slower driving into account.

In Figure 13, the layout of the proposed simulation is shown. The driving cycle (green), drivetrain (blue), control strategy (red) and power sources (yellow) form the core of the backwards model. Starting from the power sources, the maximum achievable velocity is then calculated in the forward model (purple) and compared with the demands of the driving cycle.
Specific qualities of the written simulation are:

- The combination of the forward and backward model makes it possible to profit of the simplicity of the backward approach taking into account the maximum performance of the vehicle. An alert displays immediately if the driving cycle is followed or not and how many times it occurs.
- The objective is to examine the power flows in the drivetrain and to examine the effect of the EDLC system. The simulation is built in such a way that the presence of the EDLC unit can be modified by only changing one variable.

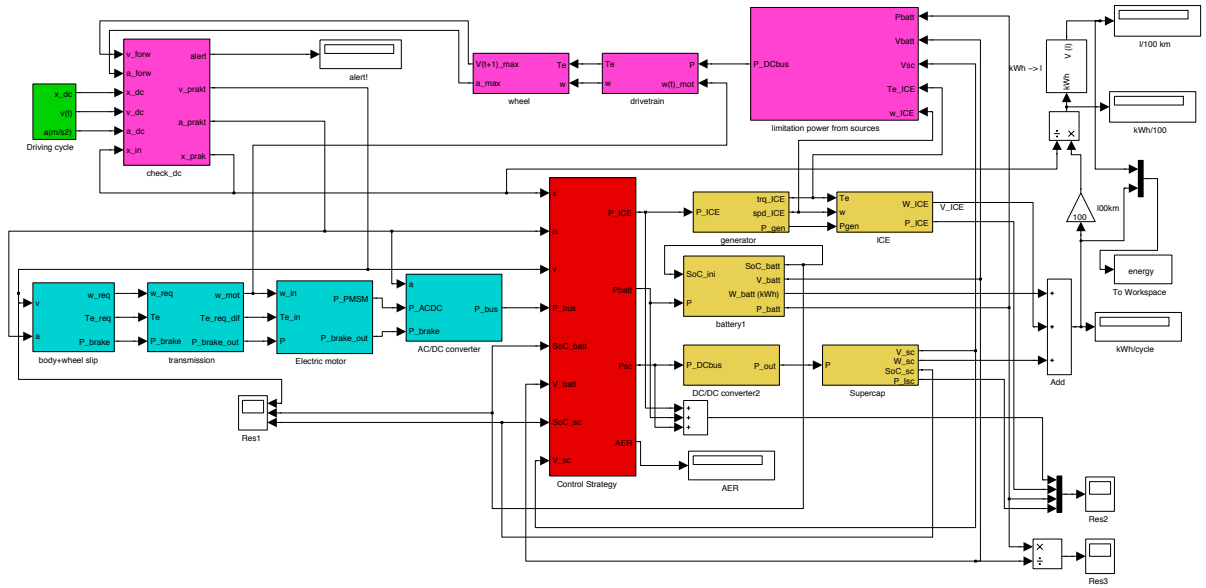

Figure 13: General simulation lay-out

3.3.2 Components

3.3.2.1 Driving cycle

A driving cycle proposes a velocity profile that the vehicle needs to follow. A lot of different driving cycles exist to describe different types of driving behaviour and the choice of one hugely impact the simulation results. A typical urban driving cycle contains a lot of accelerations and decelerations, making electrical energy sources more attractive thanks to their ability of regenerative braking. Conversely, highway driving cycles ask for a higher but almost constant speed in a region with a high efficiency of the ICE.

In this master thesis, three case studies are performed in order to obtain results for different driving styles. The first two cases follow driving cycles as proposed by the United States Environment Protection Agency (EPA). This will allow to compare the simulation results with the official fuel economy ratings of the Chevrolet Volt 2011. To define these ratings, the EPA submits the vehicle to a city and a highway driving test. The city driving behaviour is represented by the FTP-75 driving cycle (Federal Test Procedure), while the Highway Fuel Economy Driving Schedule (HWFET) describes highway driving conditions. A weighting factor for both driving behaviours (55% city driving and 45% highway driving) is used to obtain the final fuel economy rating [64]. The exact calculations are presented in 5.1 Validation.

The third case study applies the simulation to the New European Driving Cycle (NEDC). The NEDC is designed to represent the typical driving behaviour of a passenger car and is used in Europe to define the emissions and fuel consumption of a vehicle. It consists out of the ECE-15 Urban Driving Cycle (UDC) which is repeated four times and an Extra-Urban driving cycle (EUDC). The three driving cylces are displayed in Figure 14 and their main characteristics are presented in Table 5.

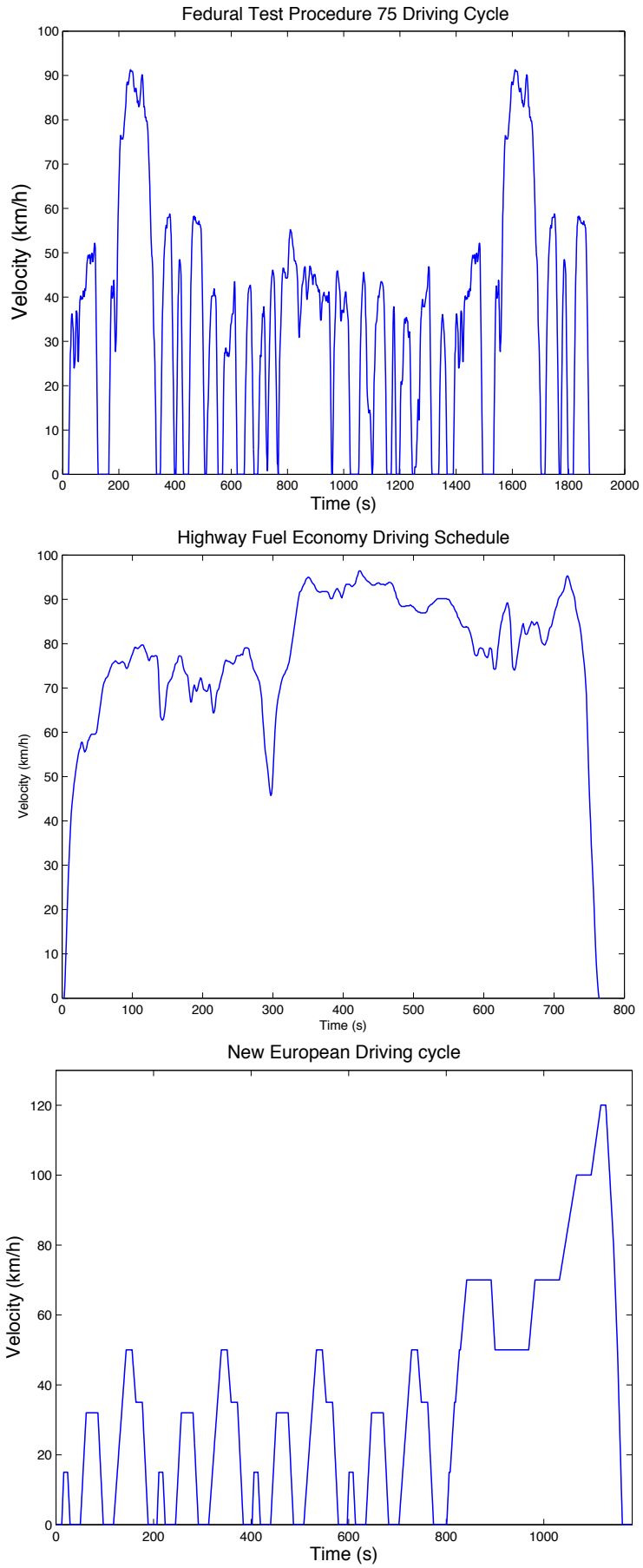

Figure 14: Federal Test Procedure 75, Highway Fuel Economy Driving Schedule, New European Driving Cycle

Table 5: Characteristics driving cycles

Parameter	FTP-75	HWFET	NEDC
Distance (km)	17,8	16,5	10,9
Time (s)	1874	765	1180
Mean velocity (km/h)	34,1	77,6	33,3
Maximum velocity (km/h)	91,2	96,4	120
Maximum acceleration (m/s²)	1,48	1,43	1,06

3.3.2.2 Longitudinal dynamics

Starting from the velocity profile, the required tractive effort at the wheels is calculated by using the longitudinal dynamics model of a vehicle. Newton's second law states that the movement of an object along its moving direction is completely determined by all the forces acting upon it in that direction. Applying this for a vehicle delivers the longitudinal dynamics model:

$$(m * \delta_J) * \frac{dv}{dt} = \sum F_i = F_t - (F_w + F_r + F_g) \quad (3.1)$$

where

m = mass of the vehicle (kg);

δ_J = rotational inertia coefficient (-);

v = velocity of the vehicle (m/s);

F_t = tractive effort (N);

F_w = aerodynamic resistance (N);

F_r = rolling resistance (N);

F_g = gradient resistance (N).

The tractive force (F_t) is produced by the energy sources. This force is necessary to overcome the vehicle's resistances and meet the demands of the drive cycle in terms of acceleration. The main resistive forces for a vehicle are the aerodynamic resistance, rolling resistance and gradient resistance [60-65].

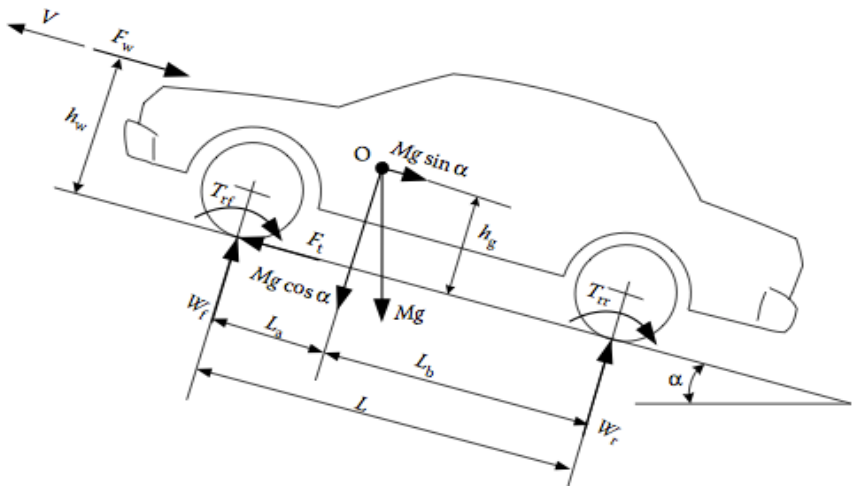

Figure 15: longitudinal dynamics of a vehicle [61]

The *aerodynamic resistance* includes the shape drag and skin effect. When a vehicle is moving forwards, it has to push the air in front of it away, what means that the vehicle encounters an increased pressure. Furthermore, because the air cannot instantaneously fill the space behind the car, a forward motion induces a region with a decreased pressure behind the vehicle. The shape drag denotes these two zones of pressure that oppose the forward motion of the vehicle. The skin effect takes into account that the air close to the vehicle moves with almost the same speed as the vehicle itself, while the air further away doesn't and this difference in speed of the air molecules provokes friction. The total aerodynamic resistance can be calculated by

$$F_w = \frac{\rho_{air} * A_f * C_d * v^2}{2} \quad (3.2)$$

where
ρ_{air} = density of air (1,225 kg/m^3 at 15°C);
A_f = frontal area of the car (m^2);
C_d = drag coefficient of the car (-).

The *rolling resistance* takes into account the losses due to the deformation of the tire. While driving, the load of the car causes a deflection of the tire's round shape. The hysteresis of the rubber in the tire induces a loss term that can be calculated by

$$F_r = C_r * m * g * \cos(\alpha) \quad (3.3)$$

where
C_r = rolling resistance coefficient (-);
g = gravitational constant (= 9,81 m/s^2);
α = slope (rad).

When driving on a slope, the *gradient resistance,* which takes into account the component of the gravitational force in the direction of movement, must also be included in the simulation model:

$$F_g = m * g * sin(\alpha) \quad (3.4)$$

In standard driving cycles, no information about the slope of the trajectory is given. Accordingly, the gradient resistance isn't taken into account [65].

3.3.2.3 Transmission

The global transmission of the drive exists out of a differential and a transmission. The transmission is necessary to match the torque and speed of the motor with those at the wheels. In practice, series PHEVs usually don't need a gearbox due to the favourable torque-speed characteristics of an electrical motor: at low speeds, a high torque can be produced in order to deal with high accelerations. These accelerations aren't required at higher speeds, so the decreasing torque doesn't pose problems. The transmission can then be modelled as a single gear transmission.
The differential is a gearbox that allows the wheels on the same axis to have different speeds, what is necessary when turning. It also can be modelled as a single gear and its effect can easily be taken into account as part of the global drivetrain transmission. The speed and torque behind the transmission becomes:

$$\omega_{out} = i_g * \omega_{in} \tag{3.5}$$

$$Te_{out} = \frac{Te_{in}}{\eta_{trans} * i_g} \tag{3.6}$$

where

i_g = transmission ratio (-);

ω_{out} = shaft velocity behind the transmission (rad/s);

ω_{in} = shaft velocity before the transmission (rad/s);

Te_{out} = torque behind the transmission (N.m);

Te_{in} = torque before the transmission (N.m);

η_{trans} = efficiency transmission (%).

3.3.2.4 Electric motor

Physically, the EM provides the mechanical power to the wheels. This power is delivered by the energy sources in the form of electricity at the level of the DC-bus. A DC/AC converter is needed to feed the motor with AC voltages and currents.

Today, a wide variety of motor types do exist. While simple DC-motors where the first motors to be used in electric vehicle applications, the induction machine and Permanent Magnet Synchronous Machine are currently preferred because of their ability to reach higher speeds (thus higher power), efficiencies and specific power. Switched Reluctance motors also deserve attention, but ask for a more complex control and still face noise problems [66-68].

Different techniques exist to model the electrical motor. One can define the motor by using physical equations, equivalent circuits (analytical models) or measured efficiency characteristics. The last solution is preferred in this simulation because of its simplicity. The efficiency maps are taken out of the database of ADVISOR 2002, which contains data of several EMs with a rated power in the range of 15 kW up to 187 kW. The efficiency map is inserted in a look-up table in Simulink. By entering it with the required speed and torque values, the efficiency for that specific situation is obtained. This efficiency then is used to compute the required power at the DC/AC converter entrance. Constraints in terms of power, torque and speed are added in order to guarantee safe operation of the EM.

The AC/DC converter transforms the DC power at the DC-bus into AC power that feeds the EM. To account for its losses, it is modelled by a constant efficiency of 95% in both directions [69].

3.3.2.5 ICE-Generator

The ICE-generator unit comprises the ICE, the generator and the AC/DC converter. The ICE is the source of the mechanical power, which is transformed into electrical AC power by the generator and finally rectified by the AC/DC converter in order to deliver DC power at the DC-bus. In a series PHEV, the ICE is decoupled from the wheels thanks to the generator. This has the advantage that the ICE is able to run constantly at its most efficient working point. The generator and AC/DC converter then must be dimensioned such that their most efficient region matches the operating point of the ICE.

Efficiency maps of ADVISOR 2002 are used to model these components. Both components are physically coupled and are chosen to run at their most efficient point, so their speed and torque values are equal and constant. The losses in the AC/DC converter are taken into account by using a constant efficiency of 95% [7].

One can remark that the efficiencies of the ICE, the generator and the EM are all modelled by using efficiency maps of the library of ADVISOR 2002. These data will not correspond to the efficiencies that can be obtained with modern technologies. Since 2002, the search to minimize the fuel consumption has steered a gradual improvement for these components [2]. This inaccuracy is tolerated, as it will not change the analysis of the power flows in the RESS.

3.3.2.6 Battery

Batteries for PHEV applications are commonly of the lithium-ion family. In this master thesis, a high energy LFP battery with characteristics listed in Table 6 is used. The data are experimentally obtained by researchers at VUB in regard of the SuperLIB project [70].

Table 6: Battery cell characteristics [70]

Parameter	
m_{batt} (kg)	1
V_{batt} (dm^3)	0,59
$U_{n,batt}$ (V)	3.3
$C_{batt,ref}$ (Ah)	45
$I_{batt,max}$ (A)	3*It
$I_{batt,,min}$(A)	-2*It

The lifetime of the battery at different discharge rates is presented in Figure 16. The cycle life of a battery is defined as the number of charge and discharge cycles the battery can undergo before its capacity has dropped to 80% of its initial capacity [28]. Figure 16 clearly indicates the negative effect of higher currents on the lifetime. The obtained cycle life is experimentally defined after repeatedly discharging the battery to 100% Depth of Discharge (DoD). The number of cycles increases drastically when diminishing the DoD, justifying the choice to maximally discharge the battery system to 30% State of Charge (SoC).

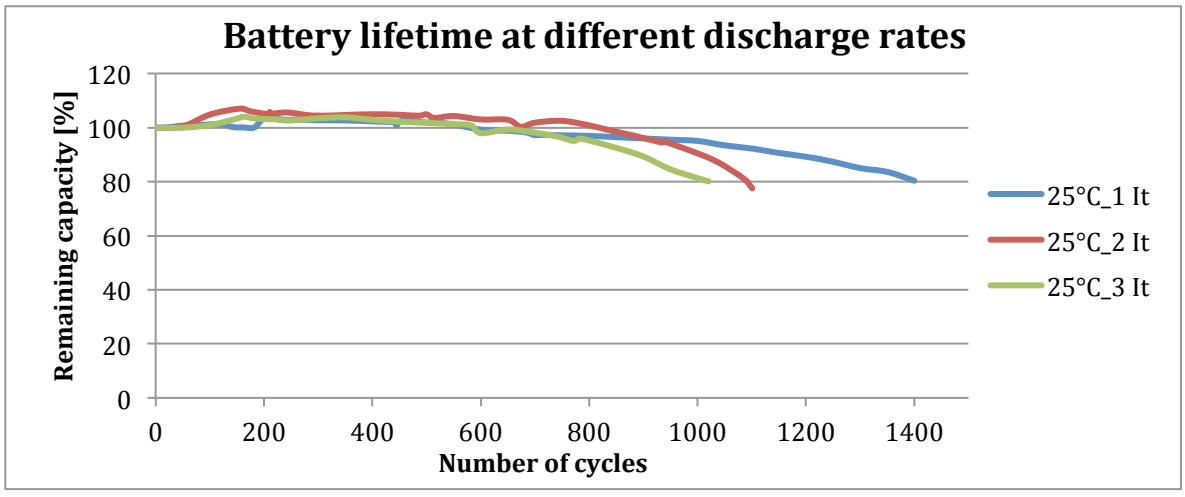

Figure 16: Battery lifetime at different discharge rates [70]

To model the battery, the R_{int} model is selected [39]. It is the simplest, but also less accurate electrical model of a battery. It defines a battery as an ideal voltage source with an internal resistor to account for the thermal losses. In practice, both the open circuit voltage U_{oc} and the internal resistance R_{int} are function of the SoC, State of Health (SoH) and the temperature of the battery. The resistance also varies with the current and is different during charging and discharging. To take these effects into account, a variable open circuit voltage and resistance could be used.

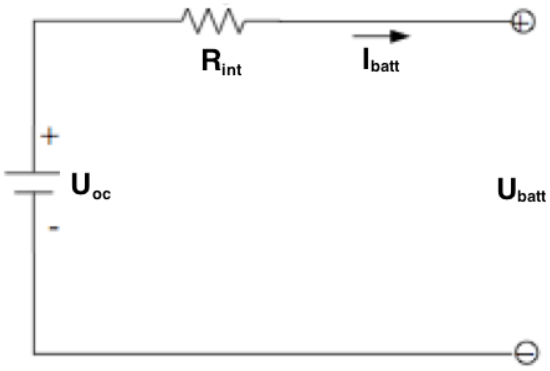

Figure 17: R_{int} model of a battery [39]

For this battery type, data for the internal resistance at different SoC levels and discharge rates were available. The open circuit voltage is modelled as a constant voltage of 3,3V. This assumption causes an error in comparison to the real open circuit voltage of an LFP battery (see Figure 18). However, by imposing an operating area for the battery system in SoC interval [30%, 100%], the error stays limited.

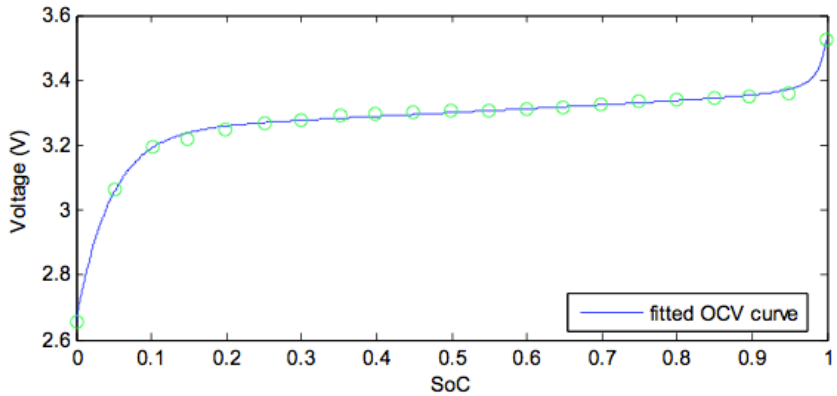

Figure 18: Open circuit voltage in function of DoD for an LFP battery [40]

The of a battery can be computed by counting the used capacity [61]:

$$SoC_{batt}(t) = SoC_{batt,in} - \frac{I_{batt} * \Delta t}{3600 * C_{batt,ref} * \left(\frac{I}{I_{ref}}\right)^{n-1}} \tag{3.7}$$

where

$SoC_{batt,in}$ = initial state of charge of the battery (%);

$C_{batt,ref}$ = reference capacity of the battery with a continuous discharge current I_{ref} (Ah);

I_{ref} = continuous discharge current at which the reference capacity is defined (A);

n = Peukert constant (1,01 to 1,03 for LFP batteries [23]).

The term $C_{batt,ref} * \left(\frac{I}{I_{ref}}\right)^{n-1}$ denotes the change in capacity of the battery if discharged at other currents than the reference discharge current. However, for lithium ion batteries this term stays very close to the reference capacity due to the small Peukert constant.

3.3.2.7 EDLC cells

Maxwell is one of the leading companies regarding ELDC technology. In their K2 series, they offer cells with a capacitance up to 3000F and accordingly very high power performance. These are the typical EDLC cells that can be used in transportation applications. An overview of the cells with capacitances varying from 1500 to 3000F is presented in Table 7.

Table 7: EDLC cell characteristics [71]

Parameter	BCAP1500	BCAP2000	BCAP3000
Mass (g)	280	360	510
Capacitance (F)	1500	2000	3000
Nominal voltage (V)	2,7	2,7	2,7
Maximum voltage (V)	2,85	2,85	2,85
ESR (mΩ)	0,47	0,35	0,29
EPR (Ω)	900	643	519
Specific energy (Wh/kg)	5,4	5,6	6,0
Specific power (W/kg)	6600	6900	5900
Lifetime (cycles / year)	1000000 / 10	1000000 / 10	1000000 / 10

To model the EDLC, an equivalent circuit with the capacitance C_{EDLC}, the Equivalent Series Resistance ESR and the Equivalent Parallel Resistance EPR is used (Figure 19). The ESR represents the ohmic losses, mainly due to the contact resistance between electrode and electrolyte. The EPR takes the static losses due to self-discharge of the capacitor into account.

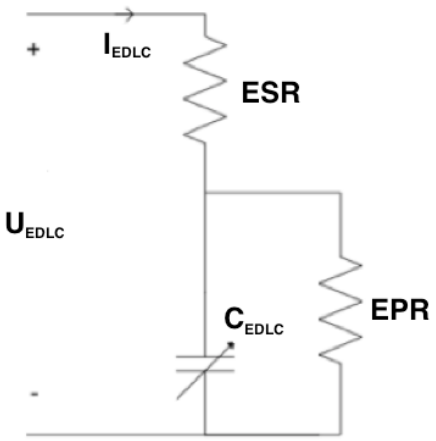

Figure 19: Equivalent circuit EDLC cell [39]

The energy stored in an EDLC system is directly related to the voltage of the EDLCs

$$W_{EDLC} = \frac{C_{EDLC} * {U_{EDLC}}^2}{2} \tag{3.8}$$

Due to this relation between energy content and voltage difference, the SoC of an EDLC cell can easily be computed out of its voltage:

$$SoC_{EDLC} = \frac{\frac{1}{2} * C_{EDLC} * U_{EDLC}(t)^2}{\frac{1}{2} * C_{EDLC} * U_{max,EDLC}^2} = \frac{U_{EDLC}(t)^2}{U_{max,EDLC}^2} \tag{3.9}$$

The disadvantage of this behaviour is that the potential difference over the EDLCs endures large fluctuations with changing SoC, while the battery voltage is fairly constant. Due to the large variation of the voltage, an EDLC is practically only used in the interval [$U_{EDLC,max}$, $U_{EDLC,max}/2$]. This means that only 75% of the energy of an EDLC cell is storable:

$$\begin{aligned} W_{EDLC,us} = & \int_{t_0}^{t_e} P_{EDLC}\, dt = \int_{t_0}^{t_e} U_{EDLC}.I_{EDLC}\, dt = \int_{t_0}^{t_e} U_{EDLC}.C_{EDLC}.\frac{dU_{EDLC}}{dt}\, dt = \\ & \int_{\frac{U_{EDLC,max}}{2}}^{U_{EDLC,max}} U_{EDLC}.C_{EDLC}\, dU_{EDLC} = \frac{3}{4} W_{EDLC,max} \end{aligned} \tag{3.10}$$

As explained in 2.3.3 Hybrid RESS, the EDLC system is connected to the DC-bus through a DC/DC converter in order to control the power flows in the hybrid RESS. In PHEV applications, the DC/DC converter must be a bidirectional converter. During acceleration, the voltage of the EDLC system must be increased, or boosted, such that power can flow from the EDLC system to the DC–bus. During braking, the voltage must be decreased or bucked in order to send power from the DC-bus to the EDLC system [41]. The exact efficiency of the converter depends on the working conditions, but a constant efficiency of 95% is used due to reasons of simplicity. The choice is based on results of a 30 kW interleaved four-channel DC/DC converter [72].

3.4 Power control strategy

3.4.1 Requirements

The efficiency of a hybrid drivetrain depends on the efficiencies of its components and on the control of the power flow from and to the different energy sources. The power control strategy brings all the components together and must make sure that each power source is used in its most efficient way in order to maximally benefit from the hybrid concept. But apart from the efficiency, the power control strategy must also meet the requirements in term of driveability and safety, e.g. no link between the SoC of an energy source and safety of the driver.

In this master thesis, a series PHEV with a RESS existing of a battery system and an EDLC system is controlled. The general requirements of the PHEV are:

- Meet the demands of the chosen driving cycles,
- All systems must stay within their safe operating area in order to guarantee safety and driveability;
- Start driving in all electric mode and only use the ICE when the RESS is not able to safely provide the traction power anymore;
- Maximize fuel economy of the RESS:
    - Use the EDLC system to supply peaks during load power, while the battery delivers the average power
        - SoC of EDLC system must be high at low velocities in order to handle accelerations;
        - SoC of EDLC system must be low at high velocities in order handle braking.

3.4.2 Applied control strategy

3.4.2.1 ICE – RESS

The *thermostat control strategy* or *engine on – off strategy* is selected to control the ICE – RESS system. With this strategy, the ICE-generator unit is completely controlled by the SoC of the battery. The RESS propels the vehicle in Charge Depleting (CD) mode until the SoC of the battery drops under a certain level. At that moment the ICE will start running at its most efficient working point and will provide power to the wheels and to the battery in order to charge it. When the SoC of the battery again has reached a certain higher level, the ICE is shut down and the vehicle is driven in CD mode again [73]. The thermostat control strategy is illustrated in Figure 20. In this figure, the term PPS means Peak Power Storage and plays exactly the same role as the RESS in the explanation above.

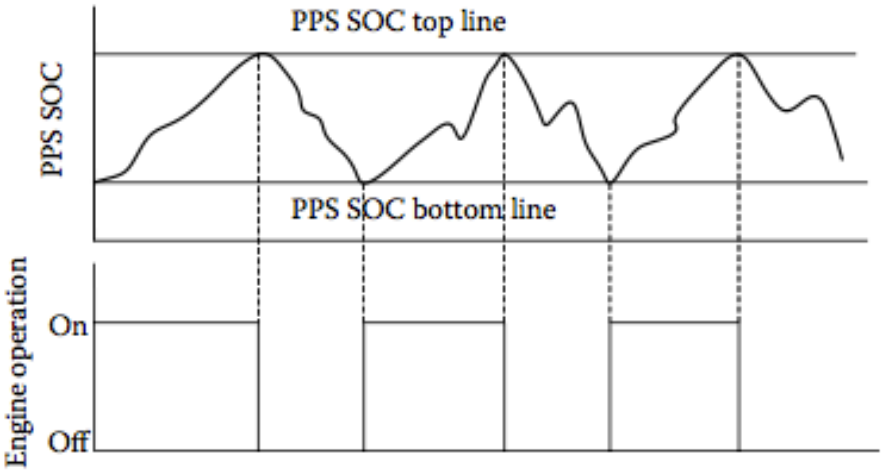

Figure 20: Thermostat control strategy [73]

3.4.2.2 RESS control strategy

The global overview of the control scheme of the RESS is presented in Figure 21. The hybrid RESS must supply / absorb the load P_{ress}, which is defined by subtracting the power delivered by the ICE of the power required to follow the driving cycle calculated at the DC-bus.

In order to make a distinction between the peak power, which must be provided by the EDLC system and the average power, which is supplied by the battery, a *low pass filter* (orange) is installed. The low pass filter blocks the high frequency component of P_{ress}, resulting in a slowly varying signal. The output of the filter represents the power that is delivered by the battery system. The difference between the load and the battery power is supplied by the EDLC system.

A *SoC-control* (blue) block is added to make sure that the EDLC system is able to deliver and absorb the required power under all circumstances. In this block, the SoC of the EDLC system is regulated by comparing the actual SoC of the EDLC to a reference SoC, which at his turn depends on the vehicle's speed. The result is a power difference ΔP that is added to the EDLC system and drawn from the battery system.

The other blocks represent *constraints* (yellow) on the current drawn from the EDLC and the battery system, the maximum current rate of the battery and the voltage of the battery and EDLC system [11,13,39,46].

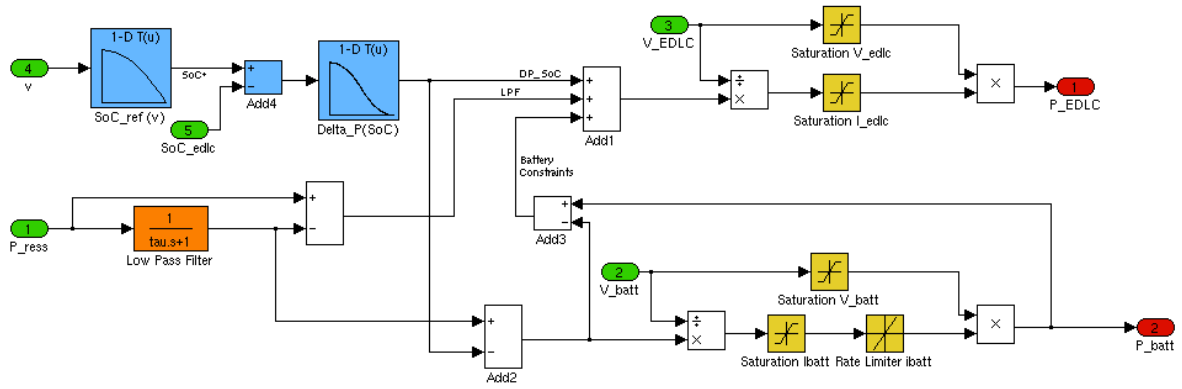

Figure 21: Control strategy

3.4.2.2.1 Low pass filter

The low pass filter is the main instrument used to divide the power asked from the RESS into power from the EDLC system and from the battery system. The filter attenuates the high frequency signals and the output is the power demand for the battery system.

The transfer function of a low pass filter in the Laplace domain is

$$H_{LP}(s) = \frac{1}{\tau * s + 1} \tag{3.11}$$

where τ is the time constant of the filter[4].
The output of the filter, also called the moving average power, becomes

$$P_{batt} = \frac{1}{\tau * s + 1} * P_{ress} \tag{3.12}$$

and the power that needs to be delivered by the EDLC system is

$$P_{EDLC} = P_{ress} - P_{batt} \tag{3.13}$$

The time constant of the low pass filter is a very important design parameter. Hadartz and Julander use a time constant of 16 seconds in [39], while Yu et al. chose 10s in [74] and Cheng et al. 8 seconds in [75]. The last author justifies his choice by stating that the acceleration time also is 8s, meaning that the EDLC system mainly deals with the accelerations and the battery provides the average power to maintain the velocity of the vehicle.

3.4.2.2.2 SoC-control

The control of the SoC of the EDLC system is performed by a proportional P controller, which generates an extra power signal ΔP in order to guide the SoC of the EDLC system to its reference value. This reference value varies with the velocity of the vehicle. The purpose of the SoC control is to make sure that the EDLC system will be able to deliver power when the vehicle speed is low and store power when the vehicle speed is high [11]. The SoC controller contains two lookup tables: one that relates the velocity with the reference SoC and one to compute the power difference in function of the difference in SoC.

[4] Time after which the output signal has reached 63% of the input signal

3.4.2.2.3 Constraints

After the computation of the ideal power distribution between the battery and the EDLC systems, the physical limitations of both sources have to be considered. The following constrains are added in order to make sure that the energy sources are handled safely:

- Current of the battery system:

The 3C discharge rate and 2C charge rate define the maximum and minimum current through the LFP battery (see Table 6):

$$I_{batt,max} = 3 * 45A = 135\ A \quad (3.14)$$

$$I_{batt,min} = -2 * 45A = -90\ A \quad (3.15)$$

- Current slope of the battery system:

A rate limiter imposes a maximum current slope of 1/10 of the peak current per second [75]:

$$\left(\frac{dI}{dt}\right)_{max} = 13{,}5\frac{A}{s} \quad (3.16)$$

- Voltage of the battery system

The voltage of the battery system cell varies around its nominal value of 3,3V. High current demands can however cause a significant voltage drop. The safe operating area of the battery voltage is defined as

$$U_{batt,max} = 3{,}65V \quad (3.17)$$

$$U_{batt,min} = 2{,}0V \quad (3.18)$$

- Current of the EDLC system:

A current limit of 400A is chosen, which is also used as constraint in [76] and as upper limit for experiments in [10]. The datasheet of the EDLC cell indicates that higher currents can be provided (non repetitive even up to 2200A [71]) but this demand could cause a dramatic increase in temperature ($P_{diss} = R_{int} * I^2$) and even damage the EDLC cell.

- Voltage of the EDLC system:

The voltage of the EDLC system can vary in the interval [$U_{EDLC,max}/2$, $U_{EDLC,max}$]. Lower voltages would have a negative effect on the efficiency of the EDLC system and DC/DC converter and ask for too high currents. In order to make sure that the voltage stays in its safe operating area, a hard and a soft limit that limit the power output of EDLC system are imposed:

$$P_{EDLC,lim} = M * P_{EDLC} \quad (3.19)$$

with

$$\begin{cases} M = 0 & \text{if } P_{ress} > 0 \text{ and } SoC_{EDLC} \geq 100\%; \\ M = -20 * SoC_{EDLC} + 20 & \text{if } P_{ress} > 0 \text{ and } SoC_{ELDC} > 95\%; \\ M = 1 & \text{if } 30\% \leq SoC_{EDLC} \leq 95\%; \\ M = 20 * SoC_{edlc} - 5 & \text{if } P_{ress} < 0 \text{ and } SoC_{EDLC} < 30\%; \\ M = 0 & \text{if } P_{ress} < 0 \text{ and } SoC_{EDLC} \leq 25\%. \end{cases} \quad (3.20)$$

3.4.2.3 Regenerative braking

One of the major advantages of introducing a RESS in vehicular applications is its ability to store energy during braking. In a conventional car, braking occurs with mechanical friction discs that dissipate all the braking energy in the form of heat. In a PHEV, the braking energy can flow through the drivetrain to the RESS where it can be stored. In a hybrid RESS, the braking energy is preferably sent to the EDLC system due to its low internal resistance, high efficiency and ability to store large amounts of energy in short time periods.

Even when using a regenerative braking system, mechanical friction brakes always coexist with the electrical system in order to ensure braking performance. A distinction between two hybrid braking systems can be made: the parallel hybrid braking system, where both the electrical and mechanical brakes are used in parallel and a series hybrid braking system. In the series braking system, all the energy is recovered by the electrified system up to the maximal power it can absorb. The mechanical brakes are used to cope with the excessive braking power. This topology is chosen because it allows more energy regeneration, although it is more complex due to the high braking power at which the mechanical brakes are suddenly used [67,77].

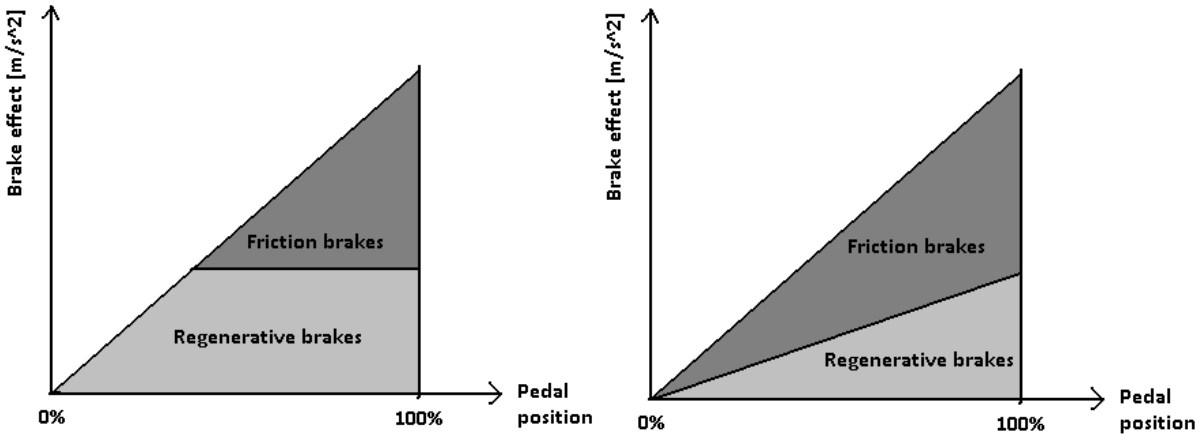

Figure 22: Series and Parallel regenerative braking system [77]

The recoverable energy is available in the form of kinetic and/or potential energy. Due to the use of driving cycles without any slope in their trajectory, only kinetic energy is taken into account. A constant regeneration efficiency is often used to model the regenerative braking. It expresses the amount of kinetic energy that finally reaches the RESS. The rest is needed to overcome the resistances and losses in the drivetrain or is lost in the friction brakes at low velocities. Barrero et al. mention in [11] that 60-65% of the kinetic energy can be restored, while Gantt et al. obtain a regenerative braking efficiency of 55% by using a braking fraction of 85% and a transmission efficiency of 65% [78]. In this model, the same braking fraction of 85% is used to calculate the available regenerative energy at the wheels, which is then passed through the drivetrain where the efficiencies of the components take their losses into account.

4 Dimensioning of the powertrain components

A Plug-in Hybrid Electric Vehicle (PHEV) can be configured in different ways, by using different drivetrain topologies and/or control strategies. These configurations have to be optimized for the applied load situation. An important part in this optimization is the dimensioning of its components, as it must ensure good performances with a minimum total weight, volume and cost. In this section, the method to dimension the different components is explained. The scope of this master thesis is to analyse the power flows in the RESS of the PHEV, not to design a PHEV. The simulation is therefore applied to the case of the Chevrolet Volt.

Table 8: Chevrolet Volt parameters [46,79]

Parameter	Chevrolet Volt
Published data	
m	1715 kg
$m_{batt,mod}$	198 kg
r_w	0.33 m
C_d	0.287
A_f	2.16 m^2
Assumed data	
C_r	0.010
δ_J	1,08
η_{trans}	95 %
P_{aux}	700 W
P_{HVAC}	1857W

Figure 23: Chevrolet Volt [46]

The published data in Table 8 are data released by General Motors about the GM Volt. The other data are estimates based on values found for other applications. δJ is the rotational inertia coefficient that takes the effect of the rotational inertia into account [79]. η_{trans} is the efficiency of the transmission system and takes the losses in the single gear transmission and differential into account. The auxiliary power and HVAC power (Heating, Ventilation and Air Conditioning) are both extra loads that demand energy for other reasons than propelling the vehicle. Although their exact value is dependant on the driving conditions, weather…, they can be modelled as a constant extra power demand. The HVAC is the largest of all ancillary loads. In this simulation, an HVAC power of 1,86 kW is assumed [80]. In [81], Hayes et al. mention that the HVAC power in the Nissan Leaf at peak moments (starting at a cold day) can even be 6 kW. Other auxiliary equipment such as power steering, lights, compressors, radio,… add another 700W [62].

4.1 Electric motor

To estimate the power rating of the Electric Motor (EM), three performance characteristics are generally taken into account: maximum cruising speed, gradeability and acceleration. In [73], the authors mention that the power rating of the motor drive is dictated by acceleration requirements rather than by maximum cruising speed or gradeability. To estimate the power rating of the EM, the authors propose a methodology based on the required acceleration (starting at 0m/s) and the calculation of the aerodynamic and rolling resistance.

The power to accelerate is estimated by

$$P_{n,EM} = \frac{\delta_J * m}{2 * t_a} * \left(V_f^2 + V_b^2\right) \tag{4.1}$$

where
$P_{n,EM}$ = nominal power of the EM (kW);
δ_J = Rotational inertia coefficient (-);
m = mass of the vehicle (kg)
t_a = acceleration time (s);
V_f = final speed of the vehicle (m/s);
V_b = base speed of the vehicle (m/s).

The base speed of the motor is defined as the lowest speed at which the motor works in its constant power area (see Figure 24). The base speed of the vehicle can be calculated by taking the transmission ratio into account. The average power to overcome the aerodynamic and rolling resistance during the acceleration is

$$\bar{P} = t_a * \int_0^{t_a} \left(m * g * C_r * v + \frac{\rho_{air} * A_f * C_d * v^3}{2} \right) dt \tag{4.2}$$

where v is the vehicle speed at time t. The vehicle speed can be estimated in function of the final velocity of the vehicle by

$$v = V_f * \sqrt{\frac{t}{t_a}} \tag{4.3}$$

Substituting relation (4.3) into (4.2) and integrating the power term gives the power that is necessary to overcome the vehicle's resistances. Adding the acceleration power described in (4.1) results in an estimation for the rated power of the EM:

$$P_{n,EM} = \frac{\delta_J * m}{2 * t_a} * \left(V_f^2 + V_b^2\right) + \frac{2}{3} * m * g * C_r * V_f + \frac{1}{5} * \rho_a * C_d * A_f * V_f^3 \tag{4.4}$$

The application of equation 4.4 is performed by starting from 0m/s to the maximum velocity achieved with the maximum acceleration of the driving cycle. The EM's highest power rating is observed in the HWFET and became 48,7 kW [73].

The final choice of the EM is a Permanent Magnet Synchronous Motor (PMSM) with a maximum power output of 53 kW. It is the smallest EM out found in the ADVISOR database that is able to deliver the peak power 48,7 kW in the HWFET driving cycle. Compared to the 110kW EM of the Chevrolet Volt, the chosen 53 kW PMSM has a much lower power range. However, the Chevrolet Volt is able to accelerate from 0 to 60 miles per hour (97 km/h) in 8, 53s [46]. The acceleration necessary to accomplish this is 3,14 m/s², while the maximum acceleration in the considered driving cycles only is 1, 48 m/s². During the next step of the design phase, the maximum power in the EM is checked for every drive cycle and the choice of the EM is validated as it can at every moment provide the required power.

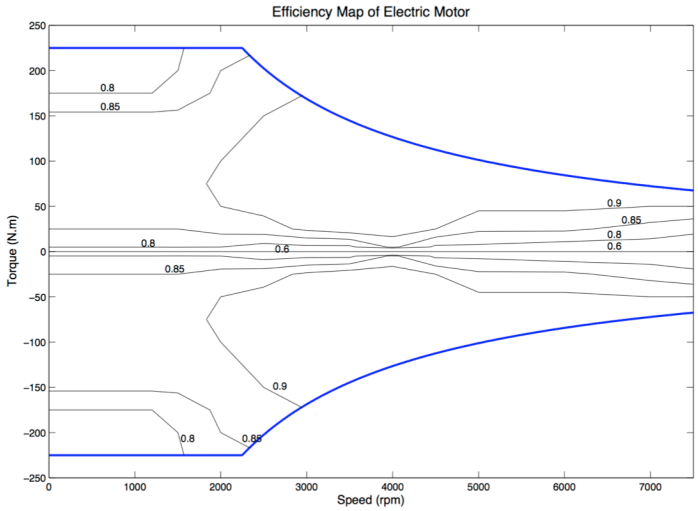

Figure 24: Torque-speed characteristic of the electric motor

4.2 Transmission

Due to the favourable torque-speed characteristic of the PMSM (see Figure 24), only a single gear transmission is necessary. The transmission must match the maximum speed of the motor with the maximum speed of the wheels.

$$i_g = \frac{n_{EM,max} * \frac{(2 * \Pi)}{60} * r_w}{V_{max}} \tag{4.5}$$

where

i_g = transmission ratio (-);

$n_{EM,max}$ = maximum velocity of the EM (rpm);

r_w = wheel radius (m);

V_{max} = maximum velocity of the vehicle (m/s).

4.3 ICE-generator unit

In a series PHEV, the ICE – generator unit commonly is used as 'back-up' energy source that only starts when the RESS is not anymore able to provide the required power. At the moment that the ICE is running, it is used at its most efficient point and the full RESS plays the role of peak power unit: when the power provided by the ICE is not able to meet the requirements of the driving cycle, the RESS supplies the difference. At moments that the ICE produces more power than necessary, the excessive power flows to the RESS to charge the battery and/or EDLC system.

The sizing of the ICE should be based on the average power demand for the drive cycle. The ICE has to be able to provide this power at its most efficient point and charge the RESS (slowly) during driving.

4.4 Batteries

During charge depleting mode (CD), batteries execute the same task as the ICE – generator unit during charge sustaining (CS) mode: they provide the average power to propel the vehicle (power requirement). The battery system also has to store a certain amount of energy in order to make sure that an acceptable distance can be driven (energy requirements).

The energy requirements of the battery system depend on the desired All Electric Range (AER) of the PHEV. In order to completely drive a certain driving cycle in all electric mode, the energy content of the battery system must at least be

$$W_{batt,mod} = \frac{P_{avg} * t}{3600} \tag{4.6}$$

where
W_{batt} = necessary energy content of the battery (kWh);
P_{avg} = average power required in the FTP cycle (W);
t = time to drive the driving cycle (s).

For example, the required energy content of the battery system for the NEDC is 2,68 kWh. Using the proposed 45Ah LFP battery cells (see Table 6), the amount of cells can be calculated by

$$n_{batt} = \frac{W_{batt,mod}}{W_{batt} * \Delta SoC_{batt}} = \frac{W_{batt,mod}}{C_{batt,ref} * U_{n,batt} * \Delta SoC_{batt}} \tag{4.7}$$

where ΔSoC_{batt} takes the operational SoC window of the battery (70%) into account. It results in one string of 26 battery cells in series. Such a battery system however does not make sense in PHEV applications. The battery system for a PHEV is in practice always larger. This battery pack would be designed to drive the NEDC (10,9 km), while the Chevrolet Volt for example has an AER of 56 km. To reach this distance, it contains 288 Lithium ion cells connected in three parallel strings of each 96 cells in series [46]. These strings of 96 cells produce a DC bus voltage of almost 360V. This high voltage bank has the advantage of lowering the current and thus lowering the ohmic losses. Moreover, as the electrical equipment in HEVs (converters, motor and generator) is designed at voltages of 330 or 360V, it is much more convenient to use a larger battery module. With this type of LFP battery cells, one string of 100 cells connected in series allows reaching 330V and results in a battery pack of 14,9 kWh of which 10,4 kWh is exploitable. Based on Table 4, where an overview of the commercial BEVs and PHEVs is presented, one can consider a battery pack of around 16 kWh as common practice. Extra strings can be added in order to enlarge the power capacity and double the energy content of the pack, but the cost, weight and volume of the battery pack also would double.

The conversion from battery cell parameters to module parameters is assumed to be ideal, while the battery management system, wiring resistance and contact resistance at the interconnections of the cells in reality create additional losses.

4.5 EDLC system

An EDLC system is used in a hybrid configuration with batteries in order to provide the peak power and reduce the stress on the battery. When one determines the size of the EDLC system, the required power and energy for these peaks have to be taken into account. To do this, the methodology presented in Figure 25 is followed [9].

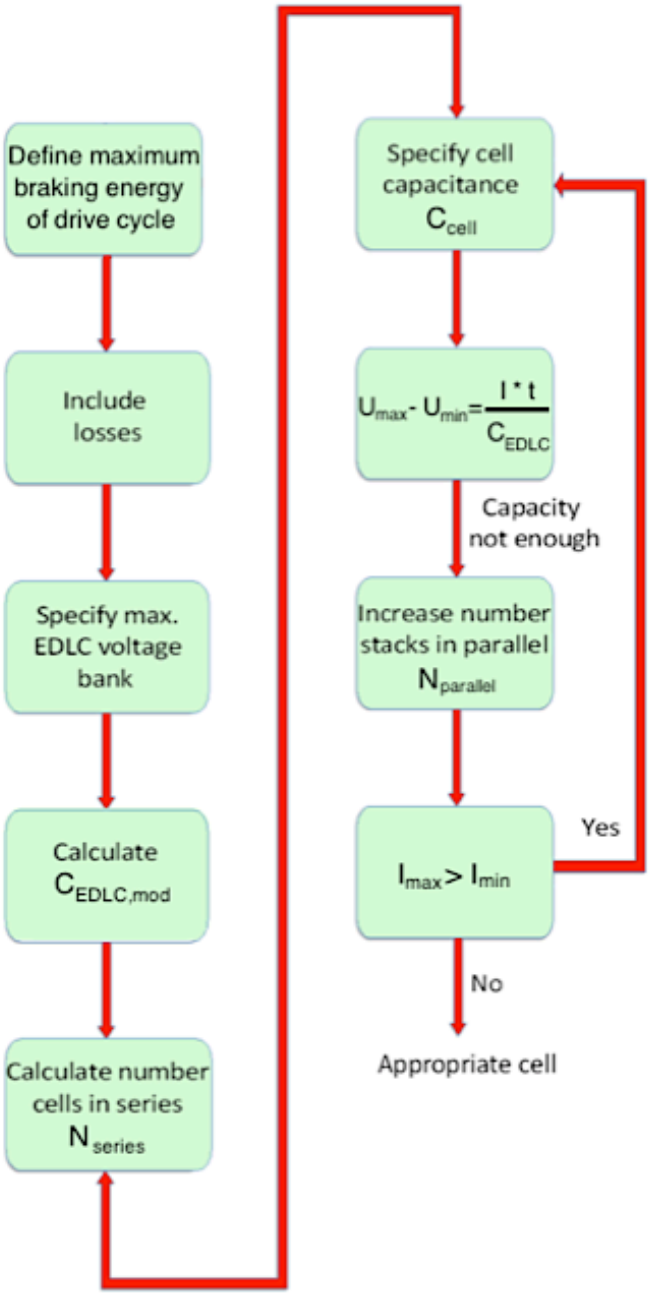

Figure 25: Methodology to dimension the EDLC system [9]

The maximum energy that has to be stored in the EDLC system is equal to the kinetic energy released during a full brake from the maximum velocity of the driving cycle to standstill:

$$W_{brake,max} = \frac{m * {V_{max}}^2}{2} \tag{4.8}$$

For the NEDC, the maximum velocity is 120 km/h what results in a kinetic energy of 186,3 Wh. Of this energy, maximally 60-65% can be collected and stored in the RESS [11]. The rest of the energy is lost due to rolling and aerodynamic resistances or dissipated in the components.

The maximum voltage bank of the EDLC system is dependent on the application. The ELDC voltage is specified by taking a discrete set of possibilities into account: Maxwell sells 125V modules containing 48 EDLC cells of 3000F. By connecting multiple of these modules in series, the bank voltage can be increased. The NEDC requires at least two modules of 125V and the EDLC system's capacitance becomes:

$$C_{EDLC,mod} = \frac{W_{brake,max}*2}{U_{n,EDLC,mod}{}^2} \tag{4.9}$$

The application on the NEDC results in a total capacitance of 23,7F for the EDLC system. The total system exists out of two modules of 48 cells that are connected in series [82]. In order to increase the EDLC voltage and minimize the ohmic losses, these two modules are preferably also connected in series. The cell capacitance can be calculated by equation 4.11

$$U_{n,EDLC,mod} = N_s * U_{n,EDLC} \tag{4.10}$$

$$C_{EDLC,mod} = \frac{N_p}{N_s} * C_{EDLC} \tag{4.11}$$

where
N_s = number of EDLC cells connected in series (#);
N_p = number of EDLC cells connected in parallel (#).

The calculated necessary cell capacitance becomes 2273F and justifies the choice of EDLC cells with a capacitance of 3000F, as it is the only possibility that is able to satisfy the energy requirements of the NEDC. The power requirements are checked by

$$U_{EDLC,max} - U_{EDLC,min} = \frac{I_{EDLC}*t}{C_{EDLC}} \tag{4.12}$$

where I_{EDLC} is the current through the EDLC system and t is the deceleration time of the full brake. If the total capacitance is not enough to store the charge released during the brake, an extra string must be connected in parallel to the existing string. As shown in Figure 25, the final check is to compare the current through the EDLC with the maximum allowable current through the EDLC. If the EDLC is under all circumstances of the driving cycle able to provide the required current, the cell is dimensioned correctly with respect to the energy and power requirements of the EDLC system. This application of this methodology on the NEDC, FTP-75 and HWFET resulted in an EDLC system configuration of two 125V modules containing respectively cells with a capacitance of 3000F, 1500F and 1500F[5].

[5] The 125V modules containing EDLC cells with a capacitance of 1500F or 2000F are theoretically considered in this master thesis to optimize the size of the EDLC cells but are not sold by Maxwell.

5 Results and discussion

5.1 Validation of the proposed model

The simulation results can now be compared to the official fuel economy rating of the Chevrolet Volt 2011. The rating is obtained by experimental verification of the fuel consumption for a certain driving pattern and is released by the United States Environmental Protection Agency (EPA). The EPA defines the fuel economy rating as a combination of the vehicle's fuel economy during city driving (FTP-75) and highway driving (HWFET driving cycle). The 'typical' driving behaviour in the USA is assumed as 55% city driving and 45 % highway driving, leading to the final fuel economy rating as defined in equation 5.1 [64].

$$FE_{final} = \frac{1}{\frac{0,55}{FE_{city}} + \frac{0,45}{FE_{hw}}} \tag{5.1}$$

where FE stands for fuel economy and is expressed in miles per gallon. To compute the city and highway fuel economy, the simulation model is run in a battery stand – alone configuration and the HVAC power demand is shut down, conform to the test procedures described by the EPA [83]. The official MPG data released by the EPA also use an adjustment factor in order to take non dynamometer effects (traffic, weather, road conditions,…) into account. For the specific cases of the FTP-75 and HWFET driving cycle, these factors are respectively 90% and 78% [64].

For Plug-in Hybrid Electric Vehicles (PHEVs), a distinction in fuel rating during charge depleting (CD) in all electric mode and charge sustaining (CS) is made. A comparison between the simulated equivalent fuel economy and the official fuel economy of the Chevrolet Volt 2011 is presented in Table 9.

Table 9: Official and simulated fuel economy of the Chevrolet Volt [83]

	Official Chevrolet Volt 2011	**Simulated results**		
		City	Highway	Combined
CD mode (all electric)				
FE (l/100 km)	2,53	2,26	2,04	2,16
AER (km)	56.3	52,1	66,8	57,8
CS mode				
FE (l/100 km)	6,36	6,20	6,36	6,27

One can observe that the simulated fuel consumption during CD in all electric mode is lower than the officially released fuel consumption of the Chevrolet Volt 2011. This discrepancy could be the result of the simplified modelling techniques combined with an underestimation of different parameters such as the rolling resistance coefficient, auxiliary power demand, the efficiencies of the components etc. The simulated All Electric Range (AER) resembles closely official AER of the Chevrolet Volt. This is due to battery pack chosen in this simulation. It has a slightly lower energy content, what contradicts the effect of the lower fuel consumption.

The good result of the CS fuel economy in comparison to the official rating was not expected as the topology of the drivetrain of the Chevrolet Volt (see Figure 26) is not exactly the same as the series topology used in the proposed model. Although different sources refer to the Chevrolet Volt as a Series PHEV (for example in [19], [31] and [69]), it actually also contains a planetary gear that allows the Internal Combustion Engine (ICE) to directly power the wheels – cfr. the combined series parallel hybrid topology - instead of flowing through the generator, converters and electrical motor (EM). This feature allows reducing the losses in the components of the drivetrain during CS mode and is also used when the vehicle is driving faster than 110 km/h in CD mode [46].

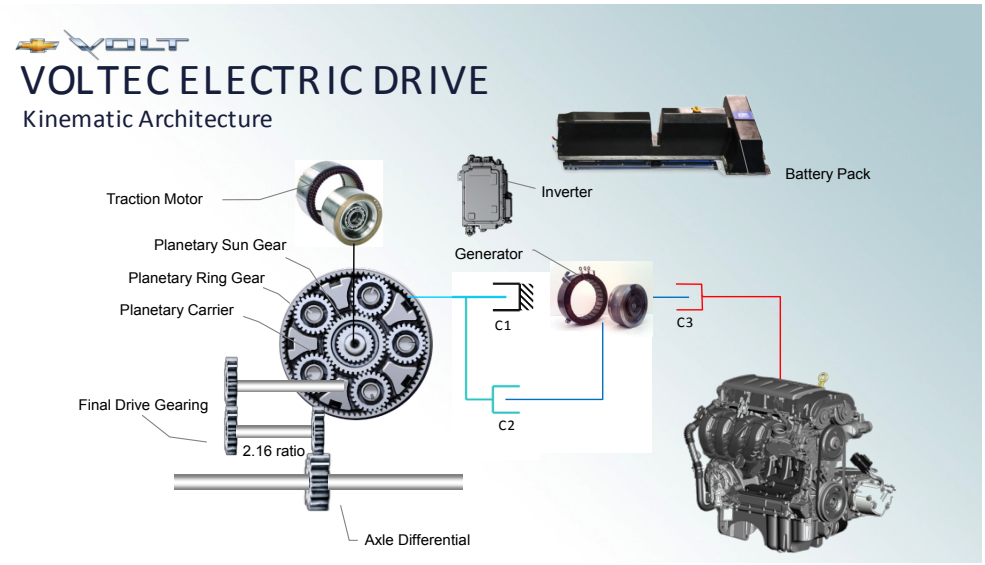

Figure 26: Chevrolet Volt's drivetrain [46]

5.2 Optimization of the hybrid RESS

The general control principles of the hybrid RESS are explained in 3.4.2.2 RESS control strategy. The behaviour of the battery and Electrical Double Layer Capacitor (EDLC) system still has to be optimized by choosing the proper design parameters. The most important one is the time constant of the low pass filter. In this section, its influence on the lifetime, efficiency and size of the RESS is examined more in detail while keeping in mind the cost of the total RESS.

5.2.1 Influence time constant of low pass filter

The time constant of the low pass filter regulates the distribution of the power between the battery and the EDLC system. It controls how fast the moving average power provided by the battery system changes. A large time constant smoothens the battery power and reduces the battery peak power and stress, improving the lifetime of the battery pack. However, the EDLC system must be dimensioned larger to handle the enlarged peaks. This results in a larger weight, volume and cost of the RESS. In order to define the optimal design constants, an improvement factor is calculated to analyse the benefits of the hybrid RESS.

For these three cases, the optimal time constant of the low pass filter is defined by calculating the improvement factor for each time constant. To define the improvement factor, the battery current, the RESS efficiency, the EDLC performance (power and energy) and the acceleration profile of the driving cycle are examined for a specified EDLC system.

To take the effect of the time constant on the battery current into account, the root mean square (RMS) battery current is calculated for both the stand-alone battery system and hybrid RESS. The relative improvement of the RMS battery current is calculated by

$$I_{RMS,impr} = \frac{I_{RMS,s-a} - I_{RMS,hybrid}}{I_{RMS,s-a}} * 100 \quad (5.2)$$

In the same way, the relative improvement in RESS efficiency can be calculated (equation 5.5). The efficiency of the stand-alone system takes the internal heat losses in the battery into account, while the losses in the DC-DC converter and EDLC system are added for the hybrid system.

$$\eta_{impr} = \frac{\eta_{hybrid} - \eta_{s-a}}{\eta_{s-a}} * 100 \quad (5.3)$$

These relative improvement factors are supplemented by a penalty factor for the EDLC performance. This penalty factor is introduced in order to take the moments that the EDLC system is not able to deliver the required power into account. This loss of performance mainly occurs at moments that the voltage of the EDLC system is close to its constraints (see 3.4.2.2.3 Constraints). The penalty factor is defined as

$$PF = \frac{P_{EDLC} - P_{EDLC,lim}}{P_{EDLC}} \quad (5.4)$$

where
PF = penalty factor (-);
P_{EDLC} = Power demand of the EDLC system, defined by the control strategy (kW);
$P_{EDLC,lim,}$= Constrained power that practically can be provided by the EDLC system (kW).

Finally, starting from the acceleration profile of the examined driving cycle, the distribution of the acceleration time is calculated and added in order to match the acceleration time with the operating time of the EDLC. The total improvement factor becomes

$$Impr = w_1 * I_{RMS,impr} + w_2 * \eta_{impr} - w_3 * PF + w_4 * Acc \quad (5.5)$$

where
Impr = Total improvement factor (-);
Acc = Distribution of the acceleration time (-);
w_i with i= 1,..,4 = weighting factor (-).

As the last two terms in equation 5.5 can not be defined relative to the battery stand-alone system, the introduction of a weighting factor is necessary in order to scale the outcome of the penalty factor and acceleration time distribution with the relative terms. The weighting factors are experimentally defined.

5.2.2 Result optimization time constant

Figure 27 shows the improvement factor in function of the time constant is shown for the three driving cycles with each their specific size as calculated in 4.5 EDLC system.

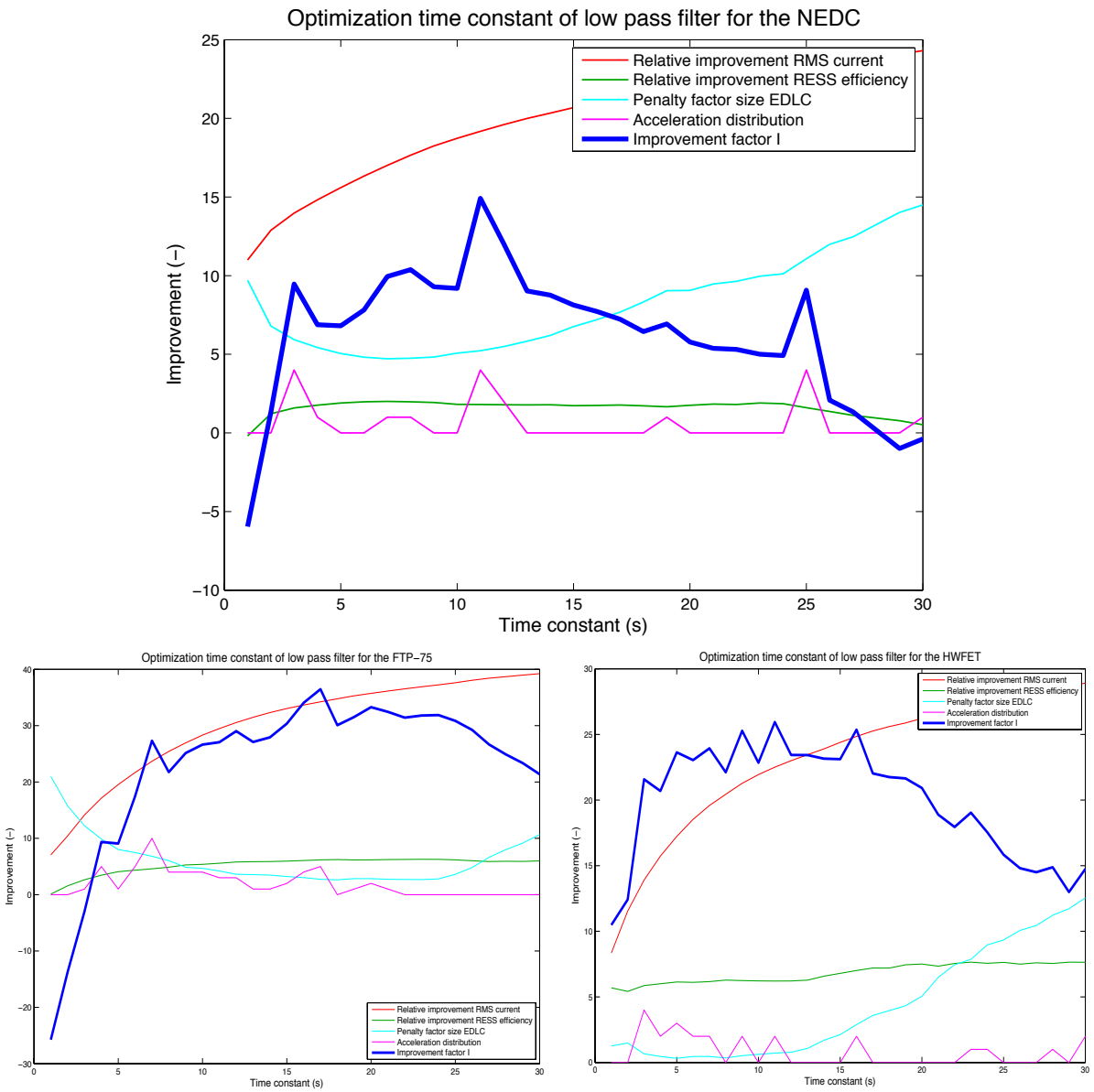

Figure 27: Optimization time constant filter for the NEDC (up), FTP-75 (under left) and HWFET (under right)

It results in an optimal time constant of 11s, 17s and 11s for respectively the NEDC, FTP-75 and HWFET. These results are comparable to the time constants retrieved in literature that vary between 8 and 16s [14,39,75]. The large time constant of the FTP-75 is due to the dimensioning method, in which the calculated required cell capacitance is matched with a discrete set of existing EDLC cell capacitances. It led to a slightly over-dimensioned EDLC system in terms of energy requirements. One could thus consider reducing the energy content of the EDLC module by using cells with a lower capacitance or by using only one module of 125V. The first option however can cause problems vis-à-vis the power requirements, while the latter option would double the step up ratio of the DC/DC converter. The step up ratio of an interleaved multichannel DC/DC converter however should be limited to four [72], what wouldn't be guaranteed by only using one module of 125V.

Other conclusions that can be drawn are:

- At the optimal time constant of 11s, the penalty factor for the NEDC is not zero. This is due to the definition of the voltage limit of the EDLC cells: the soft voltage limit makes sure that the SoC of the EDLC system doesn't drop below 25% or surpasses 100%. This soft limit imposes its constraint when power is drawn from the EDLC system with a SoC smaller than 30% or when power is sent to the EDLC system at a SoC higher than 95%.
- The relative improvement of the RESS efficiency and battery RMS current are positive for the optimal time constant in the three different case studies. This corresponds with the expectations and the results found in literature [9,40].

5.3 Simulation results

In the previous sections, the basic design principles of the drivetrain's components and control strategy have been presented and validated. The validated model now is applied to the three considered driving cycles in order to analyse the power flows in the hybrid RESS and compare the performance of the battery stand alone-system with that of the hybrid RESS. The performance in this case refers to energy content, power capacity, lifetime, efficiency and cost. The figures that are presented below are all the result of the application of the NEDC, while the tables contain information of all the driving cycles. The interested reader can find the figures of the simulations applied to the FTP-75 and HWFET in the annex.

5.3.1 Power flow in hybrid RESS

The distribution of the load between the different energy sources of the active hybrid RESS is shown in Figure 28 and Figure 29, where the latter presents a zoom on the first 200s (ECE drive cycle). The ICE was not used when only following the NEDC once as the State of Charge (SoC) of the battery system did not drop below 30%. The power provided by the battery system is mainly the moving average power coming from the low pass filter, modified by the SoC controller of the EDLC system and by the constraints on the battery and EDLC system. The EDLC system provides the difference between the total power demand and the battery power. The effect of the auxiliary power, which is modelled as a constant power demand during the whole driving cycle, becomes clearly visible during idling.

One can notice that the peak power of the EDLC system during the brake around 1140s is more than 60 kW. The low SoC at that moment results in a low output voltage of the EDLC system and a peak current of 381A through the EDLC system. All the released energy during this peak can thus be stored in the EDLC system without dissipating any of the available energy mechanically, as the peak current is below the limit of 400A. One can also remark that the peak power during braking is in general larger than the peak power during accelerations. In the latter situation, the acceleration is divided between the battery and the EDLC system while the power sent to the EDLC system during a deceleration is partly coming from the braking energy and partly from the battery that was delivering traction energy before the brake. This is also the reason why the battery is addressed to store braking energy around 1150s. The EDLC system collects all the braking energy and the additional power delivered by the battery in the beginning of the brake. The result is that the SoC of the EDLC system has risen rapidly during the deceleration and cannot store all the braking energy. During the remainder of the deceleration, the battery system stores the rest of the braking energy.

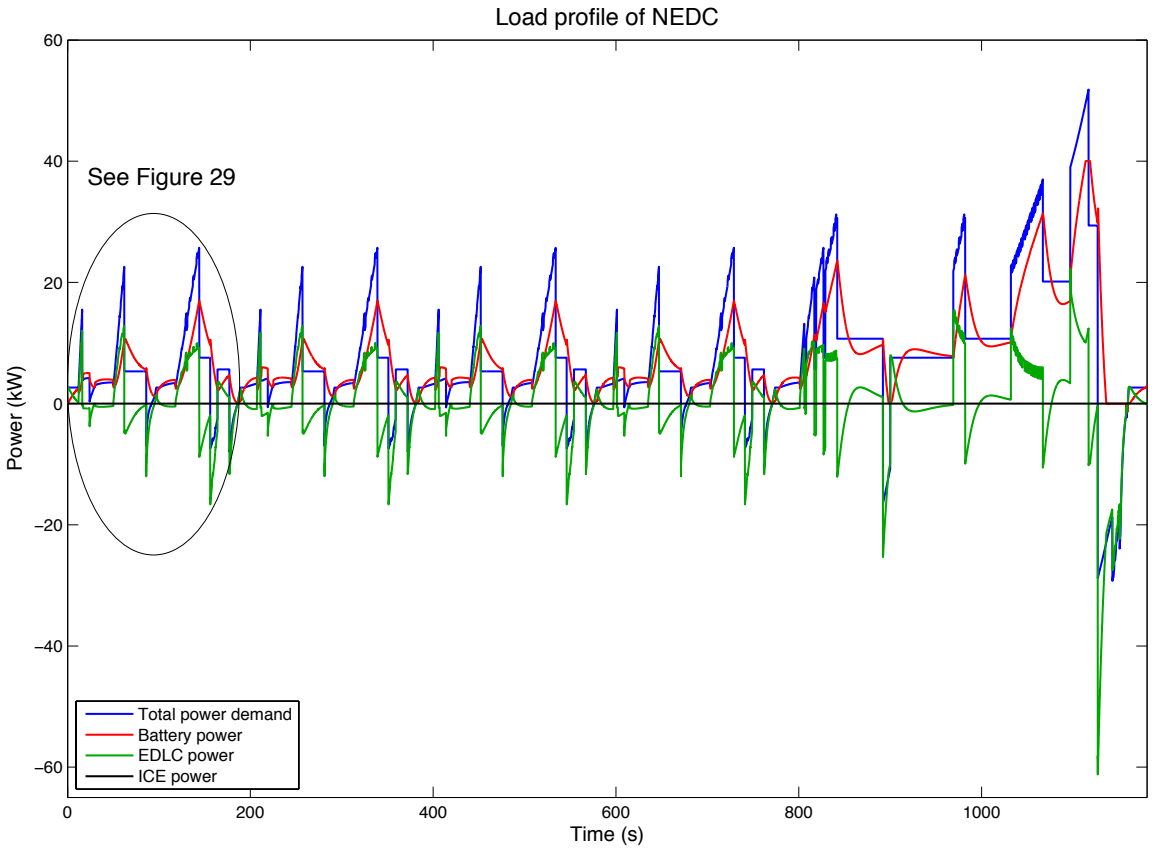

Figure 28: Load distribution between the energy sources during NEDC

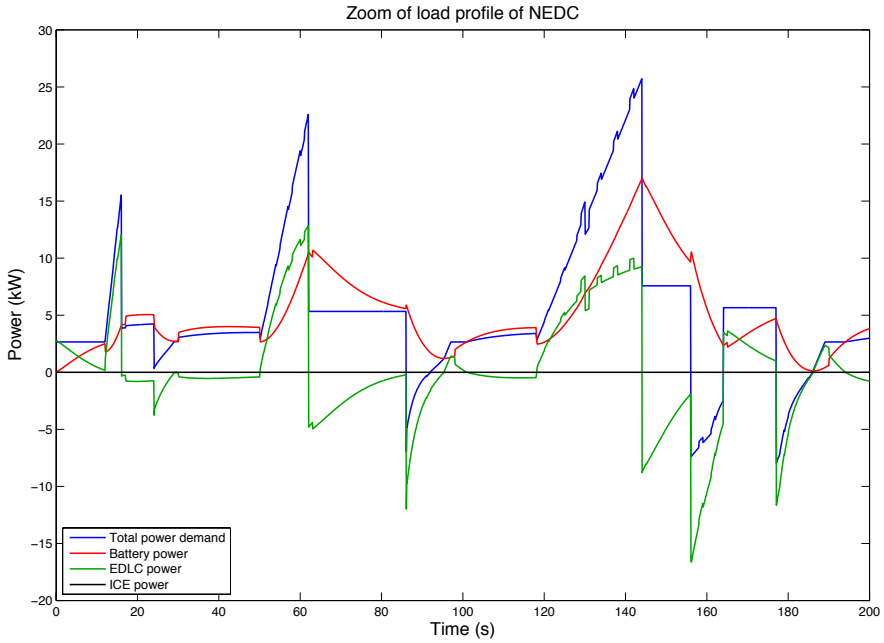

Figure 29: Zoom on load distribution between the energy sources during NEDC

Figure 30 shows the SoC evolution of the EDLC system during the NEDC. It proves that the EDLC system never leaves its safe operating region: its SoC never exceeds 100% or drops below 25%. The effect of the SoC controller can also be seen during idling. The SoC controller causes a power flow between the battery and EDLC system in order to make sure that the SoC matches the reference SoC and ensures its performance during the drive.

The battery system is not charged during the execution of the NEDC (except shortly around 1150s) because of the control strategy that sends all the regenerative braking energy to the EDLC system. This is translated in a monotonically decreasing battery SoC. By driving the NEDC multiple times, the SoC finally will drop to 30% and the ICE will start delivering. This power will be used to propel the PHEV and to charge the battery conform the Engine on/off strategy.

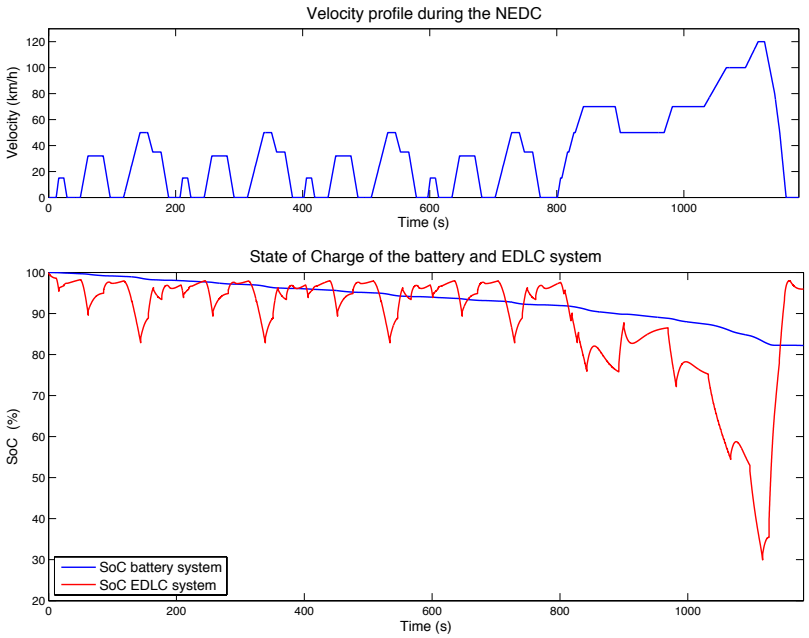

Figure 30: State of Charge evolution of the EDLC system during the NEDC

5.3.2 Comparison stand-alone and hybrid RESS

The most important performance characteristics of the RESS vare presented in Table 10. These parameters allow making a comparison between the battery stand-alone system and the hybrid RESS in terms of power capability, efficiency, lifetime and cost. Due to the low specific energy of EDLC cells, the energy content of the RESS is not changed significantly (energy content of the EDLC system is 273 Wh, what corresponds to 1,8% of the battery's energy content of 14,9 kWh) and is not further analysed.

Table 10: Comparison battery stand-alone and hybrid RESS performance

	NEDC		FTP-75		HWFET	
	Stand-alone	**Hybrid**	**Stand-alone**	**Hybrid**	**Stand-alone**	**Hybrid**
W_{tot} (kWh)	2,65	2,67	4,26	3,96	2,77	2,65
W_n (l/100km)	2,72	2,74	2,69	2,50	1,88	1,81
AER (km)	42,0	42,6	42,6	47,0	60,9	64,8
$I_{batt,max}$ (A)	135	135	135	83,4	135	95,1
$I_{batt,RMS}$ (A)	40,3	33,7	43,4	28,6	53,8	43,3
η_{RESS} (%)	88,2	89,6	81,6	88,8	86,1	90,9
$\Delta V_{DC\text{-}bus}$ (V)	55,6	35,7	53,4	31,4	58,0	39,6
Alert[6] (#)	6	0	53	0	14	0

[6] Represents the amount of times that the forward model has to adjust the velocity of the driving cycle due to the constraints on the components of the drivetrain

5.3.2.1 Power capability

When running the simulation in a battery stand-alone configuration, a first observation is that the required velocity of the NEDC cannot be guaranteed at all time. The constraints of the energy-optimized battery are too tight to ensure the desired performance. For example, around 1110s, the imposed velocity cannot be met and the forward calculation adapts the theoretical velocity profile into the maximal feasible velocity (see Figure 31 and Figure 32). The decrease in velocity also causes a lag in distance that has to be eliminated by a time period in which the velocity of the vehicle is higher than the required velocity. The parameter 'alert' in Table 10 reflects the shortcomings in terms of power deliverable by the RESS by counting the situations at which the velocity of the drive cycle cannot be followed.

The limitation of the 3C rate causes a problematic situation at the highlighted moment around 1110s. This constraint limits the available power of the battery:

$$P_{max,batt} = I_{batt,max} * U_{n,batt} = 135A * 330V = 44{,}8\ kW \quad (5.6)$$

Additionally, the limitation on the current slope of the battery system also causes inconveniences with respect to the acceleration performance. To overcome these inconveniences, a second string could be connected in parallel to the current battery system. This would double the current through the battery system and thus doubling the power capability of the battery pack. However, its trade off in terms of weight (extra mass of 220kg), volume (66 dm^3) and cost (9979 €) makes this option inconvenient for the analysed application. Increasing the maximal battery current and current slope could also improve the power performance of the battery stand-alone system, but would have a negative impact on the lifetime and could cause safety problems due to the increasing dissipated energy ($P_{diss} = R_i * I^2$).

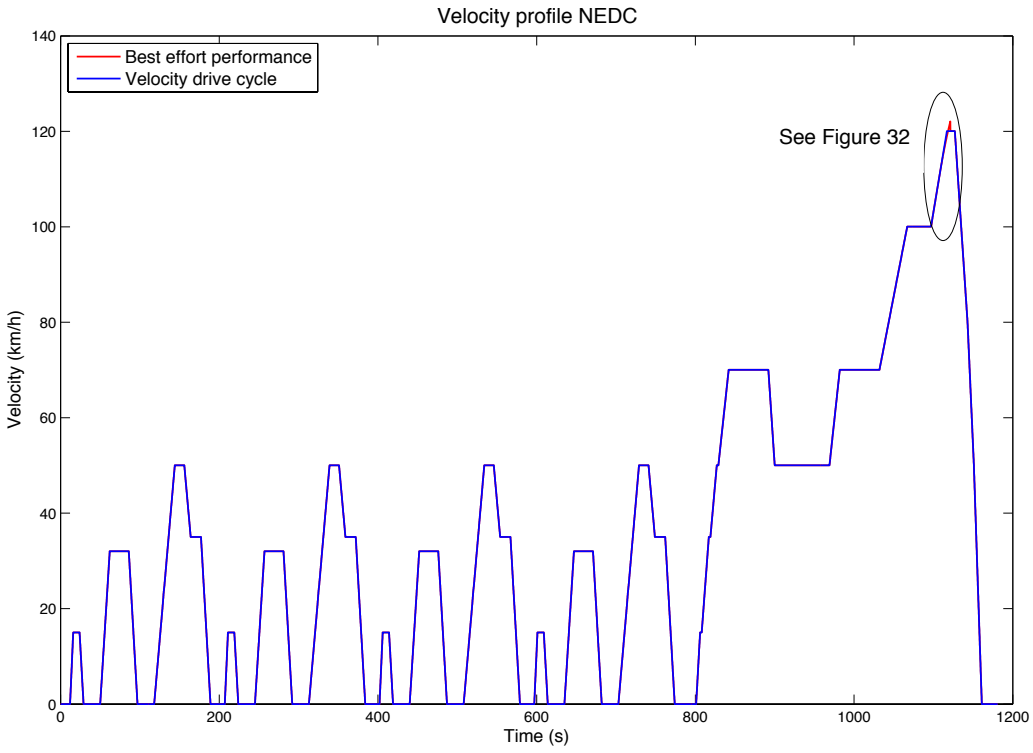

Figure 31: NEDC velocity profile and influence forward method

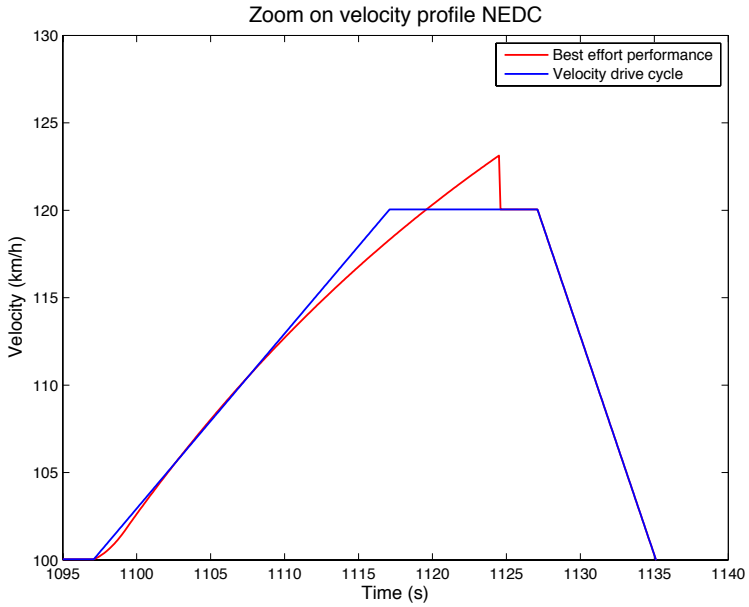

Figure 32: Zoom on alert in NEDC velocity profile

As Table 10 indicates, there is also a large variation in alerts between the different driving behaviours. The NEDC only encounters 6 problematic moments, while the FTP-75 faces the same problem 53 times. This is mainly due to the higher accelerations that are demanded often during the FTP-75. They cause too steep battery current variations in the battery stand-alone system.

The addition of the Peak Power System (PPS) in the shape of a DC/DC converter and EDLC system significantly enhances the RESS performance in terms of power. Not one alert is shown for either of the driving cycles. The fast reaction time of the EDLC cells allows ignoring the current slope of the EDLC system and the current limit of 400A makes it possible to provide a peak power of 54,7 kW even at the minimum voltage $V_{EDLC,max}/2$ with the EDLC system only.

5.3.2.2 Efficiency

In literature, a distinction between coulomb efficiency and energy efficiency is made to evaluate batteries. They describe respectively the capacity losses and energy losses during a cycle of discharging and charging up to the initial SoC and are defined by

$$\eta_C = \frac{Q_d}{Q_c} = \frac{I_d * t_d}{I_c * t_c} \tag{5.7}$$

$$\eta_w = \frac{W_d}{W_c} = \frac{I_d * \int_0^{t_d} V_d * dt}{I_c * \int_0^{t_c} V_c * dt} \tag{5.8}$$

where η denotes the efficiency (%), Q the capacity (C) and W the energy (J) during discharging (d) and charging (c) [14]. The coulomb efficiency is taken into account by introducing a factor of 99% [84] to the coulomb counter that computes the SoC of the battery system. The power dissipation in the internal resistance is used to calculate the energy efficiency.

In 5.2 Optimization of the hybrid RESS, the remark is made that the efficiency of the RESS increases by adding the EDLC system. This remark only denotes the energy efficiency and is also shown numerically for the three driving cycles in Table 10. The energy efficiency of the total RESS is calculated by

$$\eta_{RESS} = \frac{W_{tot} - W_{DC-bus}}{W_{tot}} \tag{5.9}$$

where W_{tot} is the total energy provided by the energy sources during the drive cycle and $W_{DC\text{-}bus}$ denotes the energy required at the DC-bus. The difference is per definition the energy lost in the RESS. The energy efficiency of RESS increases respectively by 1,6%, 8,8% and 5% for the NEDC, FTP-75 and HWFET. These results show the same trend as the results retrieved in literature: Hadartz and Julander presented an efficiency increase of 2,5% of the active hybrid RESS [39], Wu et al. obtained a 3,5% efficiency improvement [40] and Omar et al. achieved a driving range extension of 7% in [9]. The more pronounced improvement in efficiency in this master thesis could be the result of the current rate limiter of the battery systems, which limits the amount of energy that can stored during sudden variations of the battery power demand. This is also the reason why the improvement of the energy efficiency for the FTP-75 is that pronounced. To my knowledge, this effect is not taken into account in the articles mentioned above. The increase in efficiency of the hybrid RESS is also due to the decrease of dissipated energy in the battery system. The decrease in battery RMS current in the hybrid system can clearly be seen in Table 10 and Figure 27. The corresponding losses thus decrease quadratically with the current:

$$W_{diss} = \int_0^{t_{end}} P_{diss} * dt = \int_0^{t\_end} R_{int} * I_{batt}^2 * dt \tag{5.10}$$

The effect of the magnitude of the battery current on the energy efficiency of the battery system is shown in Figure 33. One can thus remark that the efficiency improvement will drop when a power-optimized lithium ion battery is used instead of an energy-optimized lithium ion battery, due to the higher limitations on the current slope of the battery system. Another important remark is that although the improvement in energy efficiency, the final consumption during the NEDC is larger for the hybrid RESS thanks to the additional weight of the EDLC system.

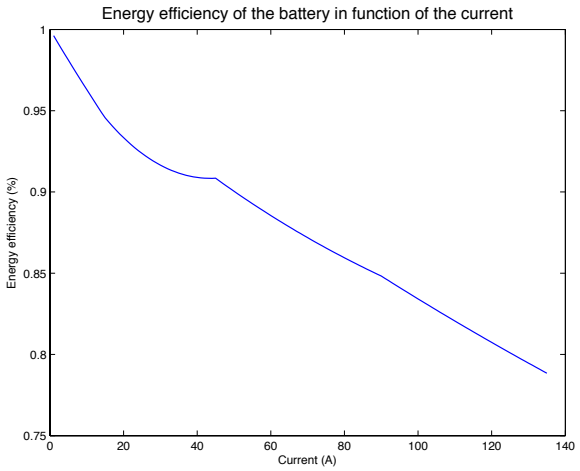

Figure 33: Energy efficiency of the battery in function of the current

5.3.2.3 Regenerative braking efficiency

In this section, the effect of the regenerative braking performance of the RESS on the improvement in energy efficiency is analysed more in detail. Four parameters are used to characterise the regenerative braking performance, based on the methodology described by Van Sterkenburg et al. in [85]:

• Brake factor (BF) is defined as the ratio of the brake energy and the propulsion energy measured at the wheels:

$$BF = \frac{W_{brake}}{W_{propel}} \tag{5.11}$$

Its value depends on the driving cycle and vehicle properties that define the power requirements at the wheels, such as the drag coefficient and rolling resistance coefficient.

Table 11 indicates that city driving, such as the FTP-75, results in a relatively high BF compared to highway driving (HWFET).

• Vehicle Propulsion Efficiency (VPE) indicates the efficiency of the vehicle when the energy sources supply power to propel the vehicle. It is also called battery-to-wheel efficiency and depends on the efficiencies of the components in the drivetrain (transmission, converters, EM, RESS).

$$VPE = \frac{W_{propel}}{W_{source,propel}} \tag{5.12}$$

where

$W_{source,propel}$ = amount of energy supplied by the energy sources during the driving cycle (kWh).

• The Vehicle Regeneration Efficiency (VRE), also called wheel-to-battery efficiency, denotes the efficiency of the conversion of braking energy into useful energy stored in the RESS.

$$VPE = \frac{W_{reg}}{W_{brake}} \tag{5.13}$$

where

$$W_{reg} = W_{source,reg} + W_{aux,reg} \tag{5.14}$$

and

$W_{source,reg}$ = part of the regenerated braking energy that is stored in the RESS (kWh);

$W_{aux,reg}$ = part of the regenerated braking energy used to drive the auxiliary power (kWh).

• System Regeneration Factor (SRF) is the ratio of the regenerated braking energy and the energy supplied by the energy sources while propelling it. The SRF shows the reduction in energy consumption thanks to the storage of regenerative braking energy.

$$SRF = \frac{W_{reg}}{W_{source,propel}} = BF * VPE * VRE \tag{5.15}$$

Table 11: Regenerative braking factors

	NEDC		FTP-75		HWFET	
	Stand-alone	**Hybrid**	**Stand-alone**	**Hybrid**	**Stand-alone**	**Hybrid**
BF (-)	35,0	35,8	53,0	53,5	29,8	30,4
VPE (-)	56,1	56,3	57,4	59,3	62,4	63,9
VRE (-)	58,6	66,5	53,4	63,8	46,6	57,0
SRF (-)	11,5	13,4	16,2	20,3	8,9	11,3

The remarks and conclusions that can be drawn from the results in

Table 11 are:

- The BF for stand-alone and hybrid RESS applied on one driving cycle should be equal to each other as it does only depend on the driving cycle and vehicle parameters. The difference that can be noted originates from the change in the velocity profile thanks to the forward simulation model and the additional weight of the EDLC system.
- The SRF is in the three cases larger for the hybrid RESS in comparison to the battery stand-alone system. One can observe that the improvement in SRF in mainly thanks to an increase in VRE for the hybrid RESS. This is due to the control strategy that preferably sends all the braking power to the EDLC system. The EDLC system is characterised by a lower internal resistance, limiting the dissipated power in the EDLC system and thus causing an increase of the efficiency of the RESS during braking.
- A significant variation in SRF can be noticed for different driving behaviours. The application of the FTP-75, that models city driving, results in almost a doubling of the SRF in comparison with the HWFET. This proves that regenerative braking is much more interesting for applications mainly subjected to city driving.
- One can also remark that the VRE is higher than the VPE when looking at the NEDC and FTP-75. This can be explained by the use of efficiencies for the components in the drivetrain that are defined equal in both directions. The control strategy sends all the regenerative braking power to the EDLC system, causing an increase in VRE thanks to its very low internal resistance.

5.3.2.4 Cycle life

An accurate analysis of the cycle life of a battery system is very complex. The ageing of a battery system is affected by a number of parameters, such as non-ideal temperature, DoD, charge and discharge current, battery stress etc. Some of these factors cause only temporary capacity losses, while others can reduce the battery's capacity permanently or damage the cell [86]. A possible approach to analyse the lifetime is to define the State of Health[7] (SoH) of a battery system. However, no general definition of the SoH of a lithium ion battery exists up to today due to the complexity [28,39,86]. Hence, most of the cycle life analyses of batteries are performed experimentally. In this master thesis, only the effect of the change in maximum current is used to examine the lifetime of the battery system. This allows numerically visualising the trend of the extended cycle life of the battery system, but should not be looked at as a final conclusion of the lifetime analysis of the battery system as it is not accurate enough.

[7] The SoH indicates the state of the battery between the beginning of life and end of life in % [86]

In order to analyse the lifetime of the battery system, the cycle life at the DoD of 70% needs to be estimated. Figure 16 already showed the experimentally defined cycle life of the LFP battery cell after discharging the cell up to 100% DoD. Based on the exponential relation between the lifetime of lithium ion batteries and the DoD described in [87], the lifetime for the different discharge rates at 70% can be calculated (see Figure 34). The cycle life at the specified SoC window becomes 2365, 1833 and 1723 cycles at respectively a maximum discharge rate of 1C, 2C and 3C. By interpolation of these results with the maximum current reached during each driving cycle, the cycle life of the simulated battery system can be estimated. The results are presented in Table 12.

Table 12: Battery cycle life improvement in hybrid RESS

	NEDC		FTP-75		HWFET	
	Stand-alone	**Hybrid**	**Stand-alone**	**Hybrid**	**Stand-alone**	**Hybrid**
$I_{batt,max}$ (A)	135	135	135	78,5	135	89,3
Cycle life (#)	1723	1723	1723	1910	1723	1820
Improvement (%)		0		10,9		5,6

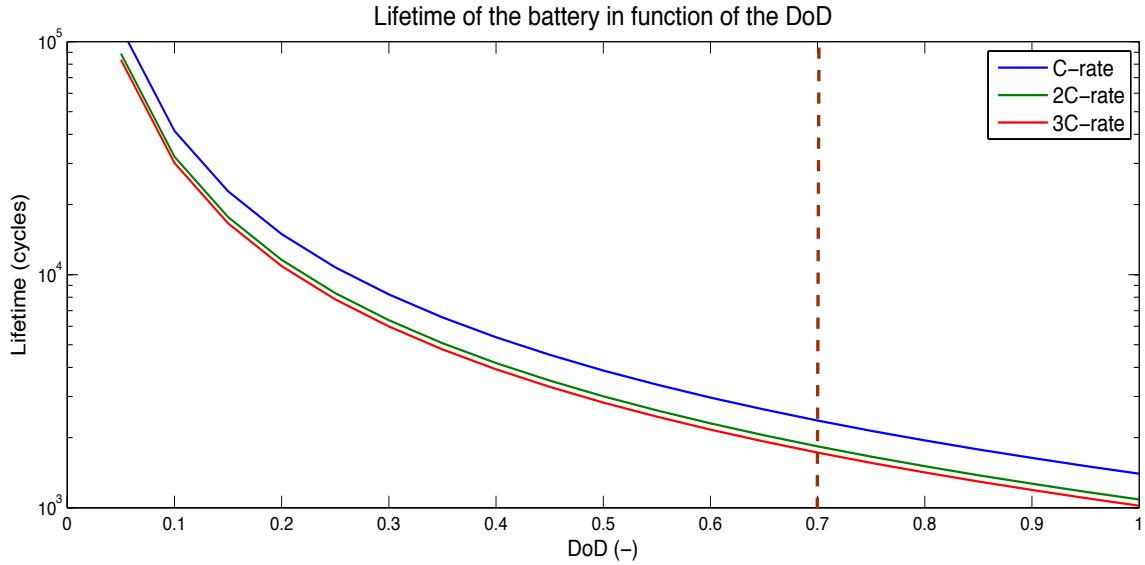

Figure 34: Battery lifetime in function of the DoD

One can conclude that the cycle life extension is significant for both the FTP-75 and HWFET. The remark has to be made that the filter time constant of 17s used in the FTP-75 benefits the reduction of the battery current in comparison to 11s used in the NEDC and HWFET. However, according to the results in Table 12, no improvement in the cycle life of the battery is observed for the NEDC although Figure 35 shows clearly the beneficial effect of the PPS on the battery current. The reason why the battery current still reaches is upper limit is that the power demand stayed high for a time period which is longer than the time constant of 11s.

Figure 35 thus shows the lack in accuracy of the result when only regarding the maximal battery current. In order to make a correct statement about the cycle life extension, a deeper examination should be executed and validated with experiments.

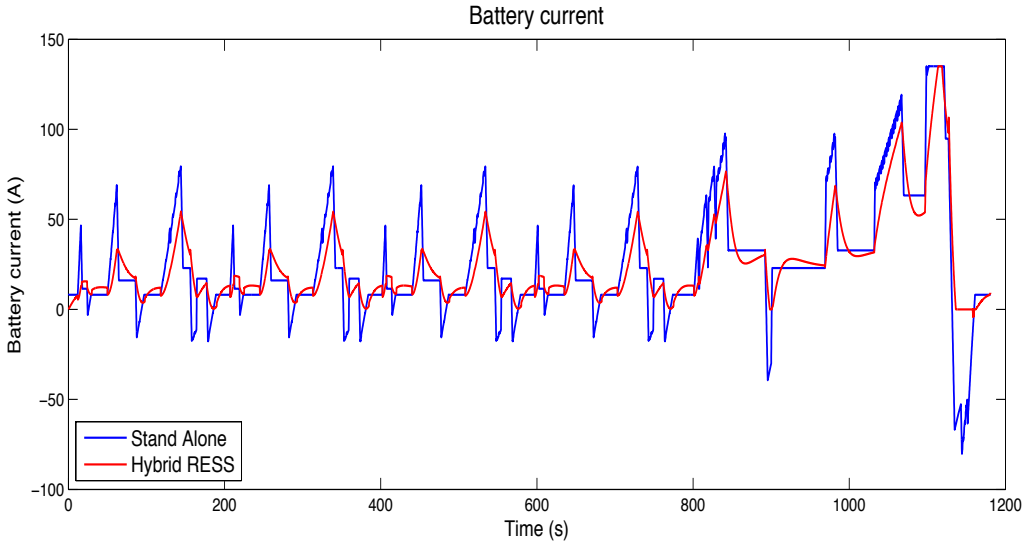

Figure 35: Battery current during NEDC

5.3.2.5 Cost, weight and volume

The cost of the RESS is one of the main challenges for PHEVs in order to become competitive with conventional cars. According to a report of the Boston Consulting Group [29], the current price of the battery system is 1000-1200$/kWh or 924-771€/kWh[8]. They also report a steep decline in price up to 2020 thanks to an increase in production of batteries and estimate that the price drops to 500$/kWh (or 385€/kWh) by 2020 [29]. A report of Element Energy defines the current price as 800$/kWh or 616€/kWh [27]. To simplify the computations, 800 €/kWh is used in this master thesis. The typical price of an EDLC cell is 0,01€/F, while the DC/DC converter used to control the power flow adds another 2000 to 3000 € to the price of the RESS [9].

The hybridization of the RESS also increases the mass and volume challenges for PHEVs. In the pursuit of minimizing the fuel consumption of a vehicle, weight is a very important parameter in order to minimize acceleration force and rolling resistance, while volume restrictions present tight boundary limits for the placement of the components of the electrified drivetrain. The battery pack exists out of individual cells and a battery management system (BMS), casing and cooling system. One battery cell has a volume of 16,5 x 27,5 x1,3 cm^3. The mass and volume of the pack are calculated by taking into account 100 battery cells, a volume-packing factor of 90% for pouch cells [28] and a factor two for the extra mass of the mass of the module (294 kg for the pack [88] compared to 152 kg for the individual cells [89]).

The mass and volume of the EDLC system is obtained out of Maxwell's datasheet of the 125V module containing EDLC cells with a capacitance of 3000F [82]. Its mass is 60,5 kg and its volume is 61,9 x 42,5 x 26,5 cm^3. The mass and volume of the packs containing cells with a capacitance of 1500F and 2000F is obtained by scaling these results with respectively the mass and volume of the 48 individual cells. The interleaved four channel DC/DC converter adds another 4 kg to the mass and 2860 cm^3 to the volume of the RESS system [72].

[8] exchange rate of 13/05/2013 [90]

Table 13: Comparison of weight and volume of the stand-alone and hybrid RESS

	NEDC		FTP-75		HWFET	
	Stand-alone	**Hybrid**	**Stand-alone**	**Hybrid**	**Stand-alone**	**Hybrid**
Cost (€)	11880	17260	11880	15820	11880	15820
Mass (kg)	200	325	200	270	200	270
Volume (dm³)	66	208	66	154	66	154

Table 13 shows the significant increase of the final cost, mass and volume of the hybrid RESS in comparison with the battery stand-alone system. Although an improved lifetime and efficiency are observed, the increased investment cost of the hybrid RESS is too high to implement it currently in passenger vehicles. The volume of the RESS is also an important issue, as the electrified drivetrain of a PHEV already demands for an optimal use of the available space in order to add the battery system and EM. The large dimensions of the EDLC system thus clearly cause extra challenges for the volume and placement of the components in a passenger car. The good power capability and less tight volume requirements make EDLC systems currently only a valid choice for heavy transport applications like buses [11], trams and metros [9].

5.3.2.6 DC-bus voltage

Another important beneficial effect of the hybrid RESS is the reduced variation of the DC-bus voltage. A stable DC-bus voltage improves the driveline efficiency. A stable DC-bus voltage allows the EM to work in stable voltage window, improving the operation of the EM. The difference in DC-bus voltage between the battery stand-alone and hybrid RESS is shown in Figure 36.

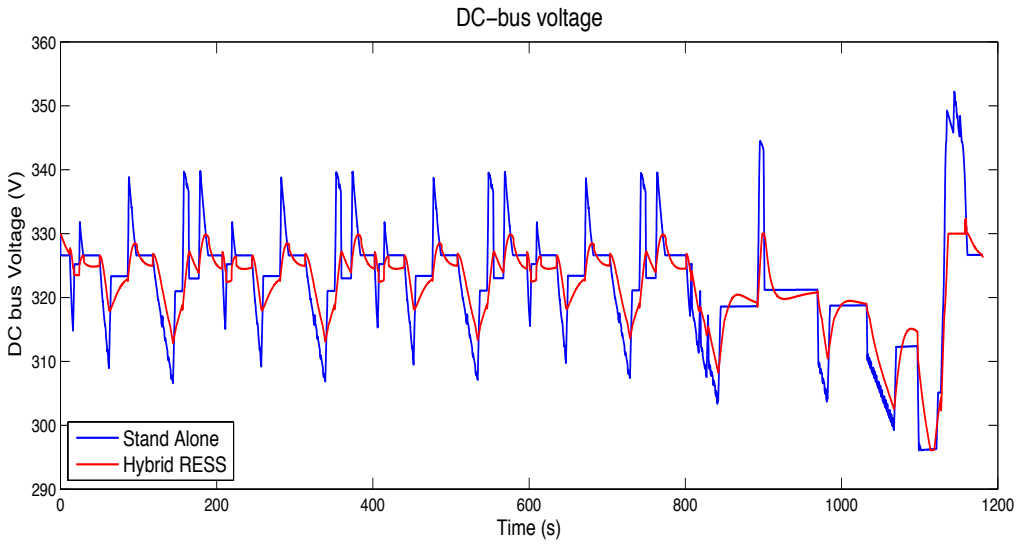

Figure 36: DC-bus voltage of the battery stand-alone and hybrid RESS during the NEDC

6 Conclusion

In this master thesis, a model of a Series Plug-in Hybrid Electric Vehicle (PHEV) has been proposed. From an extensive literature review it was concluded that the lithium ion batteries currently used as Rechargeable Energy Storage System (RESS) of PHEVs still face challenges in terms of energy content, power capability, cycle life, efficiency, safety and cost. The comparison of the battery goals proposed by the United States Advanced Battery Consortium (USABC) and Electric Power Research Institute (EPRI) clearly showed that none of the existing lithium ion technologies is currently able to meet these requirements. Moreover, optimizing a lithium ion battery for one of these characteristics inherently results in a trade – off towards one of the other parameters. To overcome this inconvenience, an Electrical Double Layer Capacitor (EDLC) system can be introduced as peak power system. Combining an energy-optimized lithium ion battery with an EDLC system is an interesting option to improve the performance of the RESS.

The proposed model is implemented in the Matlab/Simulink environment with the aim to analyse the characteristics and performance of the active hybrid RESS and compare it to the performance of a battery stand – alone system. The control strategy in the hybrid RESS aims at allocating the power peaks to the EDLC system and the average power to the battery system, while ensuring appropriate State of Charge (SoC) level of the EDLC system. A methodology to optimize the time constant of the low pass filter has been proposed.

The simulation results prove the enhanced performance of the hybrid RESS in terms of power capability, cycle life, energy efficiency and all electric range. The examination of the cycle life however only took the reduction in maximum battery current in the hybrid RESS into account, disregarding other effects such as temperature, battery stress and DoD. To make a final statement about the cycle life enhancement of the battery system in the hybrid RESS, more accurate results should be acquired experimentally. The addition of the EDLC system also enhances the braking energy performance of the RESS. An increase in System Regeneration Factor with respect to the battery stand – alone system is observed for all the driving cycles. The active hybrid RESS has also a stabilising effect on the DC-bus, benefitting the efficiency of the electrical motor. These positive effects however stand in contrast to the increased cost, weight and volume of the hybrid RESS. Current PHEVs already face a problem of competitiveness in comparison to conventional vehicles due to the increased amount of components in their electrified drivetrain. Further increasing the investment cost of the PHEVs by adding an expensive EDLC system thus clearly is not profitable. Moreover, the vehicle's fuel consumption suffers from the extra mass of the RESS. The enlarged volume of the EDLC system then again introduces extra challenges for the placement of the components in the PHEV, which is already today faced with volume restrictions due to the extra components of the electrified drivetrain. These effects still block the introduction of the EDLC system as peak power system in passenger vehicles.

6.1 Future perspectives

A lot of research is currently put in the electrification of the drivetrain of passenger vehicles. The proposed model of the series plug-in hybrid electric vehicle is used in this master thesis to compare the performance of the battery stand-alone system with the hybrid RESS. In the analysis presented above, it was concluded that the model is not sufficient to examine the cycle life improvement of the battery in the hybrid RESS. A more extensive research on this subject can be executed in order to provide a complete conclusion on the comparison of both RESS technologies. Moreover, the proposed model can also still be improved, for example by adding a temperature model to the battery to take the increase in internal resistance at higher temperatures into account.

Aside from the application described above, the model can also be applied on other configurations than the one analysed in this master thesis:

- The effects of the blended control strategy during charge depleting driving mode with a Plug-in Hybrid Electric Vehicle can be examined and compared to the characteristics of the all electric driving mode.
- The influence on the performance parameters of the RESS can be studied for other configurations of the battery system and EDLC system (see 2.3.3 Hybrid RESS)
- The concept of the peak power system can be applied to other energy storage units than the EDLC system. For example, as part of the SuperLIB project (FP7), the combination of an energy-optimized battery with a power-optimized battery for PHEV applications is investigated. The model proposed in this master thesis will be used to analyse the energy efficiency, range extension and power flows in the hybrid RESS.

List of References

[1] European Commision. Final energy consumption per sector. http://epp.eurostat.ec.europa.eu/tgm/graph.do?tab=graph&plugin=1&pcode=tsdpc320&language=en&toolbox=data (visited on 07/11/2012)

[2] International Energy Agency, "Transport, Energy and CO2: Moving towards sustainability," OECD publishing, 2009.

[3] International Energy Agency, "Technology Roadmap: Electric and Plug-In Hybrid Electric Vehicles," OECD publishing, 2011.

[4] J-M. Timmermans, J. Mathys, P. Van den Bossche and J. Van Mierlo, "Milieuvriendelijke voertuigen," in *Mobiliteit en (groot)stedenbeleid*. Brussels, Belgium, 2006

[5] Plug-in America. http://www.pluginamerica.org/ (visited on 13/10/2012)

[6] K. Lebeau, N. Omar, J-M. Timmermans, J. Van Mierlo, C. Macharis, P. Van den Bossche, J. Van Roy, M. Leemput, J. Driesen and M. Messagie, "Technologische verkenning Elektrische voertuigen," Vlaams Electro Innovatiecentrum, 2010.

[7] N. Omar, "Assessment of Rechargeable Energy Storage Systems for Plug-In Hybrid Electric Vehicles," Vrije Universiteit Brussel, Brussels, Phd thesis 2012.

[8] K. Kurani, A. Burke and J. Axsen, "Are batteries ready for plug-in hybrid buyers?," *Transport Policy*, Vol. 17, Issue 3, pp. 173-182, February 2010.

[9] M. Daowd, O. Hegazy, P. Van den Bossche, T. Coosemans, J. Van Mierlo and N. Omar, "Electrical Double-Layer Capacitors in Hybrid Topologies - Assessment and Evaluation of Their Performance," *Energies*, Vol. 5, pp. 4533-4568, November 2012.

[10] A. Burke, "Research and Development considerations for the performance and application of electrochemical capacitors," *Electrochimica Acta*, Vol. 53, pp. 1083 - 1091, January 2007.

[11] R. Barrero, X. Tackoen, T. Coosemans and J. Van Mierlo, "Hybrid buses: defining the power flow management strategy and energy storage system needs" , Stravanger, Norway, 2009

[12] M. Klohr, S. Pagiela and M. Fröhlich, "Energy Storage System with UltraCaps on Board of Railway Vehicles" in *Proceedings - 8th World Congress on Railway Research*, Seoul, Korea, 2008.

[13] J-M. Timmermans, "Modelling and Design of Supercapacitors as Peak Power Unit for Hybrid Electric Vehicles," in *Vehicle Power and Propulsion Conference*, Chicago, USA, 2005.

[14] A. Yang, Y. Xue, L. Xu, C. Zhu and R. Lu, "Analysis of the key factors affecting the energy efficiency of batteries in electric vehicle," *World Electric Vehicle Journal*, Vol. 4, pp. 9-13, 2010.

[15] J. Axsen, A. Burke and K. Kurani "Batteries for Plug-in Hybrid Electric Vehicles (PHEVs): Goals and the State of Technology circa 2008," Institute of Transportation Studies, University of california - Davis, Research Report UCD-ITS-RR-08-14, May 2008.

[16] G. Maggetto and J. Van Mierlo, "Views on Hybrid Drivetrain Power Management Strategies," in *EVS 17*, Montreal, Canada, 2000.

[17] A. Bouscayrol, K. Chen and C.C. Chan, "Electric, Hybrid and Fuel Cell Vehicles: Architectures and modelling," *IEEE Transactions on vehicular Technology*, Vol. 59, Issue 2, pp. 589 - 598 , February 2010.

[18] K. Rajashekara, S. Williamson, S. Lukic and A. Emadi, "Topological Overview of Hybrid Electric and Fuel Cell Vehicular Power System Architectures and Configurations," *IEEE transactions on vehicular technology,* Vol. 54 Issue 3, pp. 764-769, May 2005.

[19] G. Leduc, A. Muñoz and F. Nemry, "Plug-in Hybrid and Battery-Electric Vehicles: State of the research and development and comparative analysis of energy and cost efficiency," Institute for Prospective Technological Studies, European Commision, Luxemburg, 2009.

[20] US Department of Energy: Energy efficiency and Renewable Energy. Alternative fuel data center. http://www.afdc.energy.gov/ (visited on 13/10/2012)

[21] University of Delaware. [Online]. http://www.udel.edu/V2G/ (visited on 17/11/2012)

[22] A. Hubin, Course: "Batteries and Fuel cells", Vrije Universiteit Brussel, 2011.

[23] M. Daowd, O. Hegazy, J. Smekens, Th. Coosemans, J. Van Mierlo and N. Omar, "Rechargeable Energy Storage Systems for Plug-in Hybrid Electric Vehicles - Assessment of Electrical Characteristics," *Energies*, Vol. 5, pp. 2952-2988, August 2012.

[24] P. Van den Bossche, G. Maggetto and J. Van Mierlo, "Models of energy sources for EV and HEV: fuel cells, batteries, ultracapacitors, flywheels and engine-generators," *Jounal of Power Sources*, Vol. 128, Issue 1, pp. 76–89, March 2004.

[25] F. Vergels, J. Van Mierlo, J. Matheys, W. Van Autenboer and P. Van den Bossche, "SUBAT: An assessment of sustainable battery technology," *Journal of Power sources*, Vol. 162, Issue 2, pp. 913–919, January 2006.

[26] A. Pesaran, Battery choices for different plug-in HEV configurations, US Department of Energy, July 2006.

[27] Element Energy, "Cost and performance of EV batteries," The Commitee of Climate Change, Cambridge, United Kingdom, Final report, 2012.

[28] Battery University. http://batteryuniversity.com/about/ (visited on 20/11/2012)

[29] The Boston Consulting Group, "Batteries for electric cars: Challenges, opportunities and the outlook to 2020." The Boston Consulting Group, Technical report 2011.

[30] M. Miller and A. Burke, "Performance Characteristics of Lithium-ion Batteries of Various Chemistries for Plug-in Hybrid Vehicles," in *EVS 24*, Stavanger, Norway, 2009.

[31] B. Kopf, D. Swan, V. Roan, M. Walsh and F. Kalhammmer, "Status and Prospect for Zero Emissions Vehicle Technology," State of California Air Resources Board, Sacramento, USA, 2007.

[32] K. Amine, H. Yomoto and P. Nelson, "Advanced Lithium-Ion Batteries for Plug-in Hybrid-Electric Vehicles," in *EVS 23*, Anaheim, USA, 2007.

[33] M. Daowd, O. Hegazy, G. Mulder, J.M. Timmermans, Th. Coosemans, P. Van Den Bossche, J. Van Mierlo and N. Omar, "Standardization work for BEV and HEV Applications: Critical Appraisal of Recent Traction Battery Documents," *Journal of Energies*, Vol. 5, pp. 138-156, 2012.

[34] M. Daowd, G. Mulder, J.M. Timmermans, Th. Coosemans, P. Van den Bossche, J. Van Mierlo, S. Pauwels and N. Omar, "Assessment of Permance of Lithium Iron Phosphate Oxide, Nickel Manganese Cobalt Oxide and Nickel Cobalt Aluminum Oxide based cells for using in Plug-in Battery Electric Vehicle Applications," IEEE Vehicle Power and Propulsion Conference,

Chicago, USA, 2011.

[35] M. Daowd, B. Verbrugge, G. Mulder, P. Van den Bossche, J. Van Mierlo and N. Omar, "Evaluation of performance characteristics of various lithium batteries for use in BEV application," IEEE Vehicle Power and Propulsion Conference, Lille, France, 2010.

[36] N. Omar, S. Pauwels, F. Leemans, B. Verbrugge, W. De Nijs, P. Van den Bossche, D. Six, J. Van Mierlo and G. Mulder, "Comparison of commercial battery cells in relation to material properties," *Electrochimica Acta*, Vol. 87, pp. 473-488, 2013

[37] M. Carlen and R. Kotz, "Principles and applications of electrochemical capacitors," *Electrochimica Acta*, Vol. 45, pp. 2483–2498, 2000.

[38] M. Daowd, M. Al Sakka, G. Mulder, Th. Coosemans, P. Van den Bossche, J. Van Mierlo and N. Omar, "Assessment of Li-ion capacitor for using in BEV and HEV applications," *Electrochemica Acta*, vol. 86, pp. 305-315, 2012.

[39] M. Julander and M. Hadartz, "Battery-Supercapacitor Energy Storage," Department of Energy and Environment, Chalmers University of Technology, Göteborg, Sweden, Master thesis, 2008.

[40] J. Zhang, L. Jiang, H. WU, C. YIN Z. Wu, "The energy efficiency evaluation of hybrid energy storage system based on ultra-capacitor and LiFePO4 battery ," *WSEAS Transactions on systems*, vol. 3, no. 11, pp. 95-105, March 2012.

[41] J-M. Timmermans, G. Magetto, P. Van den Bossche J. Van Mierlo, "Peak Power based Fuel Cell Hybrid Propulsion System," *The World Electric Vehicle Association Journal*, Vol 1, pp. 54-61, 2007.

[42] J. Chien, S. Garg, D. Gibbons, B. Ross, M. Tang, J. Xing, I. Sidhu, P. Kaminsky, B. Tenderich and J. Amirault, "The Electric Vehicle Battery Landscape: Opportunities and Challenges," Center for Entrepreneurship & Technology, University of California Berkeley, Technical Report 2009.

[43] View Change. http://www.viewchange.org/topics/byd-f3dm (visited on 14/11/2012)

[44] Wikipedia - List of modern production plug-in electric vehicles. http://en.wikipedia.org/wiki/List_of_modern_production_plug-in_electric_vehicles (visited on 18/10/2012)

[45] Green Car Congress. http://www.greencarcongress.com/ (visited on 14/11/2012)

[46] General Motors. GM Volt: specifications. http://gm-volt.com/full-specifications/ (visited on 07/02/2013)

[47] Fisker Automotive. Fisker Karma. http://onward.fiskerautomotive.com/en-us/karma/specifications/ (visited on 17/11/2012)

[48] Toyota. Toyota Prius Plug-in Hybrid. http://www.toyota.com/byt4/2012/prius-plug-in/en/condensed_ebro.pdf (visited on 14/11/2012)

[49] Ford. Ford C-max specifications. http://www.ford.com/cars/cmax/specifications/engine/ (visited on 23/11/2012)

[50] Volvo. Latest Volvo News. http://www.volvocars.com/uk/top/about/news-events/pages/default.aspx?itemid=135 (visited on 17/11/2012)

[51] Top Speed. http://www.topspeed.com/cars/porsche/2013-porsche-918-spyder-

ar100648.html (visited on 27/11/2012)

[52] BMW. BMW i. http://www.bmw-i.be/nl_be/ (visited on 17/11/2012)

[53] Daimler. Mercedes Benz. http://www.emercedesbenz.com/autos/mercedes-benz/concept-vehicles/mercedes-benz-at-the-2009-iaa-the-mercedes-bluezero-e-cell-plus/ (visited on 17/11/2012)

[54] Lotus. http://www.lotuscars.com/gb/engineering/evora-414e-hybrid (visited on 23/11/2012)

[55] Nissan. Nissan Leaf. http://www.nissanusa.com/leaf-electric-car/index?next=ev_micro.root_nav.overview (visited on 09/12/2012)

[56] Tesla. Tesla Roadster. http://www.teslamotors.com/en_BE/roadster/technology (visited on 09/12/2012)

[57] M. Cuddy, S. Burch K. Wipke, "ADVISOR 2.1: A User-Friendly Advanced Powertrain Simulation Using a Combined Backward/Forward Approach," *IEEE Transactrions on Vehicular Technology: Special Issues on Hybrid and Electric Vehicles*, August 1999.

[58] C. Mi, A. Emadi D. W. Gao, "Modeling and Simulation of Electric and Hybrid Vehicles," *Proceedings of the IEEE: Vol. 95, Issue 4*, pp. 729-745, April 2007.

[59] W. Lhomme, A. McGordon M. Delavaux, "Comparison between Forward and Backward approaches for the simulation of an Electric Vehicle," IEEE Vehicle Power and Propulsion Conference, Lille, France, 2010.

[60] G. Magetto and J. Van Mierlo, "Vehicle Simulation Programme: A tool to evaluate hybrid power management strategies based on a innovative iteration algorithm," *Proceedings of the Institution of Mechanical Engineers. Part D, Journal of automobile engineering*, vol. 215, Issue 9, pp. 1043-1052, 2001.

[61] S. Zoroofi, "Modeling and simulation of vehicular power systems," Electric Power Engineering, Chalmers University of Technology, Göteborg, Sweden, Master thesis 2008.

[62] J. Zhou, "Modeling and simulation of Hybrid Electric Vehicles," University of Science and Technology, Beijing, Master Thesis 2005.

[63] Argonne National Laboratory. Autonomie. http://www.autonomie.net/overview/index.html (visited on 19/12/2012)

[64] Energy Information Administration, "Methodologies for estimating fuel consumption using the 2009 national household travel survey," 2011.

[65] A. Emadi, M. Ehsani and Y. Gao, "Fundamentals of Vehicle Propulsion and Brake ," in *Modern Electric, Hybrid Electric and Fuel Cell Vehicles - Fundamentals, Theory and Design*, 2nd edition, USA, Taylor and Francis Group, 2010

[66] J. Van Mierlo and G. Magetto, "Electric and Electric Hybrid Vehicle Technology: a 2000/2010 perspective," in *The challenge for cities in the 21st century: transport, energy and sustainable development*, Bilbao, Spain, 2000.

[67] G. Lagunoff, "Automotive Hybrid Technology - Status, Function and Development Tools," Luleå University of Technology, Master thesis 2008.

[68] F. Monti, "Hybrid and electric vehicles: Powertrain architecture and sizing design," PhD Thesis, March 2010.

[69] A. Hackbarth, R. Madlener, B. Lunz, D. Sauer, L. Eckstein and C. Ernst, "Battery sizing for serial plug-in hybrid electric vehicles: a model-based economic analysis for Germany," *Energy policy*, vol. 39, pp. 5871-5882, July 2011.

[70] Th. Coosemans, J. Martin, V. Sauvat-Moynot, J. Salminen, B. Kortschak, V. Hennige, J. Van Mierlo, P. Van den Bossche and N. Omar, "SuperLib Project: Advanced Dual-Cell Battery Concept for Battery Electric Vehicles," in *EVS 26*, Los Angelas, USA, 2012.

[71] Maxwell Technologies. Datasheet Maxwell K2 series. [Online]. http://www.maxwell.com/products/ultracapacitors/docs/datasheet_k2_series_1015370.pdf (visited on 19/02/2013)

[72] J. Van Mierlo, H.Gualous, P. lataire and M. Al Sakka, "Comparison of 30 kW DC-DC converter topologies interfaces for fuel cell in hybrid electric vehicle," in *Proceedings of Power Electronics and Applications*, Barcelona, Spain, 2009.

[73] A. Emadi, M. Ehsani and Y. Gao, "Design principles of series (Electrical coupling) Hybrid Electric Drive Train," in *Modern Electric, Hybrid Electric and Fuel Cell Vehicles - Fundamentals, theory and design*, 2nd edition. USA, Taylor and Francis Group, 2010

[74] R. Lu, T. Wang, C. Zhu and H. Yu, "Battery/ultracapacitor hybrid energy storage system used in hybrid electric vehicles," *Journal of Asian Electric Vehicles*, vol. 8, Issue 1, pp. 1351-1356, June 2010.

[75] J. Van Mierlo, P. Lataire and Y. Cheng, "Test Platform for Hybrid Electric Vehicle with the Supercapacitor based Energy Storage," *International Review of Electrical Engineering (I.R.E.E.)*, vol. 3, Issue 3, pp. 466-478, June 2008.

[76] M. Ortúzar, E. Wiechmann and J. Dixon, "Regenerative Braking for an Electric Vehicle Using Ultracapacitors and a Buck-Boost Converter," Department of Electrical Engineering, University of Concepcion, Technical Report June 2002.

[77] A. Emadi, M. Ehsani and Y. Gao, "Fundamentals of Regenerative Braking," in *Modern Electric, Hybrid Electric and Fuel Cell Vehicles - Fundamentals, Theory and Design*, 2nd edition, USA, Taylor and Francis Group, 2010

[78] D. Perkins, R. Alley, D. Nelson L. Gantt, "Regenerative Brake Energy Analysis for the VTREX Plug-in Hybrid Electric Vehicle," in *IEEE Vehicle Power and Propulsion Conference*, Chicago, USA, 2011.

[79] General Motors. Chevrolet Volt Performance Simulation. http://www.leapcad.com/Transportation/GM_Volt_Simulation.pdf (visited on 28/04/2013)

[80] J. Liu and H-F. Liu Y. Shih, "The Analysis of the Power-Assisted Air-conditioning System in Vehicle," in *The 4th Asian Conference on Refrigeration and Air-conditioning*, Taipei, Taiwan, 2009.

[81] R. P. de Oliveira, S. Vaughan, M. Egan and J. Hayes, "Simplified Electric Vehicle Power Train Models and Range Estimation," in *IEEE Vehicle Power and Propulsion Conference*, Chicago, USA, 2011.

[82] Maxwell Technologies. Datasheet 125V HEAVY TRANSPORTATION MODULES. http://www.maxwell.com/products/ultracapacitors/docs/datasheet_bmod0063_1014696.pdf (visited on 13/03/2013)

[83] US Department of Energy. Fuel Economy. http://www.fueleconomy.gov/feg/Find.do?action=sbs&id=30980 (visited on 20/05/2013)

[84] J. C. Burns, J. R. Dahn and A. J. Smith, "A High Precision Study of the Coulombic Efficiency of Li-Ion Batteries," *Electrochemical and Solid-State Letters*, vol. 13, pp. A177-A179, 2010.

[85] E. Rietveld, F. Rieck, B. Veenhuizen, H. Bosma and S. Van Sterkenburg, "Analysis of regenerative braking efficiency - A case study of two electric vehicles operating in the Rotterdam area," in IEEE *Vehicle and Power Propulsion Conference (VPPC)*, Chicago, USA, 2011,

[86] L. Lam, "State of Health Estimation of Liion Battery Cells in Electric Vehicles," University of Technology Delft, Delft, Netherlands, Master thesis 2011.

[87] M. Thornton, J. Rugh A. Brooker, "Technolgy Improvement pathways to cost-effective vehicle electrification," in *SAE 2010 World Congress*, Detroit, USA, 2010.

[88] US Department of Energy: Energy Efficiency and Renewable Energy. Vehicles technologies program: 2011 Nissan Leaf - Advanced Vehicle Testing – Battery Testing Results. http://www1.eere.energy.gov/vehiclesandfuels/avta/pdfs/fsev/battery_leaf_0356.pdf (visited on 15/04/2013)

[89] R. Halbright, M. Weislik M. Dunn, "Lithium Battery Sustainability," Presidio Graduate School, Technical Report 2010.

[90] European Central Bank. Exchange rate US Dollar. http://www.ecb.int/stats/exchange/eurofxref/html/eurofxref-graph-usd.en.html (visited on 14/05/2013)

Appendix

FTP-75

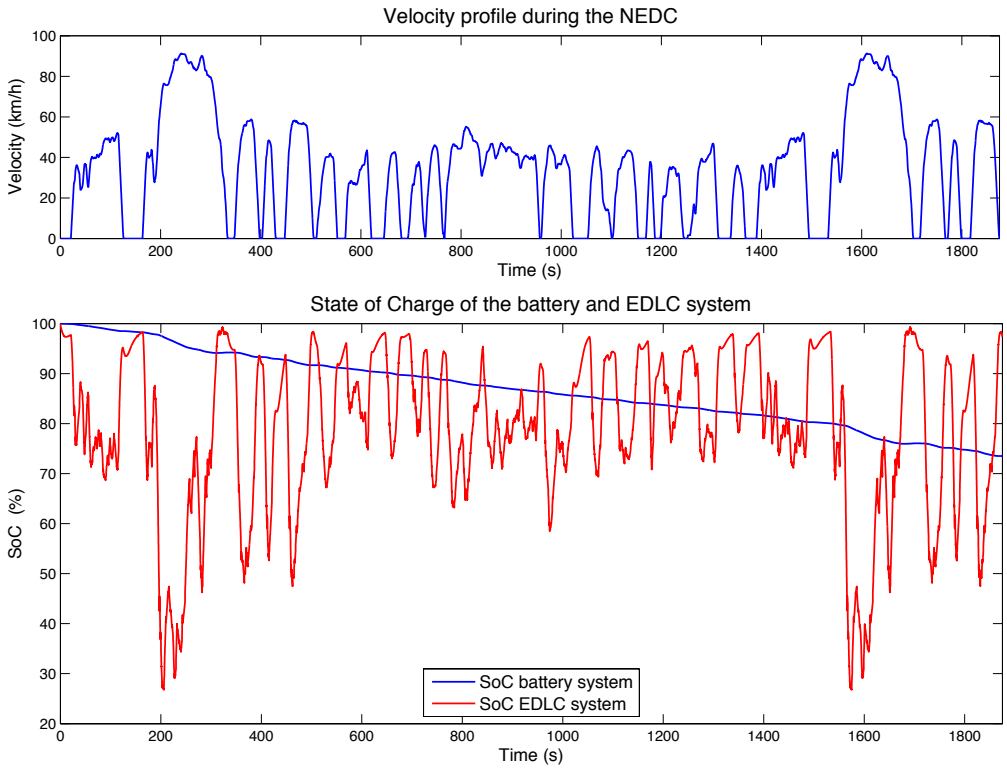

Figure 37: SoC of the battery and EDLC system during FTP-75

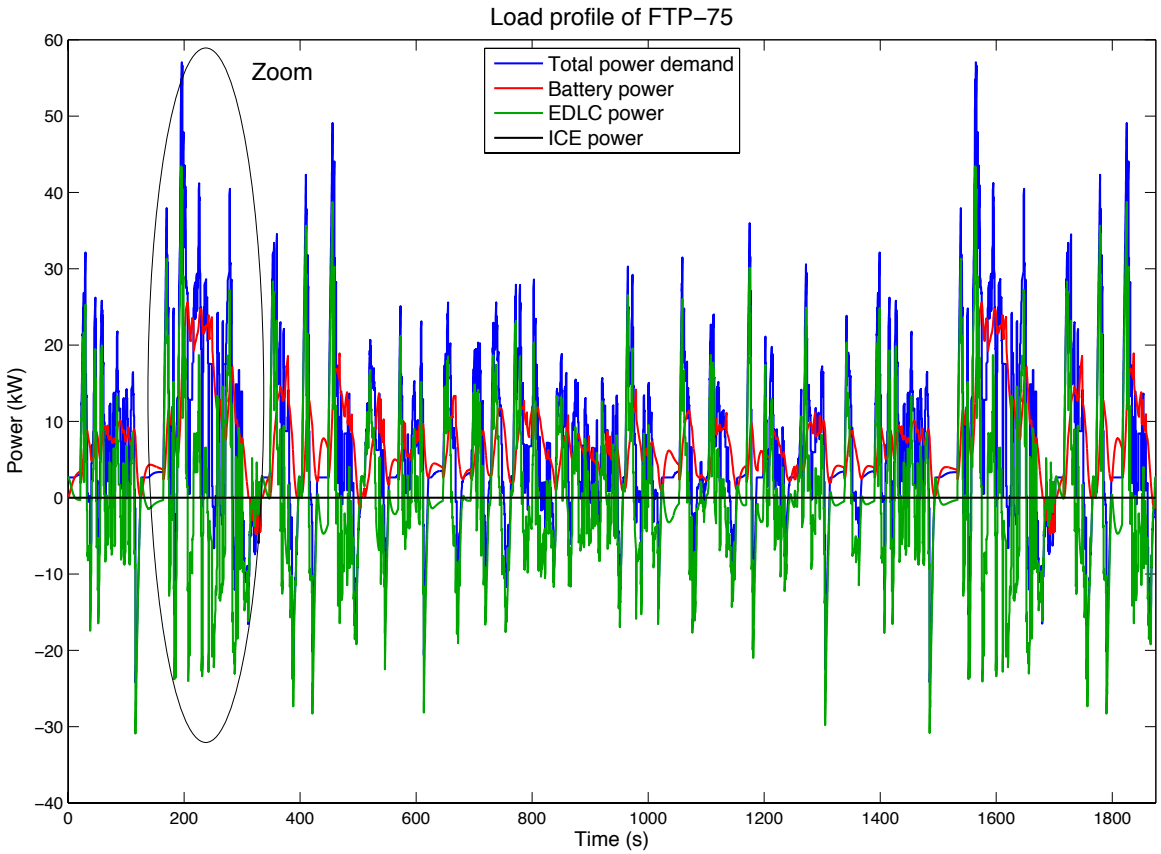

Figure 38: Load profile during FTP-75

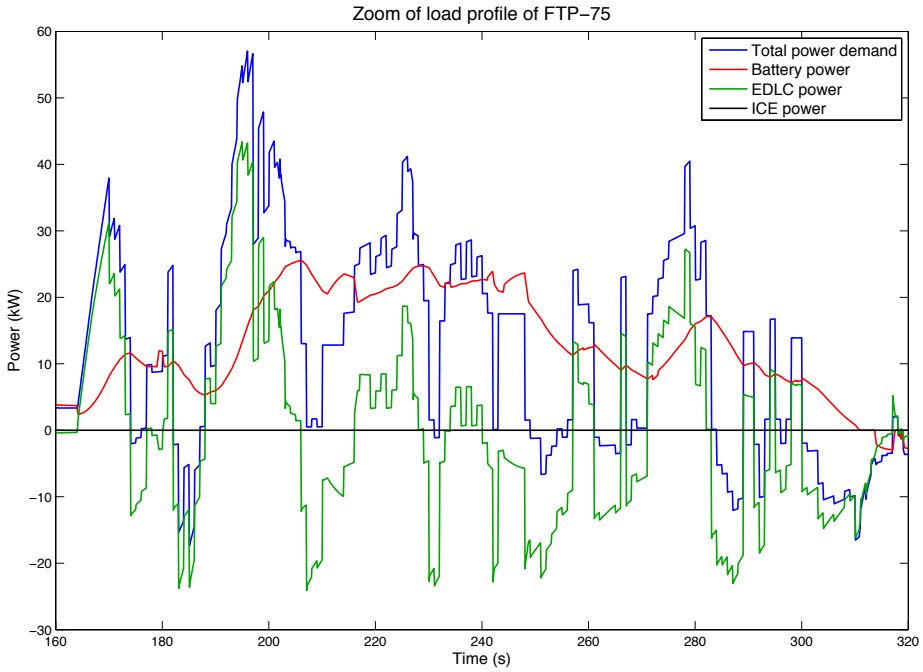

Figure 39: Zoom on load profile during FTP-75

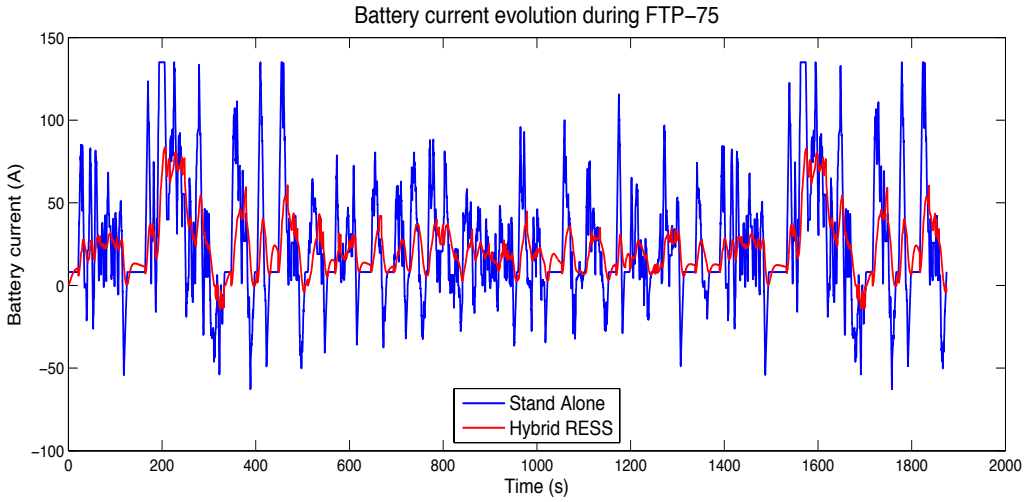

Figure 40: Battery current during FTP-75

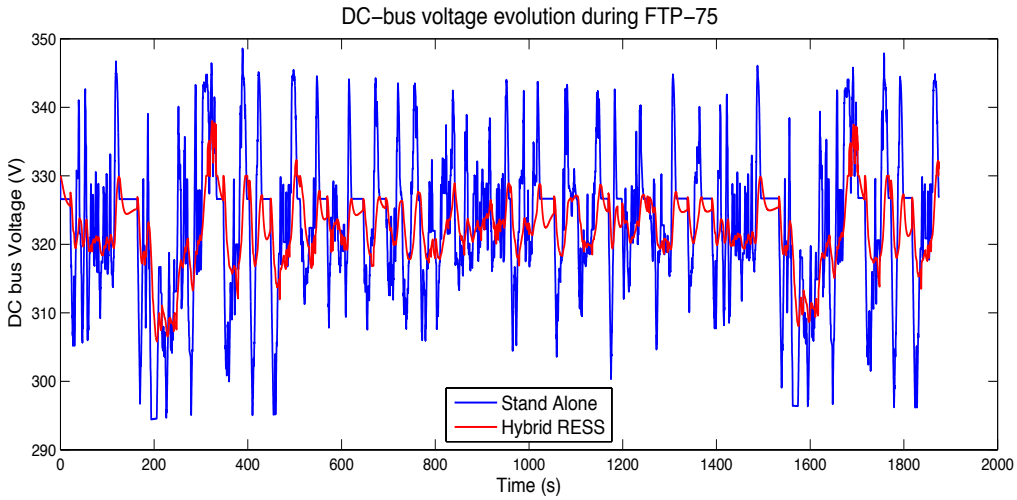

Figure 41: DC-bus voltage during FTP-75

HWFET

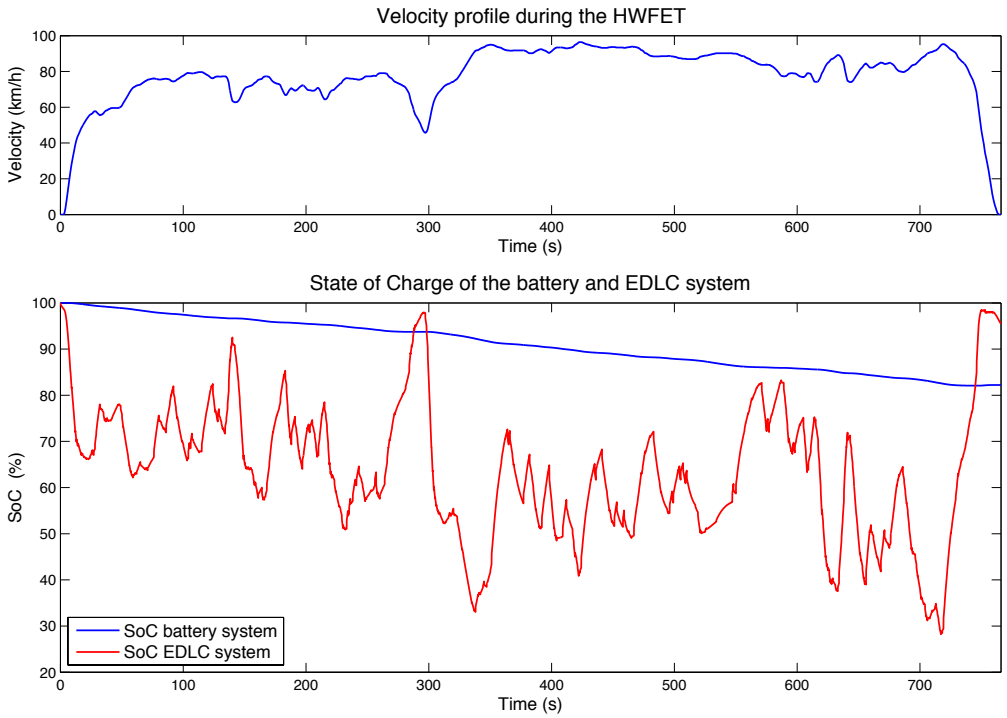

Figure 42: Battery and EDLC SoC during HWFET

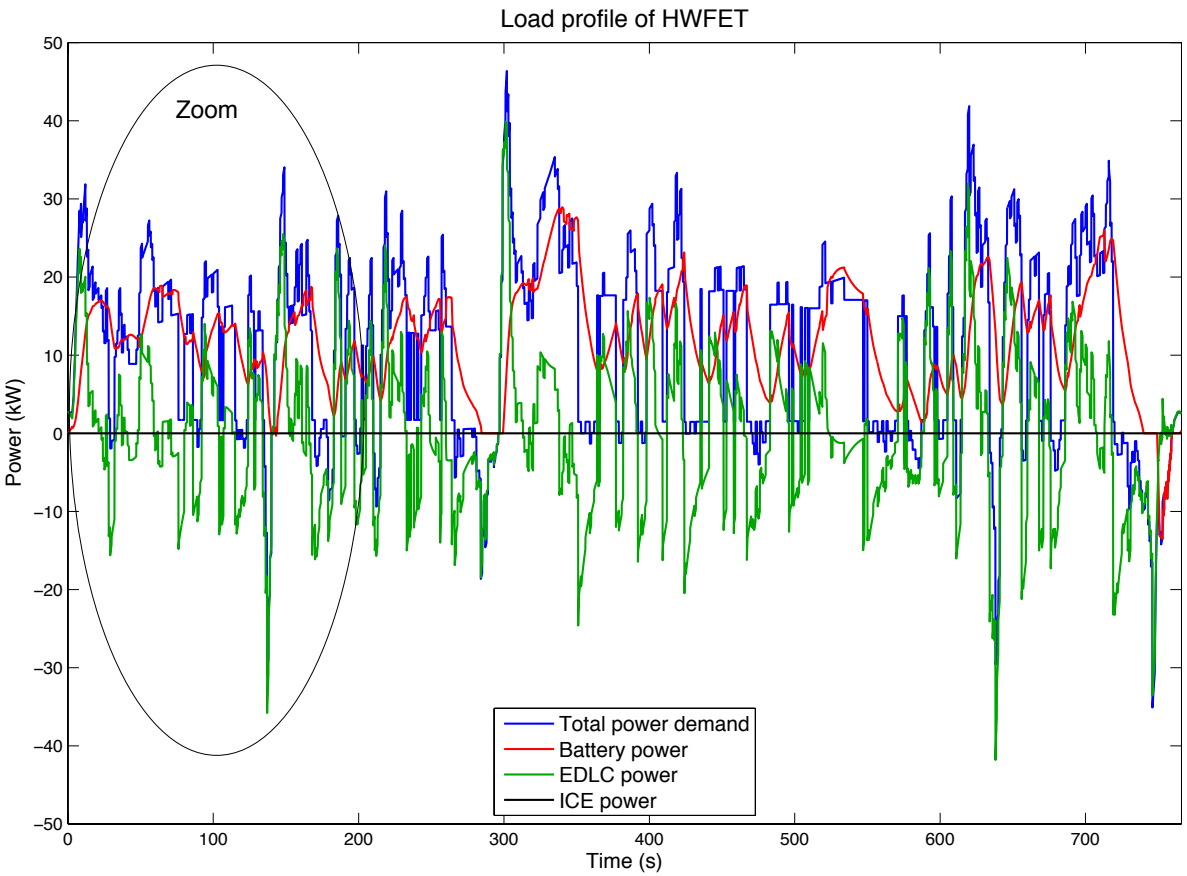

Figure 43: Load profile during HWFET

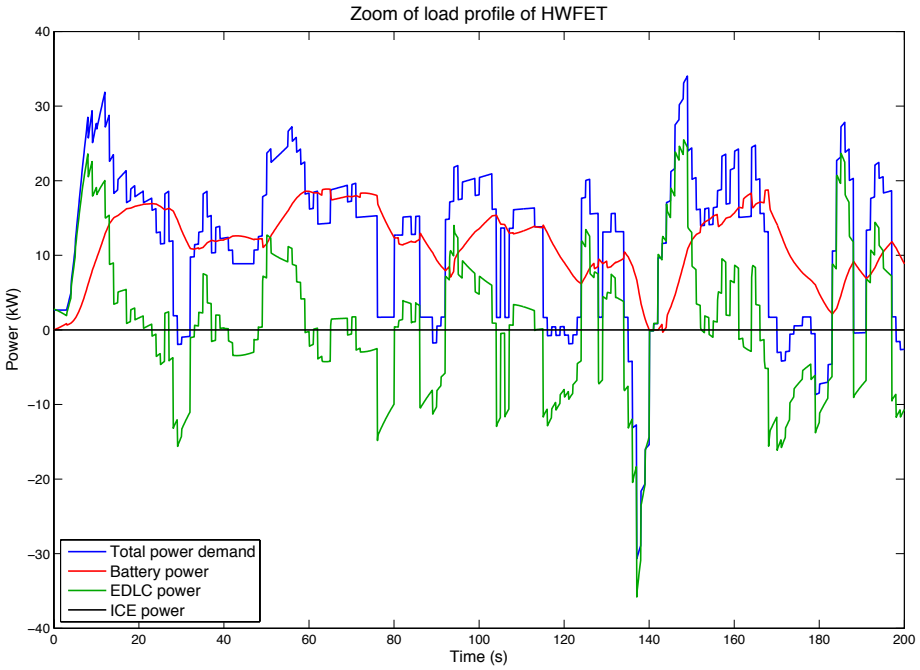

Figure 44: Zoom on load profile during HWFET

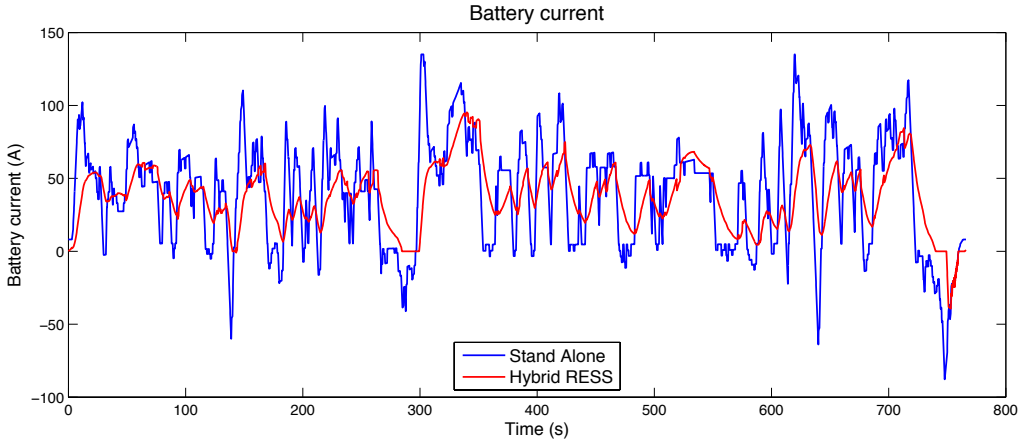

Figure 45: Battery current during HWFET

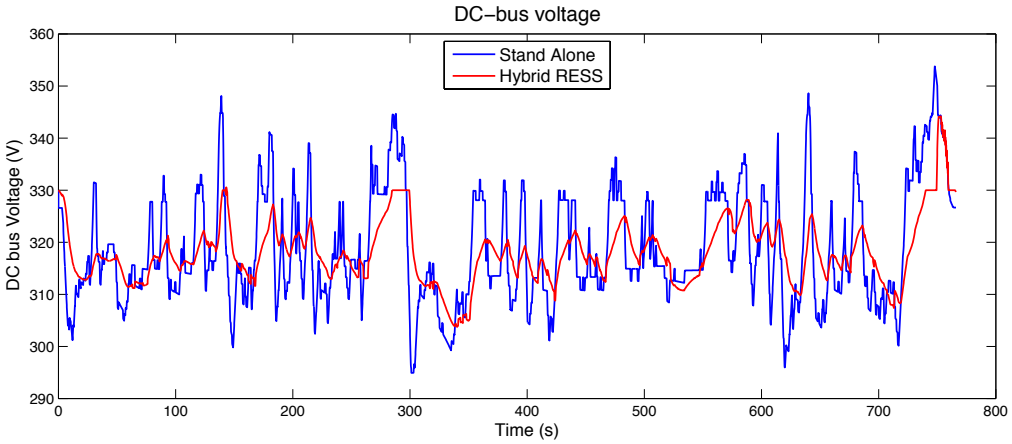

Figure 46: DC-bus voltage during HWFET